Ultra-Sensitive Molecular Detection of Explosives

A thesis submitted for the degree of Doctor of Philosophy



Merel J. Lefferts

Mansfield College

Department of Materials, University of Oxford

Trinity Term 2017

Preface

The work described in this thesis was carried out by the author, under the supervision of Prof. M. R. Castell, at the Department of Materials at the University of Oxford from October 2013 until May 2017. All the work is original, and where work of other researchers is drawn upon it has been referenced and acknowledged. The work described in this thesis has not been previously submitted for any degree at this or another university. Parts of this work have been published in peer-reviewed journals or presented at international conferences as follows:

Lefferts, M. J.; Castell, M. R., Vapour sensing of explosive materials. *Analytical Methods* **2015**

Lefferts, M.; Wu, C.; Murugappan, K.; Visser, S.; Coombes, S.; Hickey, P.; Brookes, M.; Watt, A.; Castell, M., Percolation Networks of Conductive Polymers for High Sensitivity Vapour Sensing of Explosive Materials, *presented at the 6th International Meeting on Chemical Sensors*, **2016**

Lefferts, M. J.; Murugappan, K.; Wu, C.; Castell, M. R., Electrical percolation through a discontinuous gold nanoparticle film, *in preparation*

Approximate word count of this thesis: 34.000 words.

Abstract

Explosives detection plays an important role in both military and civilian applications. However, the detection of explosive vapours remains challenging because of the low vapour pressures of explosive materials. The aim of this project is to develop a system for the ultra-sensitive molecular detection of explosives. The sensor is based on a percolation network of conductive polymers, supported on a scaffold of gold nanoparticles. By operating the sensor at the percolation threshold a higher sensitivity can be achieved compared to more traditional polymer thin film based sensors.

The first component of the sensor, the gold nanoparticle scaffold, was created by dewetting a gold thin film. The nanoparticle size and separation were controlled by controlling the initial gold thin film thickness and the annealing time and temperature. Furthermore, stepwise resistance changes were observed during gold deposition and annealing. Next, conductive polymers were deposited on the gold nanoparticle scaffolds, creating polymer networks ranging from thin films to networks close to the percolation threshold. Additionally, simulations were used to confirm that a sensor based on a percolation network has a higher sensitivity than a thin film based sensor. Finally, initial testing of sensors with various polymer coverages in the presence of ammonia has provided a proof of concept of a sensor based on a percolation network of conductive polymers.

Contents

Preface 2
Abstract 3
Contents 4
Introduction 6
Equipment 9
2.1 Ultra-high vacuum systems 10
2.2 Gold nanoparticle formation setups 10
2.3 Polymer deposition equipment 15
2.4 Imaging techniques 19
2.5 Sensor testing setup 21
2.6 Summary 22
Background A: Vapour sensing of explosive materials 23
3.1 Explosive detection 24
3.2 Animal olfaction 28
3.3 Separation and ion detection techniques 31
3.4 Polymers 38
3.5 Nanomaterials 42
3.6 Microcantilevers 44
3.7 Electronic nose approach 47
3.8 Summary 49
Background B: Practical implementation 51
4.1 Wetting and dewetting 52
4.2 Conductive polymers for sensing applications 57
4.3 Percolation networks 59
4.4 Summary 65
Gold nanoparticle scaffolds 67
5.1 Materials 68
5.2 Methods 72
5.3 Particle size and separation 75
5.4 Resistance 78
5.5 Summary and outlook 83
Conductive polymer networks 84
6.1 Materials 85
6.2 Polymer deposition methods 88

6.3 Polymer networks 95
6.4 Summary 99
Simulations of a sensor based on a percolation network 101
7.1 Simulated conductive network 102
7.2 Node distribution 106
7.3 System size 111
7.4 Maximum connection length 113
7.5 Change in conductance upon interaction 117
7.6 Dynamics 120
7.7 Summary and outlook 123
Sensor testing 126
8.1 Materials and Methods 127
8.2 Results and discussion 128
8.3 Summary 132
Summary 133
Summary for a broad audience 137
10.1 Explosives detection 138
10.2 Novel vapour sensor concept 138
10.3 Practical implementation 141
Acknowledgements 144
References 146

Chapter 1

Introduction

Explosives detection plays an important role in both military and civilian applications. One of the main challenges of explosives detection through gas analysis is the low vapour pressure of many explosive materials. The vapour pressure of, for example, trinitrotoluene (TNT) is 13 ppb[1]. Although there are many existing techniques for explosives detection, many require a form of sample preparation, such as pre-concentration, to be able to detect the small quantities of explosives. Furthermore, many of the existing techniques require large pieces of equipment. The aim of this project is to develop a very small and ultra-sensitive explosives vapour sensor.

The ultra-sensitive explosives detector will be a chemiresistor, based on a percolation network of conductive polymers, supported on a metal nanoparticle scaffold (*Figure 1.1*). The conductive polymers will be chosen such that they interact

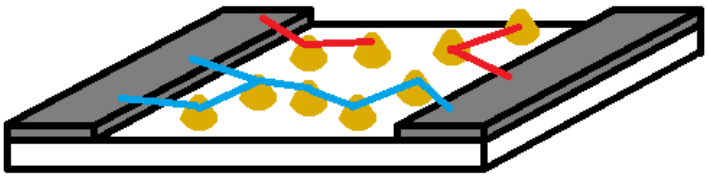


Figure 1.1: Schematic representation of a sensor consisting of an insulating substrate (white), electrodes (grey), metal nanoparticles (gold), and a network of conductive polymers, where blue signifies a conducting path between the electrodes, whereas red indicates a section of the polymer network that does not contribute to the connection between the electrodes.

with the analyte molecules. Upon interaction with the analyte the resistance of the polymer changes, which can be measured. To increase the sensitivity, compared to more traditional polymer thin film based sensors, the polymers will be deposited such that they form a percolation network. Using a percolation network of polymers will allow for a stronger overall sensor response as a result of the local change caused by the interaction between a polymer and the analyte molecule. The polymers will be deposited on a gold nanoparticle scaffold, acting as the nodes of the network of conductive polymers.

This thesis starts with an overview of the most important equipment and methods used for the work that was carried out, including sample preparation, imaging, and sensor testing methods. The next two chapters are background chapters. The first gives an overview of existing explosives vapour sensing methods. The second focusses on the background needed for the practical implementation of a sensor based on a percolation network of conductive polymers; discussing wetting and dewetting, as used for the nanoparticle scaffold formation, conductive polymers, and percolation networks.

The next chapter, chapter 5, focusses on the first component of the sensor: the gold nanoparticle scaffold. In this section the gold deposition and annealing to form the metal nanoparticle scaffold are discussed, as well as changes in the resistance of the gold layer during deposition and annealing.

In chapter 6 the conductive polymer component of the sensor is developed. Conductive polymers are deposited on both insulating substrates and insulating substrates that have been decorated with gold nanoparticles. Polymer networks close to the percolation threshold are created.

The focus of chapter 7 is on simulations of a sensor based on a percolation network. The simulations are used to study such a system and help optimise the physical sensor.

Various parameters and their effect on the resistance and percolation threshold of the sensor are discussed.

In chapter 8 the first sensing results a described. The sensors are exposed to ammonia at a range of concentrations. Furthermore, the responses of sensors with different polymer coverage are compared. A proof of concept for a sensor based on a percolation network of conductive polymers on a metal nanoparticle scaffold is given.

Finally, in chapter 9, the results described in this thesis are summarised and suggestions are made for possible future work on this topic.

Chapter 2

Equipment

In this chapter the most important pieces of equipment that are used for the work described in this thesis are introduced. This chapter starts with a description of the vacuum system and the various pieces of equipment attached to it that are used to develop the gold nanoparticle scaffolds. Next, several polymer deposition methods, used to deposit conductive polymers on the gold nanoparticle scaffolds, are discussed. Furthermore, the imaging techniques used to image the samples at various stages of nanoparticle scaffold development and after polymer deposition are discussed. Finally, the sensor testing setup is described.

2.1 Ultra-high vacuum systems

Many of the experiments described in this thesis take place in ultra-high vacuum (UHV). UHV allows for the cleanliness required for the formation of the gold nanoparticle scaffolds, and limits contamination or defects. Furthermore, the UHV systems allow for the vacuum conditions that are required for some sample preparation steps or experiments, such as vapour deposition of metals. For this reason I will start by describing the UHV systems that have been used. The equipment attached to, and installed in, the UHV chambers will be discussed in the next section of this chapter.

Two separate UHV systems have been used. One system, consisting of 2 vacuum chambers (*Figure 2.1*), was primarily used for gold evaporation and gold nanoparticle formation experiments described in chapter 5. The second UHV system consist of 3 chambers of which one is used for UHV-SEM (scanning electron microscopy) and another for scanning tunnelling microscopy (STM). Both UHV systems were produced by JEOL and can achieve pressures as low as 10^{-8} Pa.

2.2 Gold nanoparticle formation setups

A few different setups have been used for gold deposition and nanoparticle formation. All these setups consist of the same general components: an evaporator, such as a direct thermal evaporator, a Knudsen-cell, or an electron beam evaporator, a quartz crystal microbalance, and a heating holder. These pieces of equipment are described below. With the exception of the thermal evaporator in the glovebox (section 2.2.1) all of these pieces of equipment were used in UHV.

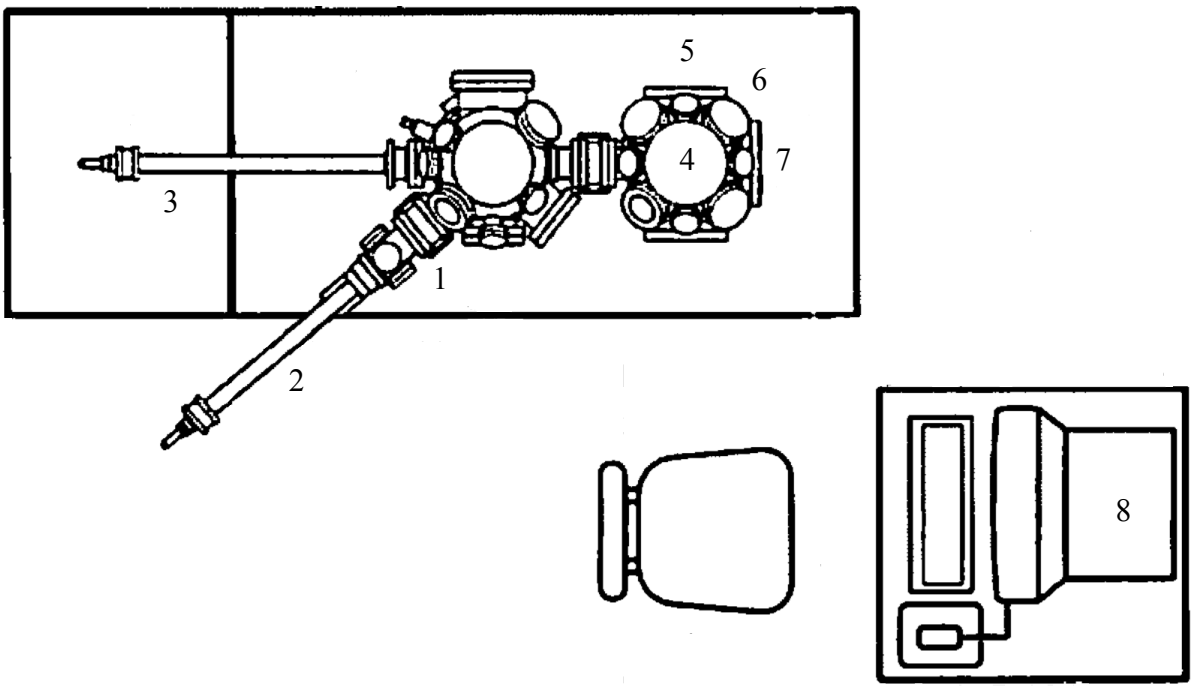


Figure 2.1: Schematic representation of the UHV system used for gold nanoparticle formation, showing the exchange chamber (1), the arms used to move samples from one chamber to another (2) and (3), the position of the sample during experiments (4), the position from which the QCM is fed through such that the crystal is close to the sample and aligned with the k-cell (5), the position of the k-cell (6), the feed through for electrical connections to the sample and heating holder (7), and the PC used for measurements (8). (Image adapted from Ref. [2]).

2.2.1 Thermal evaporator in glovebox

A direct thermal evaporator, positioned under a bell jar, in a glovebox was used for the initial gold deposition experiments. The gold was placed in a boat, directly underneath the sample, and heated by resistive heating of the boat. The best vacuum that can be achieved under the bell jar is ~10^{-6} Torr (~10^{-4} Pa), and evaporation typically takes place at approximately 2×10^{-6}-10^{-5} Torr. Once the desired vacuum pressure has been achieved, the current applied to the heating system is slowly increased until a suitable deposition rate, as measured by a quartz crystal microbalance (QCM), is reached. Under the above described conditions, gold is typically evaporated at 0.1-0.3 nm/s.

An advantage of this method is that it is possible to deposit gold on a relatively large surface area, up to approximately 100 cm^2, or on multiple samples at the same time. However, thin films deposited using this method are relatively prone to contaminations because of the relatively low vacuum and because the sample has to be transferred between different vacuum systems for the different steps of the nanoparticle formation process.

2.2.2 Knudsen cell

A Knudsen cell, or K-cell, is used for indirect thermal evaporation. A single-filament-effusion cell (*Figure 2.2*), produced by CreaTec Fischer, was used for most of the gold nanoparticle experiments described in chapter 5. The gold was placed in a pyrolytic boron nitride (PBN) crucible, inside the K-cell. The crucible is heated, by radiative heat from a tantalum wire, to 1500 °C. The temperature can be controlled by controlling the heating power applied to the tantalum wire (*Figure 2.3*). To prevent unwanted deposition while heating the crucible, the K-cell has a shutter that can cover the hole through which the vapour leaves the cell. K-cells allow for uniform and controllable temperatures within the cell, which means that the evaporation rates can be kept constant. Evaporation with this setup typically takes place at ~0.02-0.03 Å/s.

2.2.3 Electron beam evaporator

Electron beam (e-beam) evaporation can also be used to deposit thin metal films. The e-beam is attached to the second UHV system and was only used for the gold deposition on $SrTiO_3$. In e-beam evaporation a metal rod is bombarded by an electron beam, causing the metal to be evaporated. The electron beam used for evaporation is emitted by a charged tungsten filament. The e-beam evaporator used in this thesis was produced by Oxford Applied Research. This evaporator can hold 4 rods of different materials that are separated from each other to prevent contamination.

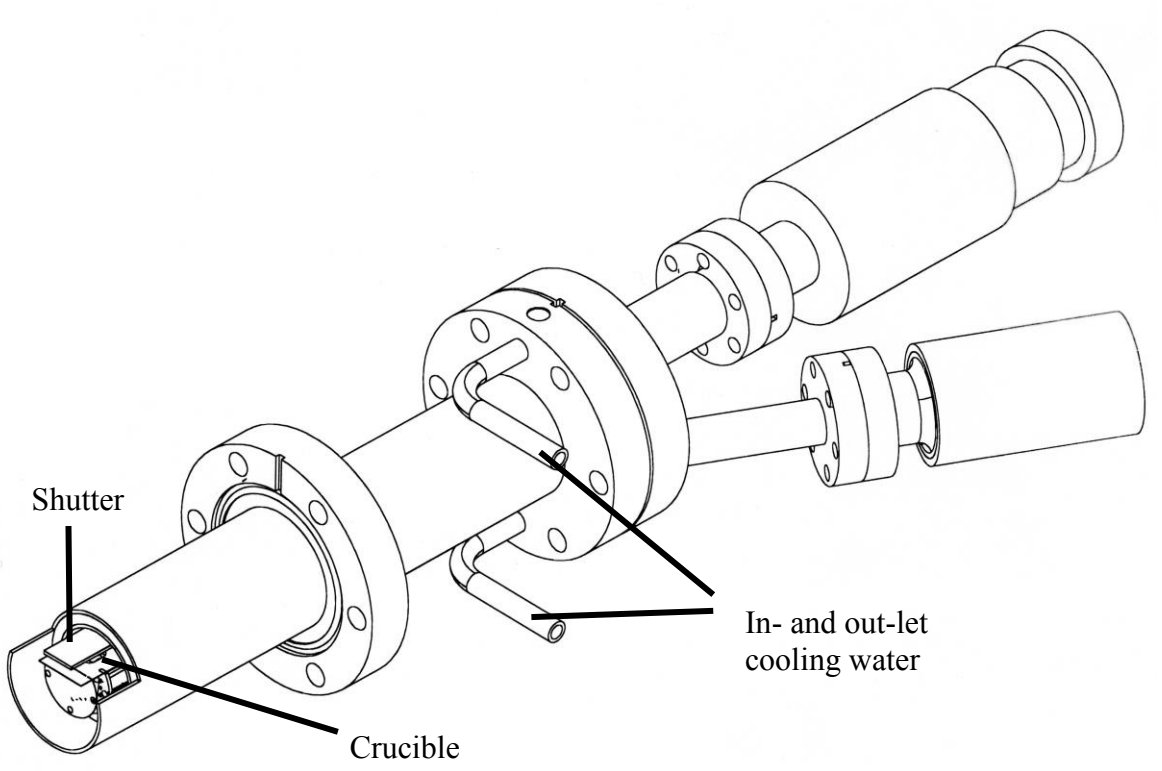


Figure 2.2: Schematic representation of a K-cell (adapted from Ref. [3]).

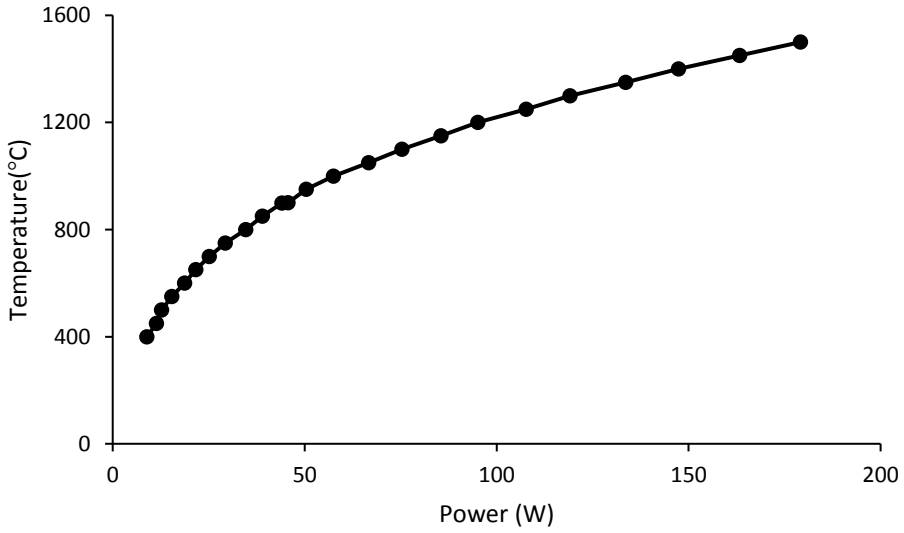


Figure 2.3: Heating power applied vs. the temperature of the K-cell as measured by the power and temperature controller of the K-cell.

2.2.4 Quartz crystal microbalance

A quartz crystal microbalance (QCM) was used to monitor the thickness of the deposited layer during thin film deposition. The key component of a QCM is a thin piezoelectric quartz crystal plate, that functions as a high frequency resonator[4]. Deposition of the evaporated material on the quartz crystal causes a decrease in the frequency of the resonator. The change in frequency is measured and used to monitor the thickness of the deposited layer. The QCM is positioned such that the amount of material deposited on the quartz crystal is the same as, or proportional to, the amount of material deposited on the sample. In this way the QCM can be used to monitor the thickness of the film during deposition on the sample. Because QCMs tend to have a high quality factor, or low resonance bandwidth, very small changes in the resonance frequency can be measured[4]. This means that the QCM is sensitive to the deposition of very thin films. A bakeable QCM produced by Inficon was used for most of the gold deposition experiments.

2.2.5 Heating holder

For this research an indirect heating holder was used to heat resistive samples in UHV. The heating holder is a sample holder, compatible with the UHV systems, which has an additional heating plate (*Figure 2.4*). A current is passed through the heating plate, which causes the plate to heat up. The sample is thus heated indirectly. This method allows for controlled and repeatable heating of a sample in UHV. Furthermore, it allows for heating while experiments take place, and measurements or images are taken of the sample. The heating holder used for this thesis was produced by JEOL.

Furthermore, a direct heating holder was used to resistively heat samples with conductive substrates. In the case of a direct heating holder there is no heating plate and the heating current is passed directly through the sample.

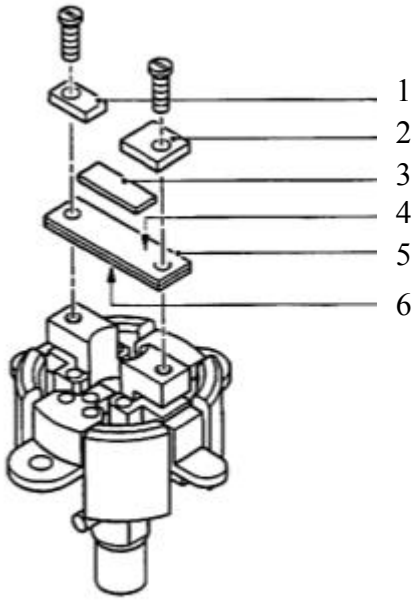


Figure 2.4: Schematic representation of a heating holder. Where 1) is a tantalum specimen retainer, 2) an alumina specimen retainer, 3) the specimen, 4) the insulator side of the heating plate, 5) the heating plate, and 6) the heater element side of the heating plate. (Image adapted from Ref. [5]).

2.3 Polymer deposition equipment

Several methods have been used for the polymer deposition work described in chapter 6 of this thesis. The polymer deposition methods include several different ways to deposit dissolved polymers, thermal evaporation of oligomers, and electrochemical polymerisation.

2.3.1 Spin coating

In spin coating a droplet of polymer solution is deposited on a stationary substrate, after which the substrate is accelerated to the desired spin speed. As the substrate is accelerated the solution spreads radially over the surface due to centrifugal force and any excess material is ejected from the surface. Next the film continues to thin until it becomes highly viscous due to solvent evaporation, or until an equilibrium thickness is reached due

to disjoining pressures. Finally, the remaining solvent evaporates, resulting in a layer of polymer on the sample[6]. Spinning ensures that the solution is spread out relatively evenly over the substrate and makes it possible to deposit thin layers.

Spin coating allows for control over the thickness and distribution of the deposited material through the choice of spin speed, solvent, and concentration of the solution. The layer thickness is proportional to the inverse of the square root of the spin speed. In addition to the spin speed, the concentration of the solution can be tailored to obtain the required film thickness. As expected, higher concentrations will result in thicker layers. Apart from choosing a suitable solvent for the chosen polymer, the solvent must wet the surface of the sample on which it will be deposited, and the solvent must be volatile. Finally, the amount of solution deposited on the sample must be sufficient to easily cover the entire surface. For the work described in chapter 6 a Speciality Coating Systems 6800 series spin coater was used.

2.3.2 Dip coating

In dip coating the sample is dipped in a polymer solution and extracted vertically. Excess solution is drained by gravity, while solvent evaporates to form a polymer film on the substrate. As in the case of spin coating the concentration and viscosity of the solution, and the volatility of the solvent affect the resulting films. Additionally the speed at which the sample is extracted from the solution plays a role. At a higher extraction speed the viscous drag of the substrate is larger. This causes a larger amount of solution to move upward with the substrate, resulting in a thicker film[7].

2.3.3 Drop casting

In drop casting a droplet of solution is simply deposited on the sample. The solvent then evaporates, leaving the polymer deposited on the substrate. This is relatively simple

method for which no special equipment is required. However, the resulting deposits are relatively thick. Furthermore this method does not allow for control over the distribution of the deposit over the substrate. This often results in the formation of droplet patterns or rings on the substrate. In some cases the substrate is not fully covered by the droplet. The thickness of the resulting layer depends on the properties of the solvent, such as the volatility, viscosity, wettability on the surface on which it is deposited, and the concentration of the solution.

2.3.4 Thermal evaporation

For thermal evaporation the polymer is placed in a boat which is heated resistively under vacuum. The polymer evaporates and the vapour is deposited on the sample. An advantage of this method is that thin, relatively uniform, layers can be deposited with precision. However, a disadvantage of this method is that only relatively small molecules can be deposited. Larger molecules are broken up during the heating. In this thesis, this method was used for the deposition of sexithiophene, an oligomer, using an evaporator built especially for polymer evaporation by Andrew Watt's group.

2.3.5 Electrochemical polymerisation

Using electrochemical polymerisation the polymer is polymerised directly onto the sample. The sample is placed in a salt solution containing the monomer, typically 1 M $LiClO_4$ and 0.1 M monomer in acetonitrile, as well as a counter electrode (Pt) and a reference electrode (Ag/AgCl). The two electrodes of the sample are connected to each other, such that they together act as the working electrode (*Figure 2.5*). Next, using a potentiostat, the sample is either held at one potential (chronoamperometry), or a range of potentials is scanned across the sample (cyclic voltammetry), causing the monomers to polymerise and

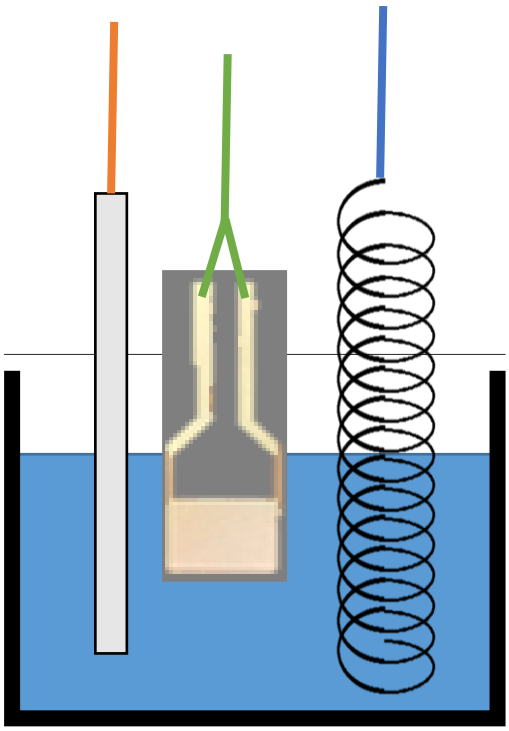


Figure 2.5: Schematic representation of the setup for electrochemical deposition, with the working electrode (green connection), the reference electrode (orange connection), and the counter electrode (blue connection).

deposit on the sample. The maximum potential was typically 1-1.4 V. Deposition only takes place when there is an electrical connection. For this reason deposition starts on the electrode and grows outwards from the electrodes once the electrodes have been fully covered with polymer. Typically the electrodes are covered after scanning across the potential range once. Any further scans increase the amount of polymer deposited between the electrodes, gradually forming a network and adding more connections between the two electrodes.

To further stabilise the polymer network and ensure that all sensor samples are tested in the same state, all samples were doped. To dope a sample it was placed in a salt solution without monomers, and held at a set potential for a set amount of time. This causes polymer film to be doped with anions, or cations, from the salt solution. The applied potential was used to control the level of oxidation, or reduction, of the conductive polymer.

2.4 Imaging techniques

Several methods have been used to image the samples at various stages of nanoparticle scaffold formation and conductive polymer deposition. The imaging methods used for the work described in this thesis are scanning electron microscopy and atomic force microscopy.

2.4.1 Scanning electron microscope

The development of electron microscopes started in the 1930s with the development of the transmission electron microscope. Later scanning electron microscopes were introduced[8]. In a scanning electron microscope (SEM) an electron beam is scanned over the surface of the sample. The principle of electron microscopy (EM) is similar to that of optical microscope, however in the case of EM an electron beam is used instead of visible light. The shorter wavelength of electrons allows for a much higher resolving power. In SEM magnets are used, instead of lenses, to direct and focus the electron beam.

An advantage of SEM is that it can be used over a large range of magnifications, from barely magnified to the nanometre scale. SEM is an especially useful technique on length scales beyond the diffraction limit of optical microscopes. A disadvantage of SEM is that the sample has to be conductive. If an insulating sample is used the sample will charge up which makes imaging difficult. It is possible to image insulating samples after coating them with a few nanometres of a conductive material such as gold or platinum. However, coating the sample is not always possible, for example when the sample has to be reused after imaging. Most samples described in this thesis have an insulating substrate. SEM images of these samples suffer from charging effects. Conductive coatings cannot be used because the samples have to be used for further experimental steps after imaging. To make imaging with SEM possible and to minimise charging effects, most SEM images in this

thesis were obtained with a low voltage, typically 1.0 - 5.0 kV, and with the electrodes of the sample connected to a conductive sample holder.

Within SEM several imaging modes can be used, for example detection electrons emitted at different angles, each providing different information about the sample. The mode that is used depends on the properties of the sample and the type of information that needs to be extracted from the image. Secondary electron (SE) detection is the most commonly used method. In SE imaging electrons from the surface of the sample are ejected due to inelastic scattering as a result of interaction with the electron beam. These secondary electrons are then detected[9]. In back scattered electron detection, electrons from the electron beam are reflected off the surface of the sample. This method is especially useful to get contrast between materials with different atomic masses[10].

The SEM systems used for the images in this thesis include the JEOL 840F and 6500F, and Zeiss Merlin 60-62.

2.4.2 Atomic force microscopy

Atomic force microscopy (AFM) was first developed by Binnig, Quate and Gerber, as a method to study the surfaces of insulators with high resolution[11]. The method uses a sharp tip, positioned close to the surface and attached to a cantilever, that is scanned over the sample surface. Variations in the forces between the tip and the surface cause the cantilever to get deflected. The deflection of the cantilever is measured, for example, using a laser beam that is reflected off the top of the cantilever. The position of the reflected laser beam is monitored using a position sensitive detector, such as a 4 segment photodiode[12].

AFM can be operated in several different modes. In the static mode the tip is in constant contact with the sample surface. A disadvantage of this method, especially when imaging relatively soft materials, is that the tip can damage the sample surface. In dynamic

imaging modes the tip oscillates above the sample surface. Changes in the frequency, amplitude, or phase, as a result of forces between the tip and the sample surface, are measured. In dynamic modes the surface damage is significantly reduced because lateral forces between the tip and the sample are minimised[13-14].

An advantage of AFM is that high resolution images can be obtained of a large range of materials. Further advantages are that AFM is not damaging to the sample and surface preparation is not needed.

The AFM system used in this work is a Park Scientific Instrument CP-II AFM.

2.5 Sensor testing setup

To test the sensor in a controlled environment a sensor testing setup was developed (*Figure 2.6*). The setup consists of a small vacuum chamber with inlets and an outlet for various gasses. Furthermore, the chamber has feedthroughs for connections to measure the resistance of the sample. It also offers the possibility of heating the sample, while testing its response. This setup allows us to measure the response of the sample in the presence of a known quantity of a specific vapour or mix of vapours, while also controlling other parameters such as temperature, pressure, and humidity.

Before testing, each sample was placed in the chamber and left to stabilise under nitrogen flow. Next, the sample was exposed for 20 minutes to a known concentration of ammonia, created by combining pure nitrogen and 500 ppm ammonia in nitrogen outside the testing chamber. After exposure, the sample was left under nitrogen flow for 70 minutes.

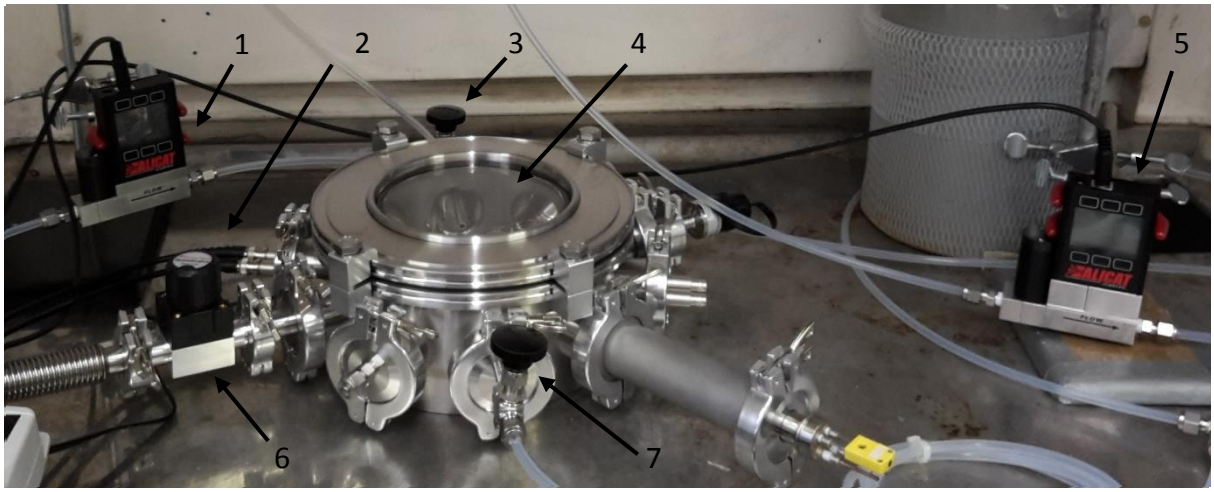


Figure 2.6: Image of the sensor testing rig where 1) is the nitrogen flowmeter, 2) electrical feedthrough to monitor the resistance of the sample, 3) the gas outlet, 4) the testing chamber, 5) the analyte vapour flowmeter, 6) the vacuum pump valve, and 7) the gas inlet.

2.6 Summary

In this chapter the equipment and methods used in this thesis have been introduced. The UHV system in which the metal nanoparticle formation takes place was described, as well as the pieces of equipment, such as a K-cell, QCM, and heating holder, attached to it. For the deposition of the next component of the sensor, the polymer layer, various possible methods were described, including drop casting, spin coating, dip coating, and electrochemical methods. SEM and AFM are the imaging techniques used for the work in this thesis. Finally, the sensor testing set up was described.

Chapter 3

Background A: Vapour sensing of explosive materials

Reliable detection of explosive substances is of critical importance in a variety of settings. For example, in a civilian context fixed monitoring stations in airports are used to prevent explosives-based terrorist attacks[15]. For military applications explosives detection is required to locate landmines and improvised explosive devices (IEDs). Finding unexploded ordinance is also a critical element in humanitarian demining activities. Explosives detection systems need to be able to detect a large range of explosive materials, including both traditional high explosive materials, such as TNT, and chemicals used in IEDs, such as ammonium nitrate. The continued development and improvement of new techniques remains important in order to overcome existing challenges and meet challenges posed by new developments in the field of explosives.

The focus of this chapter is on explosives vapour sensing. Vapours sensing can be used directly to detect vapours emitted by bulk explosives, and indirectly to detect trace quantities of explosives residue that have been vaporised within a detector. Direct vapour sensing of explosives is especially important as it allows stand-off detection of concealed explosives. It is perhaps surprising that the gold standard for vapour detection is still the olfactory sense of a trained sniffer dog. However, through the improvement of existing techniques, and the development of novel sensors, it is likely that technology will at some stage overtake animal olfaction. This chapter outlines the various explosives vapour sensing methods, both established and recent, and starts by defining explosive materials and the challenges in detecting their vapour.

3.1 Explosive detection

3.1.1 Explosive materials

Explosive materials are defined as materials that can, after initiation, undergo a very fast and self-propagating decomposition. Upon decomposition, more stable compounds are formed, and a pressure effect can take place and heat can be released[16]. For example, trinitrotoluene (TNT) whose formula is $C_7H_5N_3O_6$ decomposes into N_2, H_2, H_2O, CO and C. This is a very rapid and highly exothermic reaction, but it has a reasonably high activation energy and TNT is therefore stable in an ambient environment. Explosives can be classified in various ways. Firstly one can make a distinction based on the speed of the explosion. Low explosives detonate relatively slowly, of the order of cm/s, and there is no associated shock wave. Black powder and pyrodex are examples of low explosives. High explosives detonate at speeds of the order of km/s and cause a shock wave[16-17]. Examples of high explosives include TNT, tetryl, and picric acid (*Figure 3.1)*[18]. Although many explosive materials are

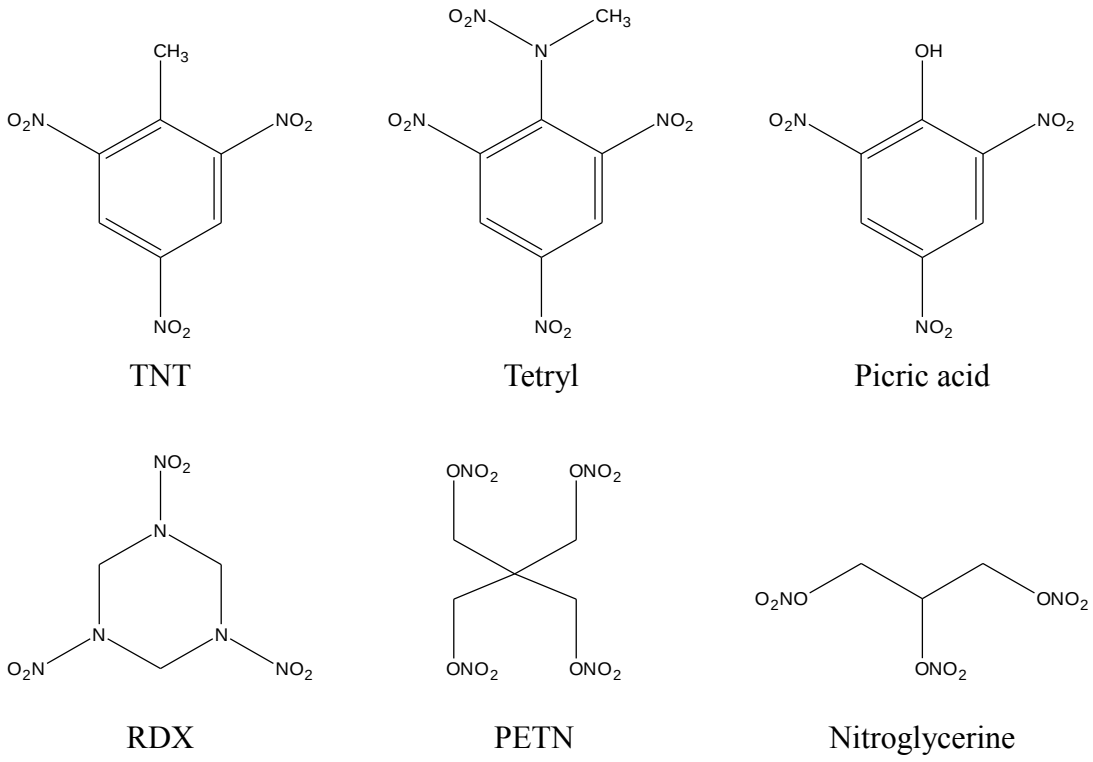


Figure 3.1: Examples of explosive materials and their structural formulas.

similar in that they often contain nitro groups they can have very different properties. Nitroglycerine, for example, is very sensitive to physical shock, making it much less stable than TNT. And cyclonite (RDX) is more powerful than TNT. High explosives can be further divided into primary explosives and secondary explosives. Primary explosives are more easily initiated than secondary explosives because they are more sensitive to impact, friction or heat[17]. Primary explosives are often used to initiate secondary explosives[16]. It is also possible to distinguish between molecular explosives such as TNT, where the fuel and oxidiser are contained in the same molecule, and binary explosives that are a mixture of a fuel and an oxidiser, for example a mixture of ammonium nitrate and fuel oil. Furthermore, explosives can be classified based on their chemistry. From a chemical point of view the following types of explosives can be identified: nitro compounds, nitric esters, nitramines, derivates of chloric and perchloric acids, azides, and various other compounds that can produce an explosion, such as fulminates, acetylides, and nitrogen rich compounds such as tetrazene, peroxides and ozonides[19].

3.1.2 Challenges to explosives detection

A large range of explosives detection methods have been developed, and some of these methods have been in use for many years. A distinction is made between methods that are used for the detection of bulk explosives and methods for trace explosives detection, noting that direct vapour sensing detects trace quantities emitted from co-located bulk materials (unlike trace particle detection where trace residues may not correlate to the presence of bulk). In the case of bulk explosives detection, imaging or investigation of the nuclear properties of a material can be used to detect macroscopic amounts of explosive compounds. Trace explosives detection is the detection of small amounts of explosives, often in the form of small quantities of explosives that have been vaporised or particulates. A distinction can be drawn between direct vapour detection in the environment and the

detection of particulates of explosive material that have been collected and then vaporised within the analysis instrument. Many of the existing technologies can be used for both these types of detection. The difference between directly detecting vapours and the detection of vaporised materials is more closely related to the sample preparation method than to the detection method itself. After all, vaporising (a sample preparation step) turns the sample into a vapour that can be analysed in the same way as an authentic vapour. Animal olfaction directly senses vapours. However, most other techniques, for example ion mobility spectrometry, mass spectrometry, and fluorescent polymer based methods, can be used for both. They can be operated both by direct sampling of the air containing the authentic vapours as well as by vaporising a sample that was collected by swiping a surface contaminated with explosive particulates. A distinction can also be made between contact and standoff detection of explosive materials. Related to this are the different ways in which samples can be collected. Contact detection requires direct collection of the sample, for example by swiping a surface, whereas standoff detection must often make use of explosive vapours. However, the equipment for standoff detection must often still be within one metre from the item or area that is screened for explosives[20].

Apart from simply being able to detect explosive materials, there are other things that should be taken into account when developing an explosives detection system. Some of these additional requirements are determined by the situation in which the device will be implemented. A device that is used as a safety measure at airports will have other requirements than one that will be used in the field during military missions. There are different requirements to the throughput and, because of elevated background levels in military environments, the dynamic range. Furthermore, during military missions portable devices are often required instead of fixed devices. Another consideration is the difference between detection and identification. In some instances a device will be used to sense

whether an explosive is present, whereas in others it is also necessary to determine which explosive compound it is. Furthermore, it can be important to consider how many different compounds, or groups of compounds, one device must be able to detect or identify.

It is furthermore possible to distinguish between methods that allow for continuous sensing and methods that allow for the analysis of individual samples. It depends on the application which of these methods is preferred. Other considerations include the detection time, the size and weight of the device, the reset time needed before a next measurement can be conducted, and the power source, and its lifetime, needed for the explosives detection device. Furthermore, it is important that an explosives detection device is user friendly and does not require much user training.

There are several challenges to the detection of explosives vapours emitted by bulk explosives. One of the main challenges is that most explosive materials have very low vapour pressures. The equilibrium vapour pressure at 300K of for example TNT is 13 ppb, that of pentaerythritol tetranitrate (PETN) is 0.026 ppb, and that of RDX 0.0084 ppb[1]. Other challenges in explosives vapour detection include the relatively small sample sizes, the variety of explosive compounds available, deliberate concealment of the explosives, and interference from other compounds that are present, including the influence of humidity and dust on the detection of explosives[1].

Since the vapour pressures of explosive materials under ambient conditions are very low, sample preparation must be done in such a way that the analyte becomes detectable. This often requires pre-concentration of the sample, for example by using a material that adsorbs explosive molecules. An example of such a pre-concentration system, incorporated in explosives detection, is single sided membrane introduction mass spectroscopy (MIMS). In this method one side of an absorbant membrane is first exposed to the air and then to the

mass spectrometer, which reduces the analyte losses compared to for example two sided MIMS[17].

Instead of detecting the explosive compounds themselves, one could also aim to detect other materials that could indicate the presence of an explosive material. One could detect associated compounds, compounds that tend to be present when explosives are present, or even taggants, materials that have been added during the production of the explosive to facilitate detection. An advantage of this approach is that taggants and some associated compounds have a higher vapour pressure than the explosive compound itself, and are thus easier to detect. However, associated chemicals are also likely to be more prevalent in the environment than explosives themselves, and thus potentially cause higher false alarm rates.

In addition to the sensitivity, the selectivity of the detection system should also be considered. The selectivity of vapour sensing detectors may be increased by using them in an array. By using them in an array it is possible to obtain a signal similar to an artificial olfactory system. The responses of a number of sensors are combined to give a fingerprint-like signal. Pattern recognition methods can be used to analyse the signal, match it to known responses from a database, and thus identify the analyte[21]. This approach will be discussed in more detail in section 7 of this chapter.

3.2 Animal olfaction

One of the most effective methods for explosives vapour sensing is to use trained animals. Trained sniffer dogs are frequently used in the detection of explosives because of their high odour sensitivity. Detection limits as low as 1.14 ppt have been reported for canine olfaction[22], and for this reason the performance of other methods is often judged in comparison with dogs[17]. The vapour enters the canine olfactory system through the nose,

where the vapour is dissolved in the mucus in the nasal cavity and interacts with receptors. This interaction causes a signal to travel through the olfactory nerve to the brain, where the signal is interpreted, leading to perception by the animal. Purging of the system must then take place to ensure that the system is reset and can be stimulated again[23]. Canine olfaction is a complicated system in which many different organs are involved. This includes the main olfactory system, where olfactory receptors, a type of G-protein-coupled receptors (GPCRs), are expressed. Olfactory receptors can be distinguished from other GPCRs by their specific amino acid patterns[24]. In addition to the main olfactory systems canine olfaction has an accessory olfaction system, consisting of the accessory olfactory bulb and the vomeronasal organ. The vomeronasal organ expresses vomeronasal receptors, binding pheromones, and formyl peptide receptors[24]. Other organs that play a role in expressing chemical receptors and may be involved in canine olfaction are Masera's organ, which expresses some olfactory receptors, and the Grueneberg ganglion, which has been shown to play a role in the expression of some vomeronasal receptors as well as the expression of trace amine-associated receptors[23-24].

Apart from simply having a sensitive olfactory system animals have to be trained to react to certain smells to alert their handler to the presence of a vapour, for example by freezing or sitting or through another behavioural response. They have to be trained to recognise that specific smells are of interest to their handler. Dogs are trained by exposing them to samples with known compounds, often at known concentrations or vapour pressures, and rewarding specific behaviour by the dog upon smelling the compound. As well as a sample of analyte material, interferents or samples of other materials and background signals can be used to make detection more difficult. These situations might be more similar to real situations where interference from materials in the environment might also play a role. It is furthermore important to eliminate unintentional cuing of canine detection behaviour by

ensuring tests are double blind where possible, i.e. the handler and any test monitors present are unaware of the presence or position of targets or interferents. The animals can be trained to react to a whole range of explosive materials, including traditional and improvised explosive materials, as well as associated chemicals such as taggants[22]. It has for example been shown in the case of sniffer dogs working in narcotics detection that they often use the smell of associated compounds to detect the analyte materials, rather than the smell of the analyte material itself[23].

In an attempt to determine the limit of vapour sensing by dogs, dogs were first trained to indicate which of five locations contained a target odorant with a behavioural response. The concentration of the odorant was then systematically lowered until the response of the dogs became dependent on chance. It has been observed that dogs can reliably find the target odorant down to concentrations of 1-2 ppt[22].

Apart from a high sensitivity, canine olfaction has several other advantages compared to instruments for vapour sensing of explosives. These advantages include good selectivity, often resulting in a smaller number of false positives, a generally faster detection rate, a high mobility, very efficient sampling, and ease in identification of the source of the vapour. A disadvantage of using dogs for explosives detection is the amount of training needed for the dog and the handler, and the fact that dogs can get tired or bored, and need care. Therefore, possibilities of using other animals, that are more cost efficient, have been investigated. This includes rats, which also have a sensitive olfactory system. Advantages of using rats for explosives detection include their small size, reduced cost of raising, training and care relative to dogs, and their relatively weak attachment to humans or specific handlers[25].

More recently the use of honey bees for explosives sensing has also been researched. Bees can be used over relatively long distances, up to 100s of metres, while the handlers are able to stay at a safe distance from the explosives. Furthermore, there is no risk of the bees setting off a mine[26]. As part of their training the bees' food is injected with a small amount of the target material, which will encourage the bees to search for 'food' with the same smell. It has been observed that bees that have been trained in this way, tend to fly along the vapour plumes towards the source of the analyte material. They then pause above the source of the vapour before they continue their flight. For bees, vapour detection has been observed at a similar sensitivity to that of dogs, in the ppt range[26]. However, the use of free flying bees has significant challenges, such as the presence of other food sources and variations in climate. The response of trained moths to explosives vapour has also been investigated[27]. Like bees, moths are relatively easy to train, inexpensive to take care of, and cannot set off an explosive. Like dogs and rats, a behavioural response to specific vapours can be harnessed in moths.

Although there are several possible ways in which animal olfaction can be used for vapour sensing of explosive materials, and animal olfaction is very sensitive, it is not always the best option. In many cases it would be better if a sensitive and selective, equivalent technological solution could be used. Instruments have many advantages over animals, for example a theoretical 24 hour 'duty cycle', the possibility to not only detect but also identify different analyte materials, the small influence of the handler, and generally long life time of the instrument[23].

3.3 Separation and ion detection techniques

A number of techniques used for detection of explosives rely on molecular separation processes, which involve separating different types of molecules in the vapour into their

fractions. For some methods the molecules themselves are broken up into fragments or their constituent elements. The most popular techniques are gas chromatography, mass spectroscopy, and ion mobility spectrometry, as discussed individually in the following sections. These techniques can be used individually, however for greater efficacy they are often used in combination with each other.

3.3.1 Gas chromatography

Gas chromatography is used to separate and analyse a variety of compounds including explosives. The compounds are vaporised without decomposing them. A carrier gas carries the vapour through a column that is coated with a liquid or polymer, called the stationary phase. Due to different interactions with the stationary phase, different constituents of the vapour have different retention times in the column, which allows for the separation of the materials present in the sample. There is a large range of detectors that can be used to detect the materials exiting the column, including electron capture detectors, thermal conductivity detectors and nitrogen-phosphorus detectors. It has, for example, been shown that gas chromatography with an electron capture detector can be used to analyse a mixture of nine explosive compounds in less than 140 seconds *(Figure 3.2*)[28]. Furthermore, gas chromatography is often combined with other detection methods, such as mass spectrometry. Explosives detection systems that combine gas chromatography and mass spectrometry are commercially available. For example, it has been shown that gas chromatography in combination with tandem mass spectrometry can be used to detect various explosives within a few minutes[29]. It is also possible to use a combination of gas chromatography columns with different separation conditions, allowing for the separation of materials that were not separated by the first column. Techniques in which two or more separation steps are used are called multidimensional separation techniques. In two-dimensional gas chromatography the sample is passed through two columns that use

different separation conditions (*Figure 3.3*)[30]. It has, for example, been shown that fast two-dimensional gas chromatography can be used for the detection of RDX, PETN and TNT[31]. Gas chromatography can be a relatively fast detection method. When short columns are used in a highly efficient setup for gas chromatography detection takes only a few seconds[17].

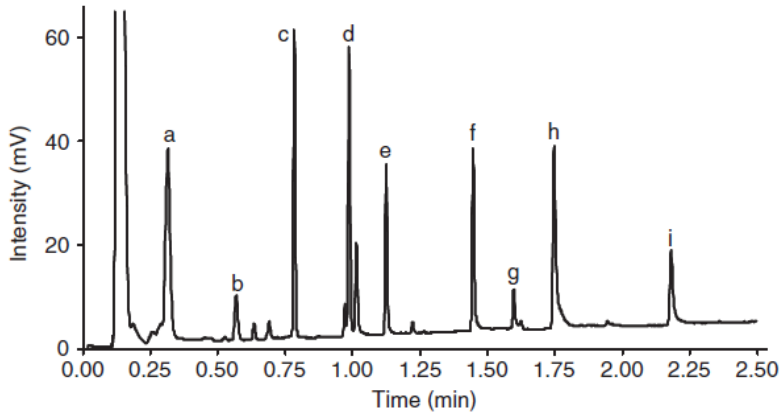


Figure 3.2: *An example of a gas chromatogram, where the peaks correspond to a) ethylene glycol dinitrate, b) 4-nitrotoluene, c) nitroglycerine, d) 2,6-dinitrotoluene, e) 2,4-dinitrotoluene, f) trinitrotoluene, g) pentaerythritol tetranitrate, h) cyclotrimethylenetrinitramine, and i) 2,4,6-trinitrophenylmethylnitramine (taken from Ref. [28]).*

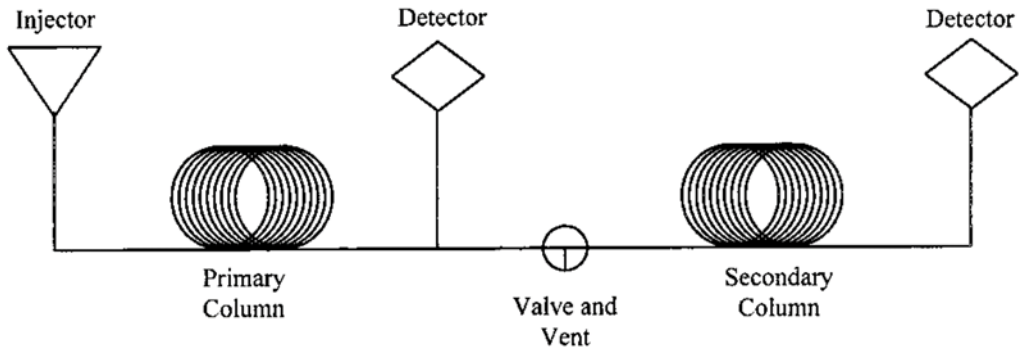


Figure 3.3: Schematic representation of a two-dimensional gas chromatography system, where the vapour is passed through two columns with different separation conditions, such as the temperature or the coating of the columns (taken from Ref. [30]).

3.3.2 Mass spectrometry

There are several spectrometry methods, including mass spectrometry that can be used for explosives detection, and have been successfully implemented in commercially available devices. In mass spectrometry the analyte is split into charged fragments, that are then separated based on their mass-to-charge ratios using a magnetic and/or electric field. The sample is introduced into a sample chamber, either at atmospheric pressure or in vacuum. It is then ionised, for example using ion impact, electron impact, vacuum ultraviolet (VUV), or resonance enhanced multiphoton ionization. The ions are then accelerated into the tube where they are separated (*Figure 3.4* and *Figure 3.5*)[32-33]. The presence and relative abundance of the different molecular fragments can be used to analyse the analyte material. An advantage of this method is the relatively short analysis time of approximately 5 seconds. One impressive example is the sub-ppt detection of RDX, within 1 to 2 seconds, without sample pre-concentration, using selective atmospheric pressure ionisation using nitrate reactant ions[34]. Work on further improvement of mass spectrometry for explosives detection is aimed at reducing cost and size, and further improvement of the portability of the equipment[17].

Apart from standard mass spectrometers used for explosives detection, such as an atmospheric pressure ionization tandem mass spectrometer, an atmospheric sampling glow discharge ion trap mass spectrometer and an atmospheric pressure ionisation time of flight mass spectrometer, systems have been developed that make use of some of the specific properties of many explosive materials. For example, many explosives have a large electron affinity. Detection systems that make use of this property include a reversal electron attachment mass spectrometer and an electron capture negative ion mass

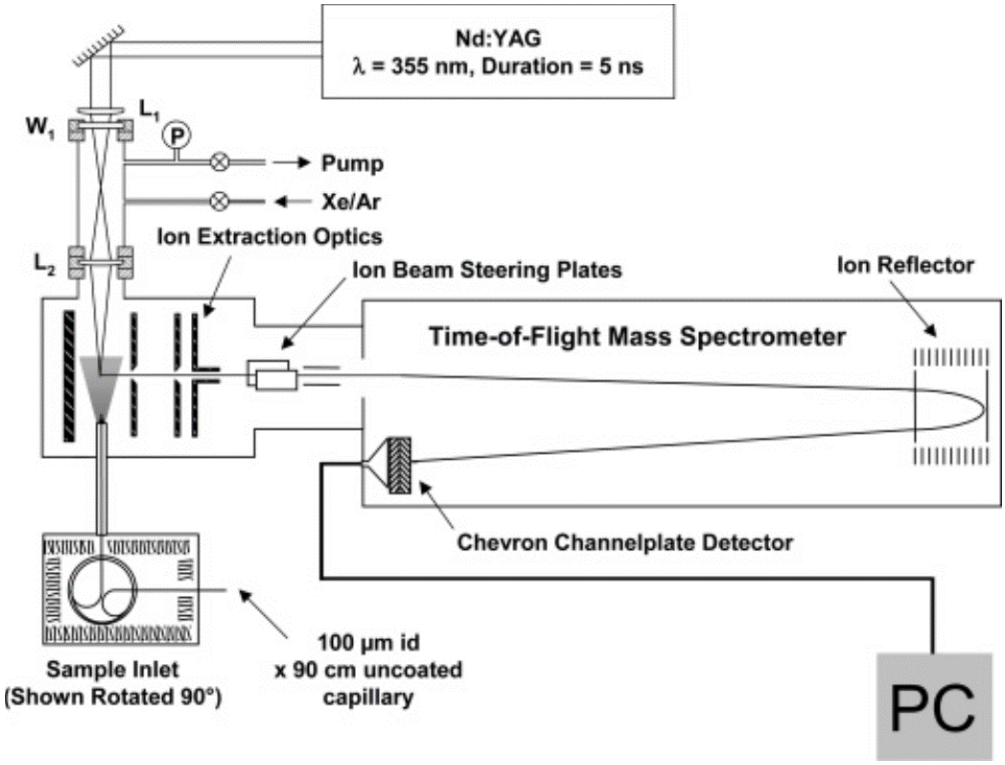


Figure 3.4: Schematic representation of a single photon laser ionisation time-of-flight mass spectrometer (taken from Ref. [33]).

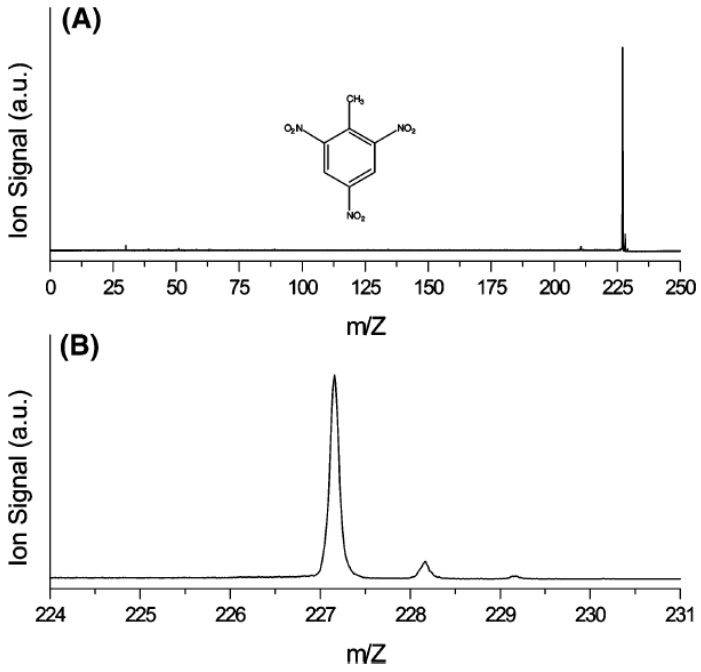


Figure 3.5: An example of a single photon ionisation mass spectrum of 2,4,6-trinitrotoluene (A) and an expanded view of the molecular ion region (B) (taken from Ref. [33]).

spectrometer. This last system makes it possible to distinguish between various explosives containing NO_2 by measuring the energy at which the NO_2 ion is formed[32].

3.3.3 Ion mobility spectrometry

Ion mobility spectrometry is used to separate ionised molecules based on their mobility in a drift gas. The flow time of the ions through an ion mobility spectrometry tube, with a gas flow and an electric field, depends on the mass, charge and dimensions of the ion, and thus allows for separation and identification of the ions. The ionisation takes place at atmospheric pressure. Usually the relative abundance of the ions is used for identification of the compound instead of absolute quantities because the ratios are less dependent on the conditions[32]. Ion mobility spectrometry is particularly suited to explosives detection because the ionisation step itself is highly selective for most explosives. Their high electron affinity causes them to be ionised when species with lower electron affinities are not ionised. Ion mobility spectrometry is currently implemented in many commercial explosives detection systems. Much work has been done to improve the sensitivity and detection speed of such systems. This can be realised by improving several individual parts of the system. It is for example possible to change the sample collection method. Ion trap mobility spectrometry is a technique that allows for higher sensitivity, by eliminating losses that occur at the shutter in conventional ion mobility spectrometry, and is thus able to detect lower concentrations[35]. It is also possible to change the ionisation technique that is used. Radioactive materials such as ^{63}Ni can be used to ionise the sample. However nonradioactive ionisation sources such as secondary electrospray ionisation (*Figure 3.6* and *Figure 3.7*) and corona discharge can also be used for the detection of explosives using ion mobility spectrometry[36]. An additional advantage of positive corona discharge ion mobility spectroscopy is that it allows for high sensitivities because a positive corona discharge results in a greater total ion current[37].

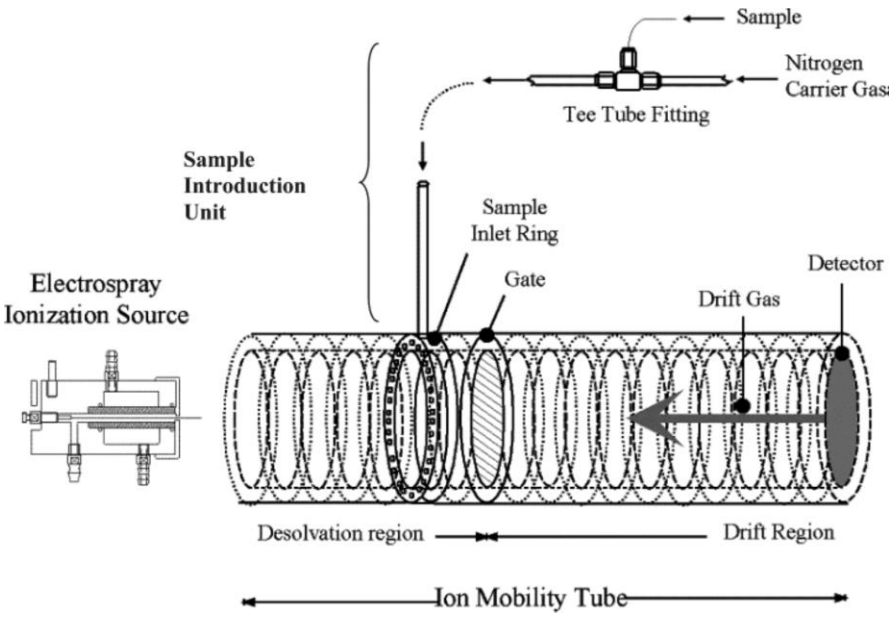


Figure 3.6: Schematic representation of a secondary electrospray ionisation ion mobility spectrometer (taken from Ref. [36]).

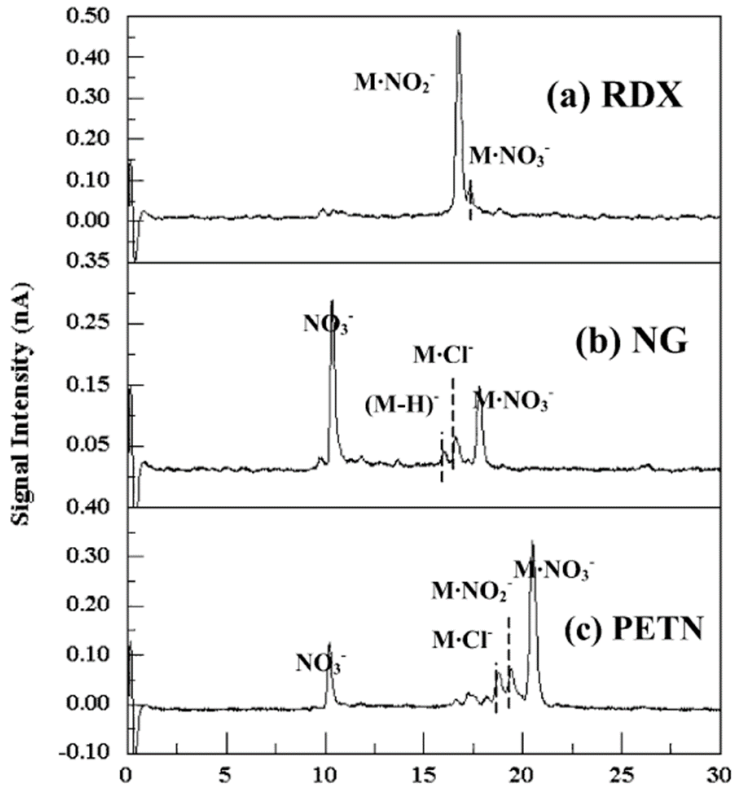


Figure 3.7: Secondary electronspray ionisation ion mobility spectra of RDX, NG, and PETN (taken from Ref. [36]).

3.4 Polymers

3.4.1 Conductive polymers

Polymers are a very versatile class of materials and can be used in a large range of applications. Initially polymers were mainly thought to be electrically insulating, however, research leading to the 2000 Nobel Prize in chemistry demonstrated the existence and versatility of conductive polymers. Due to the combination of conductivity with other properties of polymers, such as ease of processing and functionalization, conductive polymers are of interest for a large range of applications. This includes electrochemical gas sensors and other electronic devices. Conductive polymers can be used to form transparent conductors, and semiconductors in which the Fermi level can be shifted and controlled over a relatively large range[38]. For conducting polymer-based sensors it has also been shown that the responses to the analyte materials tend to be reversible[39]. Examples of conducting polymers include polyacetylene, polythiophene, polypyrrole, and polyaniline[38, 40] (*Figure 3.8*).

The intrinsic conductivity of conjugated polymers is relatively low. However, the conductivity can be increased by doping, or introducing charge carriers into the system[41]. It has for example been shown that the conductivity of polyacetylene can be increased by a factor of 10^7 through doping[38]. Although doping the polymers allows for a higher conductivity, intrinsically conductive polymers are also used for various applications. Some polymers, such as polyaniline and polypyrrole, are unstable in their undoped state, others, such as polythiophene, are stable in the intrinsic or very lightly doped state[42].

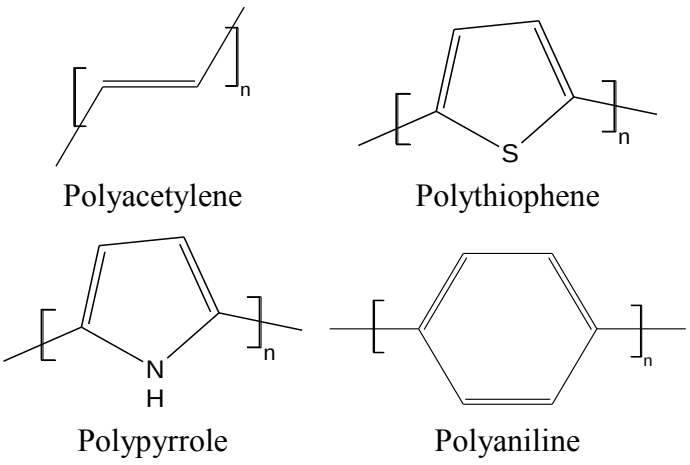
Two ways in which analyte gases can interact with conducting polymers can be distinguished. Gases can interact with a conductive polymer through a chemical reaction or by physically adsorbing onto the polymer, causing a change in the doping level or depletion

region respectively[40, 43]. In both cases a change in the electrical properties of the polymers can be measured.

There are several ways in which the polymers can be made sensitive to specific materials, or groups of materials. If the overall chemical or electrostatic properties of the conductive polymer do not allow for sensitivity to the analyte materials, this can be obtained by covalent or physical integration of synthetic or natural receptors or by imprinting[44].

Conductive polymers can be incorporated into different device configurations such as chemiresistors, chemically sensitive field-effect transistors, diodes or capacitors. A further advantage is that due to the versatility with which they can be processed they can be incorporated into the sensors in various forms[41-42]. It is possible to use polymer thin films, but also polymer based nanomaterials, which are interesting for sensing applications because they have a relatively large exposed surface area[45].

There are several properties of conductive polymers that can be used for sensing, which means that several different detection methods can be used. These methods include for example optical methods and methods based on changes in the electrical properties of



Polyacetylene Polythiophene

Polypyrrole Polyaniline

Figure 3.8: Examples of conductive polymers and their structural formulas.

the polymer[39]. Examples of polymers used for sensing applications include phospholipids for the detection of volatile anaesthetics[46], polypyrrole[47] and polyaniline[48] for the detection of ammonia, and polymer nanojuctions for the detection of TNT[49].

3.4.2 Fluorescent polymers

Fluorescent polymers can be used for explosives vapour sensing (*Figure 3.9*)[50] through a mechanism whereby the fluorescence of the polymer is switched on or off upon interaction with the analyte. In the case of a switch-off system quenching of the fluorescence is observed upon interaction, whereas in the case of a switch-on system an increase in fluorescence is observed. In most cases an on-switch system does not have an advantage with respect to an off-switch system, because both systems will suffer from background fluorescence. However the turn-on system does have a slight advantage in environments where there are many background vapours, as the turn-off, or quenching, system suffers from more false-positives due to interference from the environment[51].

The term amplifying fluorescent polymers (AFPs) is often used because there can be a gain in signal when the polymer interacts with the analyte material[51]. Amplification occurs because fluorescent polymers are an efficient electrical transport medium, allowing a delocalised exciton to sample many binding sites along the polymer chain in the life-time of one exciton. Increasing the number of pathways available for diffusion of the exciton through the polymer strongly increases the amount of amplification of the signal[51].

The use of fluorescent polymers for vapour sensing has the usual polymer advantages. Like other polymers, fluorescent polymers allow for relatively easy processing and the tailoring of the polymer to meet the requirements of a specific application. Additionally it is relatively easy to observe changes in fluorescence, either by visual inspection or through spectrometric methods.

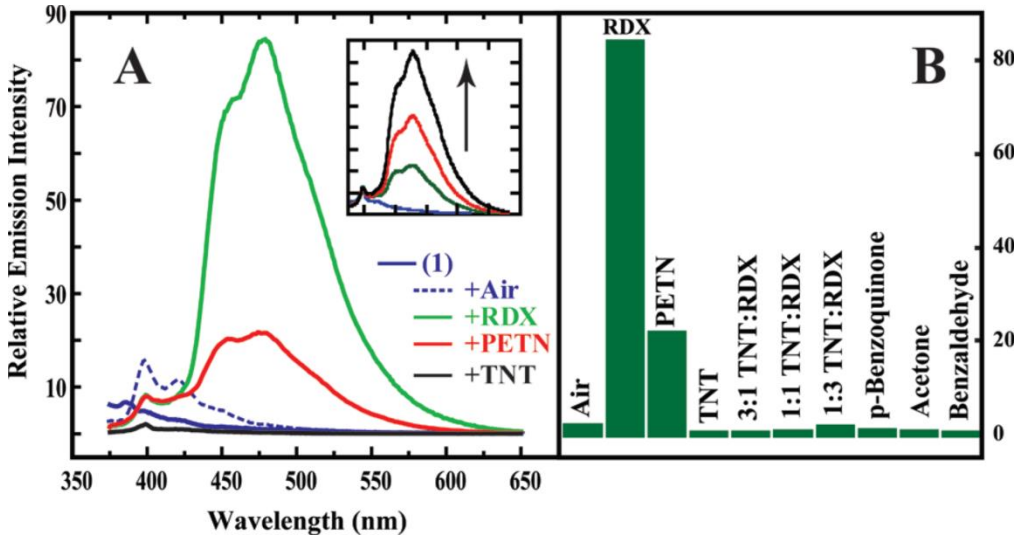


Figure 3.9: (A) Emissions profiles of a chemical sensor in acetonitrile (1), in acetonitrile after 120 s irradiation at 313 nm (air), and with RDX, PETN, and TNT in acetonitrile after 30 s irradiation. The inset shows the peak at 480 nm with increasing irradiation times (10 s intervals). (B) Emission intensity at 480 nm for various analyte materials after irradiation for 30s (taken from Ref. [50]).

An example of the application of fluorescent polymers for the vapour detection of explosive materials is the commercially available Fido device. In this system the real-time monitoring of the fluorescence of a conductive polymer thin film takes place while the system is exposed to analyte vapours. The sensitivity of this system to TNT and DNT vapours has been demonstrated to be comparable to that of sniffer dogs[51].

3.4.3 Other

Other uses of polymers in vapour sensing have been demonstrated. For example using the swelling of nonconductive polymers as it absorbs an analyte vapour[18]. A change in colour of polymers upon interaction can also be used for vapour sensing, which has not only been done with polymers but also with other chemically reactive materials[18, 52]. Furthermore, polymers can be used in combination with other techniques, some of which

will be discussed in the next sections of this chapter, to make the systems used in those techniques more sensitive to specific analyte materials. Examples of polymers used in combination with another system include surface acoustic wave (SAW) devices, where polymers are added to cause interactions with specific molecules. In the case of a SAW device a sound wave is guided across a small quartz crystal. If molecules from a vapour have adsorbed onto the crystal this will change the propagation of the sound wave. The way in which the acoustic wave is affected provides information about the properties of the vapour molecules with which it has interacted[16]. Polymer coatings are used on the sensor surface to bind specific materials to the sensor surface. It has been shown that carbowax, or polyethylene glycol, can be used to coat SAW devices for DNT detection (*Figure 3.10*)[53]. Similar to polymers, the specific interactions of biomaterials can also be used to sensitise SAW sensor surfaces[54].

3.5 Nanomaterials

There are many different types of nanomaterials, for example nanoparticles, nanowires, nanotubes, and composite materials. Many nanomaterials have properties that are changed by the adsorption of an analyte, making them suitable for sensing applications. Functionalization of the nanomaterials can also be used to allow tailoring for specific

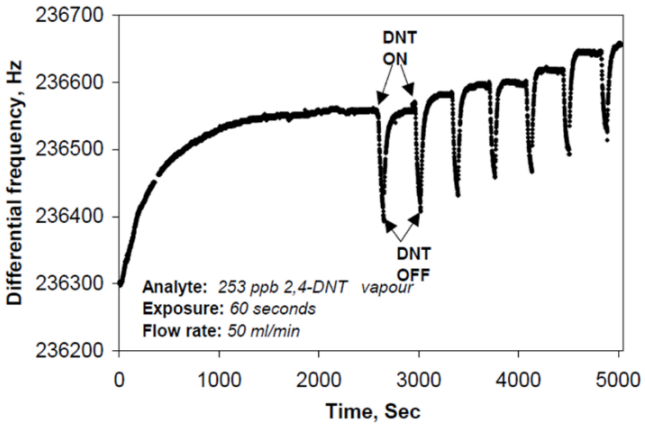


Figure 3.10: Response of a carbowax coated SAW sensor to DNT (taken from Ref. [53]).

requirements, including explosives vapour sensing[55]. Successful explosives vapour sensing has been demonstrated in a laboratory environment for systems based on various types of nanomaterials. A particularly versatile nanomaterial used in sensing are carbon nanotubes (CNTs). The electrical properties of CNTs are especially sensitive to interactions with other molecules via chemical doping and charge transfer. CNTs are well-suited for sensing applications because of their large surface to volume ratio, the possibility to tailor the electrical properties by changing the size or composition, and because it is relatively easy to incorporate CNTs into small electronic devices[56]. It has been shown that single walled CNTs have different sensitivities to the adsorption of different classes of molecules. Furthermore, their selectivity can be increased by coating the nanotubes with chemically selective layers[21].

Chemically modified silicon nanowire arrays can be used for vapour sensing of explosives, without the need for pre-concentration. When the wires are functionalised with 3-aminopropyltriethoxy silane (APTES), the amine groups can interact with the aromatic ring of TNT, which leads to changes in the conductance of the sensor. It has been shown that such as device can reliably detect TNT concentrations between ppb and ppt, and that the system can be reset by washing the surface of the sensor with a water/DMSO solution (*Figure 3.11*)[55].

Nanoparticles coated with an organic layer, forming a metal-insulator-metal system, have been used for vapour sensing. Because it is possible to tune the size, inter-particle distance, composition and functional groups of such systems, it is possible to use those properties to enhance the sensitivity, selectivity, and response time of systems in which they are used[57].

It is also possible to make vapour sensors based on localised surface plasmon resonances (LSPR) of metal nanoparticles. Changes in the LSPR spectrum of silver particles

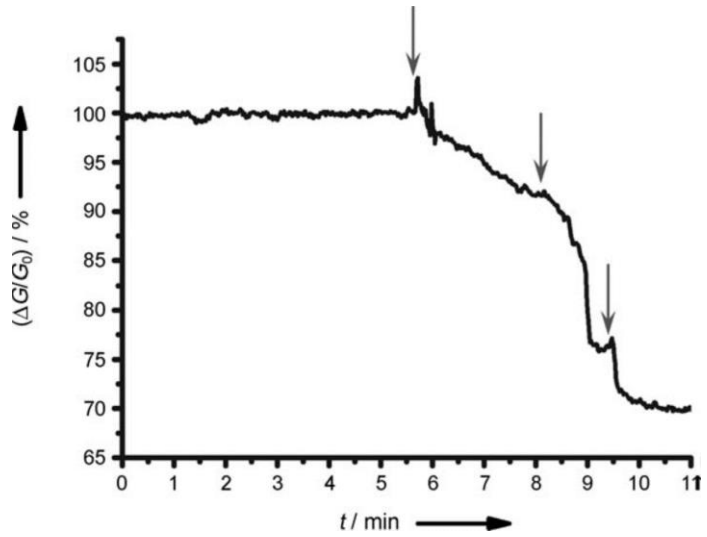


Figure 3.11: Relative conductance of a silicon nanowire based FET sensor after TNT was introduced at approximately 1 ppt in a carrier gas. The pulses (indicated by arrows) were 5 s in duration. A decrease in conductivity after each pulse is measured (taken from Ref. [55]).

were observed upon interaction with an analyte material. In this case the surface can also be modified to enhance the vapour selectivity. Detection limits in the 18-30 ppm range have been observed for this device, depending on the functionalization of the silver nanoparticles. Furthermore, it has been shown that the interaction between the sensor and the analyte molecules is reversible and the sensor reusable[58].

3.6 Microcantilevers

Nanomechanical effects caused by molecular adsorption can also be used for explosives detection. Vapour sensing of explosives using microcantilevers has been demonstrated in laboratory settings. Microcantilevers used for sensing are usually based on those used in atomic force microscopy (AFM), and are typically 100 µm long, 50 µm wide and 0.5 µm thick.

Several different sensing principles can be used (*Figure 3.12*). First of all it is possible to use the change in mass due to the adsorption of analyte molecules on the cantilever. Since cantilevers with high resonance frequencies have a high sensitivity to mass

absorption, the increase in mass changes the resonance frequency of the cantilever, which can be detected[59]. The second sensing principle makes use of changes in the surface stress. In this case one side of the cantilever is sensitised whereas the other side is passivated. When the adsorption is restricted to one side of the cantilever the cantilever undergoes bending. The bending does not depend on the mass of the adsorbed molecule but on its binding energy[21]. The change in surface stress that occurs between the sensitised and passivated sides of the cantilever upon interaction is measured[60]. In the third sensing principle changes in the bulk stress of the cantilever material are used, using cantilevers consisting of two different materials[59].

There are several ways in which the changes in bending or resonance frequency of the cantilever can be measured. Because very small deflections have to be measured the system has to be very sensitive. One of the simplest and most well-known read-out methods is optical leverage, known from AFM, where a laser is focussed on the back of the cantilever and the reflected laser light is detected by a position sensitive photodetector. However, this method is more difficult to apply to arrays of cantilevers, is not suitable for very small, for example nanometre sized, cantilevers, and can suffer from optical artefacts such as in the case of changes in refractive index[59]. There are many other read-out methods, for example

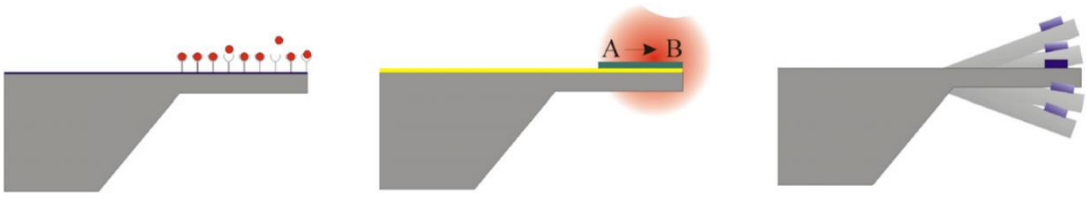


Figure 3.12: Schematic representations of the operation modes of microcantilever based sensors: surface stress changes (left), bulk stress changes (centre), and mass changes (right) (taken from Ref. [59]).

capacitive methods which can be used for nanometre sized cantilevers, piezoelectric methods which can be used for both read-out and actuation, piezoresistive and integrated optical methods, such as wave guides, which can be used for large arrays[59].

When cantilevers are used for explosives vapour sensing, the sensing relies on either the surface of the cantilever being sensitised for specific interaction with analyte molecules, or properties of the explosive materials such as phase transitions. Sensitivities to PETN and RDX in the 10-30 ppt range have been reported for functionalised cantilevers[61]. The selectivity of such systems has been shown to be dependent on the coating used to functionalise the cantilever (*Figure 3.13*)[62]. Local differential thermal analysis can also be used to obtain thermal fingerprints of the analyte material. Cantilevers are ideal substrates for this because of their low thermal mass, allowing for fast response times. Finally, the cantilevers can be used for photothermal deflection spectroscopy because the cantilevers are very sensitive to changes in temperature. In this method information about the absorption spectrum of a material can be obtained by measuring the heat produced upon absorption of light of specific wavelengths[59].

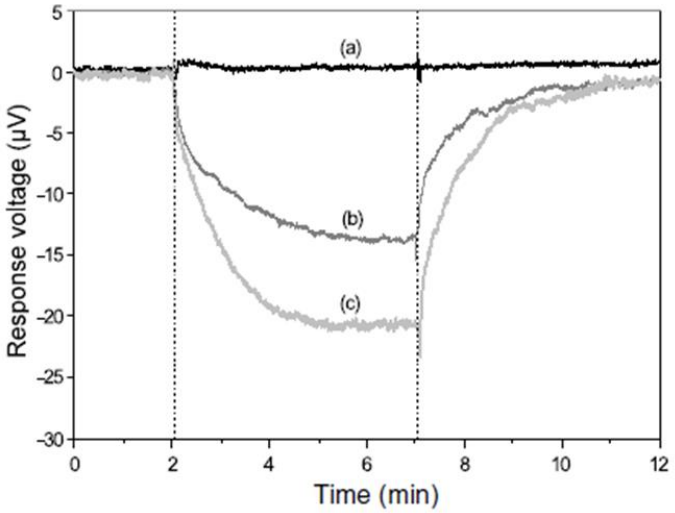


Figure 3.13: Response of a cantilever to TNT at about 7.6 ppb without self-assembled monolayer (SAM) (a), modified with a 4-mercaptobenzoic acid SAM (b), and modified with a 6-mercaptonicotinic acid SAM (c) (taken from Ref. [62]).

3.7 Electronic nose approach

Adding functionalised groups to polymers used in polymer based sensing, or coating nanomaterials or cantilevers used for sensing allows for selectivity, to one compound, or more likely to one group of materials that all have similar properties or a similar chemical group. However, this is often not sufficient to be able to distinguish between similar compounds, and to be able to detect different types of analyte materials with one sensor. Furthermore, it is important to be able to distinguish not only between different analyte materials, but also between analyte materials and harmless background signals, such as variations in humidity, air pressure, and temperature.

To allow for the required selectivity an array of sensors with different functionalization, and thus different responses to different materials, can be used. An array of sensors is able to detect different materials using a fingerprinting or electronic nose method. This is an approach similar to the olfactory system of mammals, where a number of receptors is used, that on their own are not highly selective, but the pattern of all the responses of the separate receptors combined is interpreted by the brain as a specific odour[63-64].

The sensors used in an array for an electronic nose approach can be based on many different types of sensing methods. These sensors can for example be based on polymers or nanomaterials. The detection can take place through changes in the electronic or optical properties of the materials, which means that this is a method that can be used in combination with many of the recently developed techniques. This approach is especially interesting in combination with small scale sensors.

Detection of and discrimination between various explosives vapours has been demonstrated in a laboratory environment. It has for example been shown that an array of

nanowire based field-effect transistors can be used to detect and discriminate between different explosive materials. In this case surface modification was used to create eight chemically different regions on a chip (*Figure 3.14*)[63].

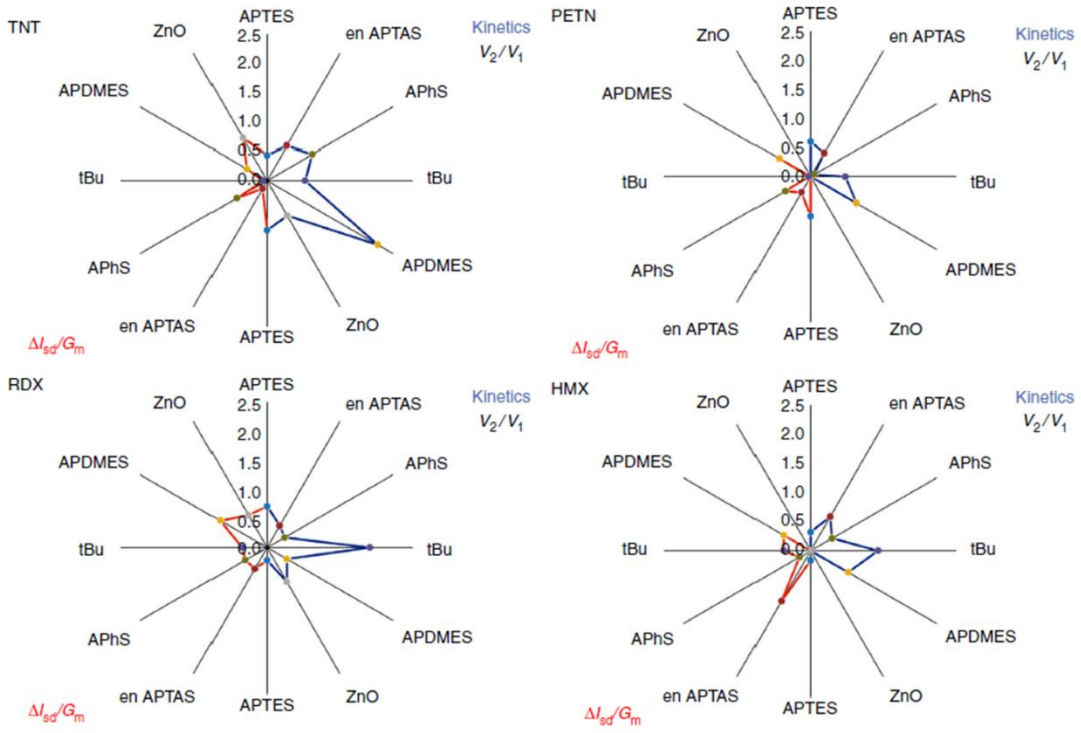


Figure 3.14: Fingerprinting results derived from a combination of thermodynamic (red) and kinetic (blue) responses of a silicon nanowire based electronic nose type sensor upon exposure to TNT, RDX, PETN and HMX (taken from Ref. [63]).

3.8 Summary

Explosives detection has many applications in both military and civilian situations. One of the main challenges are the low vapour pressures of many explosive materials, but there are many methods, both established and more recently developed, that can be used for explosives vapour detection.

Established methods play an important role in explosives vapour sensing. Animal olfaction, for example, is important because of the very high sensitivity, where dogs, as well as other animals such as rats and bees, can be used. However, the use of live animals is not always practical and many other techniques have been developed. Other traditional methods include separation methods that identify molecules or ions, such as gas chromatography, ion mobility spectrometry, and mass spectrometry.

Newer methods often use materials that allow for the creation of small electrochemical devices. Polymers, for example, are an interesting group of materials because they are easy to process and can be tailored to meet specific requirements. In polymer-based sensors changes in, for example, fluorescence or conductivity can be used to indicate the presence of an analyte material. Furthermore, polymers can be used as a coating to sensitise other types of devices, such as those based on nanomaterials or microcantilevers. Nanomaterials themselves can also be used for explosives vapour sensing and are especially interesting because their properties can be tailored and because they have a large surface area. Mechanical properties of cantilevers are used for vapour sensing using various mechanisms. Selectivity to different types of explosive can be improved by using an electronic nose approach. By using an array of sensors with different functionalization, a fingerprint-like signal can be recorded and interpreted to identify the analyte vapour.

A large range of techniques has been researched, however only few of those have successfully transitioned to field use. Ion mobility spectrometry is still the most common detection technology. Mass spectrometry is only just transitioning effectively to fieldable systems for trace detection. In the broader chemical sensor category only fluorescent polymer systems, such as the FLIR Fido systems, are being successfully implemented in the field. Many other systems that perform well in laboratory environments have not been successfully developed into fieldable systems. This is possibly due to issues with for example the sensitivity, specificity, cost, or practicality of the system. Understanding why newer methods have not transitioned effectively to commercial systems will be key to ensuring that new techniques can be exploited effectively.

Most current and future work is focussed on either improving traditional sensing methods to increase sensitivity and decrease detection times, or on developing new methods. Small scale devices and materials that are easy to functionalise and process, in combination with an electronic nose approach are especially promising.

Chapter 4

Background B: Practical implementation

The aim of this project is to develop a small and very sensitive explosives vapour sensor. The sensor will be based on a percolation network of conductive polymers on a metal nanoparticle scaffold. In this chapter the background of various components of the sensor will be discussed. The chapter will start with a background on wetting and dewetting, which plays an important role in the formation of the metal nanoparticle scaffold. Next, conductive polymers are discussed, which are deposited on top of the metal nanoparticle scaffold and are the active component of the sensor, interacting directly with analyte molecules. Finally, percolation networks are discussed. If a sensor consisting of a network of conductive polymers is operated close to the percolation threshold, this could make the sensor very sensitive.

4.1 Wetting and dewetting

Wetting and dewetting are especially important in the formation of the metal nanoparticle scaffold on which a percolation network of conductive polymers is formed. Furthermore, wetting can play a role in the formation and stability of the thin layer of polymer that will form the percolation network.

4.1.1 Theory of wetting

Whether one material wets another materials depends on the relative surface energies of the materials. The relative surface energies within the system determine whether the lowest energy state is a wetted or dewetted state, and if dewetted to what extent. The energies that must be taken into account are the surface energies of the metal, the substrate and that of the interface between the metal and the substrate (*Figure 4.1*). The Young-Laplace equation, describing an island, or film, of isotropic surface area on a solid substrate is given by[65]:

$$\gamma_{solid} = \gamma_{interface} + \gamma_{fluid} \cos\theta$$

Where γ_{solid}, $\gamma_{interface}$, and γ_{fluid} are the surface energies per unit area and θ is the contact angle at equilibrium. The wetted film is stable if $\gamma_{solid} > \gamma_{interface} + \gamma_{fluid}$. In all other cases the system will dewet if enough energy is supplied[65]. The case of a solid particle on a substrate is slightly different because the surface tension of a solid particle is anisotropic[66]. However, because the balance of surface tensions has to be evaluated over the total surface of the particle, a generalised surface tension can be used. And again solutions can be found for the balance of surface tensions, describing the non-wetting, completely wetting, and partially wetting cases[66]. In most cases when a thin film is deposited on a substrate it is in a metastable state. When such a film is heated, it will either form a more consistent wetting

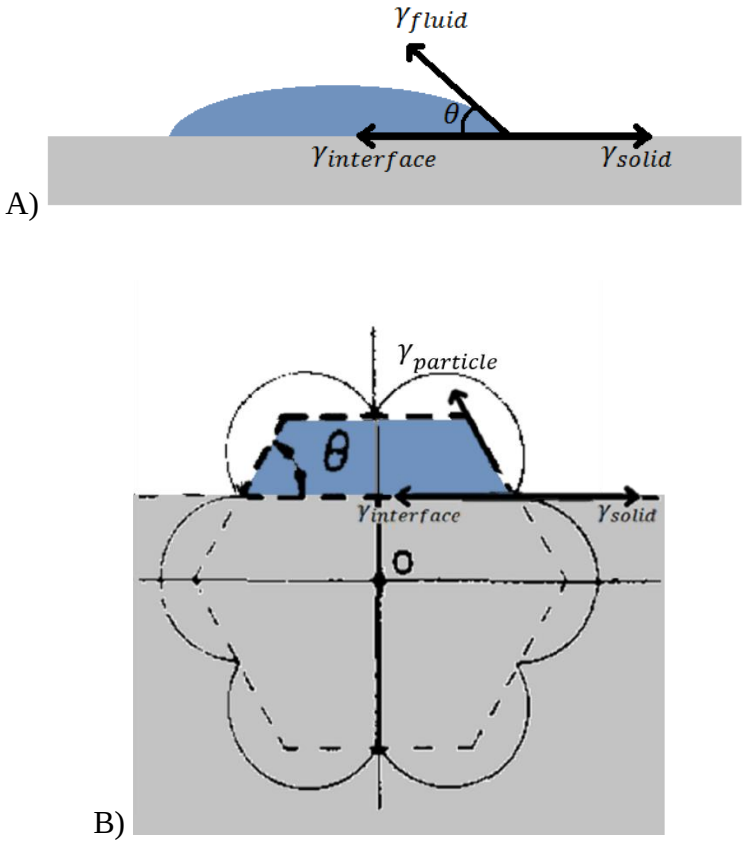


Figure 4.1: A) Schematic representation of a droplet on a solid surface. The wetting angle is given by θ, and the surface energies are given by γ_{solid}, $\gamma_{interface}$, and γ_{fluid}. B) Schematic representation of a partially wetting solid particle on a substrate for the case that $-\gamma_{particle} < (\gamma_{interface} - \gamma_{solid}) < 0$ (adapted from Ref. [66]).

layer or it will dewet and form islands. Dewetting can take place at temperatures well below the melting point of the metal[65]. Typical surface energies are 1.33 J/m^2 for gold[67], 1.2 J/m^2 for MgO[68], 78 mJ/m^2 for SiO_2[69], and 58.95 mJ/m^2 for glass[70].

4.1.2 Dewetting process

The dewetting process starts with the formation of holes in the thin film. The thin film is stable with respect to small perturbations. This means that the film remains stable, if a perturbation is smaller than the thickness of the film. If pre-existing holes are present,

dewetting can continue from those locations, and if not, holes must be formed before dewetting can start[65].

Grain structure plays an important role in the formation of holes. If the boundaries between grains are deep enough such that the groove meets the substrate this acts as a hole. Since the grooves at triple junctions tend to deepen the fastest[71], these tend to be the first places where dewetting takes place[65].

Once holes of a critical size are present in the film, hole growth can take place. Hole growth is governed by the edge retraction and the evolution of the shape of the edge of the holes. Material from the edges of the holes is transported to the flat area next to the edge. Sometimes this leads to the accumulation of material on the edge and a valley next to the edge (*Figure 4.2*). If the valley reaches all the way down to the substrate, the edge will be pinched-off from the rest of the island and forms a wire or strand. The remainder of the

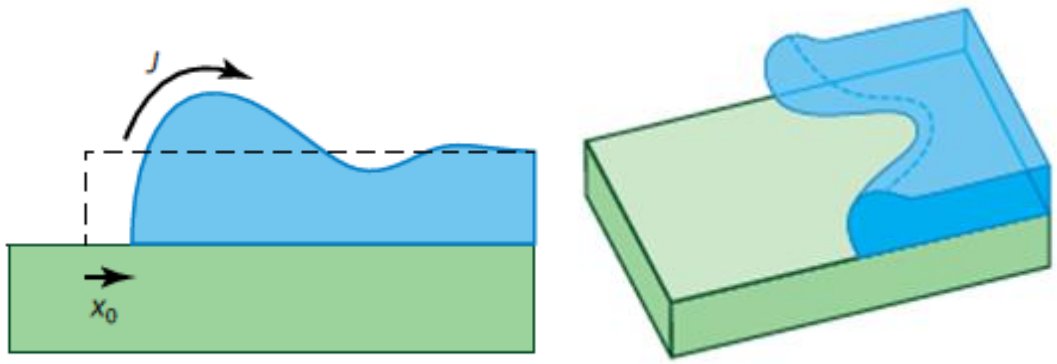


Figure 4.2: Left: Cross-section showing a schematic representation of a retracting edge. Retraction has taken place over a distance x_0, starting in a state with a flat film with a sharp corner, given by the dotted line. J is the flux of the self-diffusion taking material from the edge to the flat area behind the edge, causing mass accumulation at the edge and thus the formation of a rim. A valley is formed behind the rim, due to flux divergence behind the rim. Right: Schematic representation of a retracting edge of a film undergoing a fingering instability (taken from Ref. [65]).

island has a new edge at which transport of material continues. When there is a perturbation in the retracting edge, fingering instabilities can occur. In that case the edge is split into several fingers (*Figure 4.2*). The fingers can break up into smaller islands[65].

If dewetting only takes place at pre-existing holes, the rate of dewetting depends on the number of holes and the rate of hole growth. The rate at which an edge retracts has been found to be $t^{-1/2}$ for straight edges[72] and $t^{-3/5}$ for the edges of circular holes[73]. If holes need to be formed before hole growth can take place, the rate of dewetting depends on both the rate of hole growth and the rate of hole formation. It has been shown that in the case that the groove formation is driven by curvature-driven self-diffusion, the depth of the groove is proportional to $(tD_s)^{1/4}$, where t is the time and D_s is the surface self-diffusivity[65, 73].

Once a film has dewetted the individual particles can continue to change through Ostwald ripening. In Ostwald ripening larger particles continue to become larger and smaller particles become smaller or disappear. It is energetically more favourable to have one larger particle than it is to have many smaller particles because this causes a decrease in the total surface area of the nanoparticles[74].

4.1.3 Metal nanoparticle formation through thin film dewetting

To form supported metal nanoparticles through thin film dewetting, first a metal thin film is deposited. The metal thin film can be deposited using a thermal evaporation method, for example using an e-beam or K-cell. Next, energy is supplied to the system to encourage dewetting, for example using laser pulses[75], by heating the sample under argon flow in a quartz tube furnace[76-77], or through resistive heating in ultra-high vacuum[78].

Thin film dewetting is a convenient method for the formation of supported metal nanoparticles because it, by definition, results in a (sub-)monolayer of particles. Furthermore, this method allows for control over the size and spacing of the metal

nanoparticles, through the film thickness and annealing time and temperature. However, various other methods can also be used to create supported metal nanoparticles. These methods include sonochemistry, microwave irradiation, pulsed laser ablation, supercritical fluids[79], plasma methods, impregnation, co-precipitation, precipitation-deposition, microemulsions, photochemistry, chemical vapour deposition, electrochemical reduction, and sonoelectrochemical methods[80]. Furthermore, it is possible to use prefabricated particles and deposit them onto the substrate.

Since supported nanoparticles are of interest for several different applications, it is an advantage that the properties of nanoparticles created by dewetting a thin film can be tailored to a specific application. To create supported metal nanoparticles using this method, the materials must be chosen such that the dewetted state is energetically more favourable than the wetted state. It is also possible to tailor the surface energy of the substrate by treating the surface with a material that will change the surface such that the required properties are obtained. Furthermore, the film thickness plays a role in the formation of supported nanoparticles. It has been shown that for smaller film thicknesses the driving force for dewetting increases and the rate of dewetting is accelerated. This means that thinner films dewet at lower temperatures[65].

This method can be extended to allow for more control over the position and size of the nanoparticles. It is for example possible to use patterned substrates, instead of substrates with a flat surface. When a film dewets on a patterned substrate, islands will be formed in the positions dictated by the patterning on the substrate. The template could be made of another material, for example a polymer. Such a template could be removed after dewetting of the metal, for example by the dissolution or evaporation of the template[81].

Dewetting of thin films to create nanoparticles has been demonstrated for many different substrate-nanoparticle material combinations, resulting in nanoparticles of many different shapes and sizes[82-83]. Examples include gold and silver particles with various morphologies on MgO[84], and iron particles on $SrTiO_3$ substrates[78] (*Figure 4.3*).

4.2 Conductive polymers for sensing applications

To form an explosives vapour sensor based on a percolation network of conductive polymers, the supported metal nanoparticles are used as a scaffold on top of which the conductive polymers are deposited. In such a vapour sensor individual analyte vapour molecules interact with the polymer molecules that form the network. These interactions cause a change, for example in the resistance of the conductive polymers, which can be measured.

4.2.1 Conductive polymers

Conducting polymers are conductive because they consist of alternating single and double bonds. This means that the orbitals of the carbons atoms have a sp^2p_z configuration,

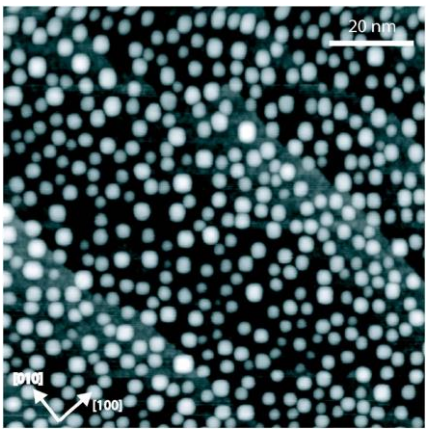


Figure 4.3: As demonstrated in this STM image by Silly et al., Fe nanoparticles can be formed when Fe is deposited on a $SrTiO_3$(001)-c(4x2) substrate and annealed at 360°C for 10 minutes (taken from Ref. [78]).

because the p_z orbitals of neighbouring carbon atoms overlap. Electron delocalisation takes place along the backbone of the polymer, making charge mobility along the polymer chain possible[38]. The π-electrons fill the π-band, while the π*-band remains empty. Therefore there are no partially filled bands, which means that conductive polymers are often semiconductors[38]. There are a number of factors that influence the conductivity of conjugated polymers. For optimal conductivity the overlap between the orbitals of adjacent carbon atoms must be optimised, as is the case for a flat molecule. If there is rotation in the molecule the overlap is reduced, which leads to a lower conductivity. Some molecules are more sensitive to this rotational effect than others, depending on the intramolecular interactions[85]. Another factor that limits the conductivity of a polymer is disorder. Improving the structural order of a polymer improves the mobility[38].

Conductive polymers are a very versatile group of materials because there are many different types of polymers, and polymers can be tailored to many different applications. Furthermore, because most polymers are soluble in common solvents, polymers can be processed relatively easily, allowing for them to be incorporated in various systems. Conductive polymer are an especially interesting group of materials because they combine these properties of polymers with electrical conductivity. Furthermore, conductive polymers can be used to form transparent conductors, and semiconductors in which the Fermi level can be shifted and controlled over a relatively large range[38]. Examples of conducting polymers include polyacetylene, polythiophene, polypyrrole, and polyaniline[38, 40].

4.2.2 Conductive polymers for sensing

Conductive polymers have various properties that allow them to be used for sensing. Therefore they can be used in systems based on various sensing mechanisms. Changes to the properties of the polymer, caused by an analyte molecule, could for example be detected

using optical methods, mass spectroscopy, and the detection of changes in resistance of the polymer[39]. An additional advantage of using polymers for sensing applications is that the responses to the analyte materials tend to be reversible[39]. Section 3.4 has already covered the use of conductive polymers for sensing applications and gives several examples of conductive polymer based sensors.

4.3 Percolation networks

Most traditional conductive polymer based sensors are based on polymer thin films. However, operating a vapour sensor based on a network of conductive polymers close to the percolation threshold could result in a higher sensitivity.

4.3.1 Percolation

Percolation was first discussed by Flory and Stockmayer, in the 1940's, as part of their discussion of polymerisation and gelation[86]. The first mathematical descriptions of percolation theory were formulated by Broadbent and Hammersley in 1957, as part of a discussion about random processes[87-88]. Since that time the mathematical description and modelling of percolation has evolved to be able describe and predict characteristics of numerous systems. Percolation can also be used for various applications, including sensing applications.

When Broadbent and Hammersley first gave a mathematical description of percolation, they set out to describe a system of flow through a porous medium with randomly blocked channels[87]. Another random process that at that time had been known for a long time and studied extensively is diffusion[89]. For that reason, they started by stressing the differences between percolation and diffusion. They described that in the random motion of a fluid through a medium the motion can be either limited by the properties of the fluid

or by the properties of the medium. In the first case they speak of a diffusion process, in the second case of a percolation process[90-91].

A percolation network can be described as a network of open and closed bonds or channels along which percolation can take place[86]. Possibly the most used example of a percolation network is that of a porous stone that is submerged in water. In this case one might wonder whether the water will reach the centre of the stone. The answer depends on the pores in the stone. If there are enough open pores, leading to the centre of the stone, the water will reach the centre. If there are not enough open pores the water cannot reach the centre of the stone. In the same way one could consider, for example, an orchard. If the trees are too far apart for an illness or fire to spread from one tree to another the bond between the two trees is considered to be closed, otherwise it is open and the illness or fire could spread to the next tree. If there are enough open bonds, in other words a large enough fraction of the trees are close enough to each other to allow spreading, percolation takes place and an illness or fire starting on end of a forest or orchard could spread and reach the other end[91].

A distinction is made between two types of percolation; bond percolation and site percolation. In the one case the bonds or channels can be either open or closed, this is called bond percolation. In the other case the sites, or atoms, can be either occupied or empty (*Figure 4.4*). Furthermore, every bond percolation system can be reformulated to give a site percolation system on a different lattice, but the inverse is not true[91].

The open bonds or available sites together form clusters, or connected areas. When there is a small number of connections or open bonds, small isolated clusters consisting of neighbouring sites that are connected, are present. When more connections are made these expand, until they finally merge. When the connections within the network are maximised, the entire network consists of one big cluster[88].

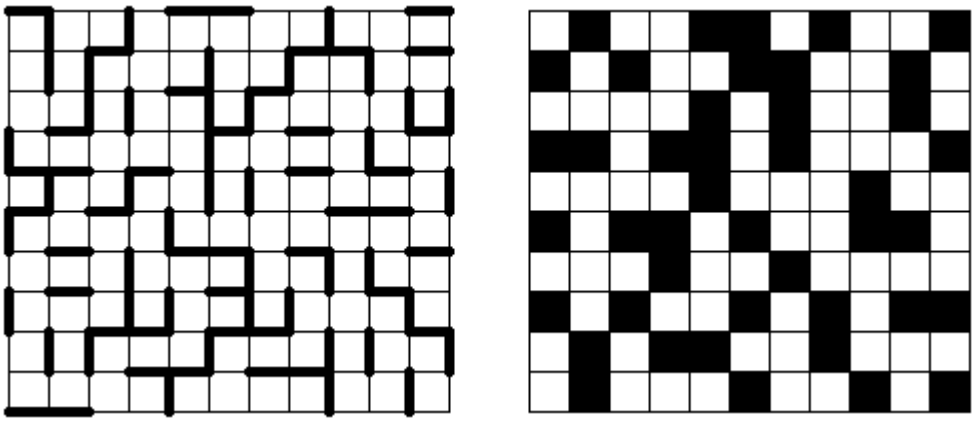


Figure 4.4: Schematic representation of bond percolation (left), where the bold lines indicate open bonds, and site percolation (right), where the black squares indicate available sites.

Percolation describes that a system can be open or closed to phenomena on a macroscopic scale. The percolation threshold is the threshold between the opening and closing of the system[86]. This means that there is a threshold where the number of open and closed bonds in the case of bond percolation, and the number of occupied and empty sites in the case of site percolation, is such that above this threshold there exists a connection between two ends of the network. While below the percolation threshold this connection does not exist.

Closely related to the percolation threshold is the critical probability. Above the critical value of the percolation probability percolation takes place. The critical probability depends on the details of the percolation system under consideration. Critical probabilities are different for lattices with different geometries (*Figure 4.5*). Critical probabilities have been determined for all Archimedean lattices[92]. For a square lattice, for example, the critical probability is ½ [93]. Similar to networks of different geometries, bond percolation and site percolation systems often do not have the same critical probability[94-95].

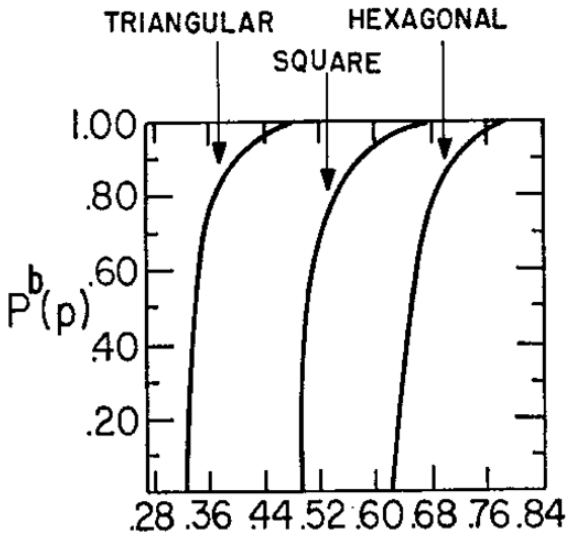


Figure 4.5: Percolation probabilities for 2D bond percolation in triangular, square, and hexagonal lattices, with respect to the fraction of open bonds (taken from Ref. [96]).

Apart from considering bond and site percolation on lattices of various geometries, the number of dimension of the percolation network should be considered. It is clear that 2-dimensional and 3-dimensional systems are different because flow takes place along a different lattice. However in the case of thin films, the thickness of the film plays a role in the behaviour of the system. The properties of such systems cannot be described by only 2- or 3-dimensional percolation. Instead percolation in a thin film can be described by a crossover between 2- and 3-dimensional percolation networks. However, it has been shown that for thin films with a finite thickness it is often possible to renormalize the system such that it can be described as a 2-dimensional percolation network[97].

It is possible to introduce more restrictions to a percolation network. In the most general case of a percolation network, the bonds or sites and their probabilities to be open or closed are independent of each other. However, there are percolation networks where this is not the case and the sites or bonds are not independent of each other[98]. This is the case

when the opening or closing of one bond influences the probability of another bond to be open or closed.

An additional condition that could be added to a percolation network is one restricting the direction of flow through the network. In the most general case percolation is undirected. This means that flow through a channel in the network can take place in both directions. In the case of directed percolation, the flow through the network is restricted to one direction. Directed percolation occurs when an external force dictates the direction of the flow through the medium[99].

4.3.2 Applications of percolation theory

Percolation has been studied extensively as a mathematical theory. Furthermore, percolation theory can be used to describe or predict existing phenomena, such as epidemiology[100] and oil recovery[101]. It is also interesting to investigate ways to use percolation networks for new applications. Percolation networks are interesting for various applications because of the sharp change that occurs at the percolation threshold. This means that, when operating close to the percolation threshold, a small change could result in a large response or even the macroscopically turning on or off of the system.

Understanding of percolation also allows for materials to be tailored such that the desired properties for a certain application are obtained, for example in the case of conductance in granular metals. These materials can be seen as a conductor-insulator mixture, and the conductance through them can be described by percolation. By co-sputtering a metal and an insulator, a film of metal granules surrounded by an insulating layer can be produced. As expected for a percolation network, the size of the granules, analogues of the connected clusters, strongly influences the conductance through the material[102].

Apart from the cluster size or concentration of connections, for some systems other factors seem to influence the conductance as well. For example, in the case of nanorods that form a network of sticks, the alignment of the rods plays a role. For single walled carbon nanotubes it is observed that the percolation probability is higher for a system with slightly anisotropic alignment than for an isotropic system. The difference between those two cases is smaller for systems with a higher nanorod concentration[103].

4.3.2.1 Sensing applications

Percolation is especially interesting for sensing applications. When a sensor is operated around the percolation threshold this allows for a high sensitivity of the sensor to a small amount of analyte. This high sensitivity is especially interesting when very low concentrations of analytes have to be detected, for example in explosives vapour sensing. Operation around the percolation threshold has been investigated for various types of sensor systems, including thin films, nanowires, carbon nanotubes, and polymers.

In a percolation network for sensing applications nanowires or carbon nanotubes[104] can be used as the bonds or edges of the network. Most nanowire or carbon nanotube based networks rely on a change in the conductivity under influence of the analyte to detect the analyte. This means that apart from using materials that respond to the target material, the network must be conducting.

Tin dioxide thin films can be used as gas sensors. Upon variation of the film thickness, grain size and stoichiometry, changes in the electrical performance, and reaction to an analyte, of the system were observed[105]. A strong influence of the thickness of the film on the sensitivity of the gas sensor was observed. It was observed that thinner films, that were also closer to the percolation threshold, were more sensitive than thicker films[105].

It has been shown that SnO_2 nanowires can be used as a gas sensor[106]. The density of the deposited nanowires was such that this system was close to its percolation threshold[106]. Furthermore a system was produced that uses a gradient in the density of the nanowires and a temperature gradient across the system. The combination of these gradients is used to create different conductivity patterns and discriminate between gasses, to create an electronic-nose type sensor[107].

Furthermore, a relative humidity sensor based on multiwall carbon nanotube/polyimide composite films operating around the percolation threshold has been described[108]. The change in resistance upon increased multiwall carbon nanotube loading is as expected for a percolation network. The sensitivity to humidity is attributed to charge transfer between the multiwall carbon nanotubes and adsorbed water molecules[108].

Percolation networks have also been used in the form of polycrystalline oxide films. The boundaries between the crystallites inhibit conduction. This sensor is based on the principle that the presence of a reducing or oxidising gas, by influencing the depletion layer at the grain boundaries, causes a lowering in the energy barrier. This allows for conduction between the grains. If this happens at several grain boundaries such that a conducting path is formed, the change in conductivity over the entire system can be detected[109].

4.4 Summary

The aim of this project is to develop an explosives vapour sensor based on a percolation network of conductive polymers, supported on a metal nanoparticles scaffold. This chapter provides background information required for the two main components of the sensor; metal nanoparticles formed by dewetting and conducting polymers, and the principle behind the sensor; percolation.

The metal nanoparticle scaffold is formed by dewetting a metal thin film. The relative surface energies of the metal and the substrate determine if the lowest energy state is a wetted or a dewetted state. In many cases when a thin film is deposited on a substrate it is in a metastable state and will dewet when enough thermal energy is supplied.

Once the metal nanoparticle scaffold has been formed the conductive polymers can be deposited on top. Conductive polymers are a very versatile group of materials because in addition to the usual advantages of using polymers, such as easy processing and the large range of materials available, they are also conductive.

If the sensor is operated close to the percolation threshold of the polymer network, this could increase the sensitivity of the sensor. Since in a percolation network a small local change to the network could have a macroscopic effect on the network, a small change to the sensor caused by interaction with an analyte molecule, could have a large effect on the entire sensor, making it a very sensitive system.

Chapter 5

Gold nanoparticle scaffolds

Supported metal nanoparticles on an insulating substrate are the first component of the vapour sensor described in this thesis (*Figure 5.1*). The metal nanoparticles form a scaffold between which the conducting polymer network will be deposited. In this chapter I will describe the formation of supported gold nanoparticles using the deposition and dewetting of a gold thin film.

I will start this chapter with a description of the materials that have been used and the reasons why they have been chosen. Next, I will discuss the methods that have been used, and the importance of a clean environment for the formation of the nanoparticles. Then I will discuss the effect of the gold layer thickness, and the annealing time and temperature on the resulting nanoparticle scaffolds. Finally, I will describe the changes in the resistance of the gold film during deposition and annealing.

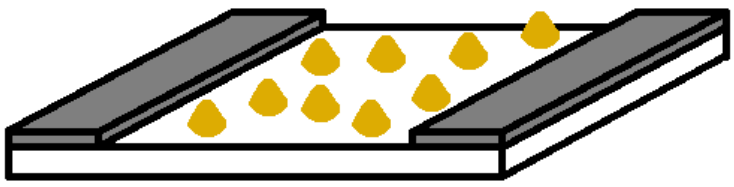


Figure 5.1: A schematic representation of supported nanoparticles (gold), between two electrodes (grey), on a substrate (white).

5.1 Materials

The nanoparticle scaffolds of the vapour sensor consist of 3 components; the supported nanoparticles, the substrate, and the electrodes. The materials chosen for each of the components have to meet the requirements set by the application, the sensor production methods, and the materials used for the other components. In this section I will explain the choice of materials for the nanoparticle scaffolds.

5.1.1 Nanoparticle material

In the vapour sensor described in this thesis the supported nanoparticles act as the nodes of the conductive polymer network. The nodes have to be conductive and relatively inert because they should connect the conductive polymers that form the network, but not interact with the analyte molecules. Furthermore, the relative surface energies of the nanoparticle material and the substrate must be such that dewetting is energetically favourable and individual supported nanoparticles can be formed (see section 4.1). Finally, it must be possible to find polymers that are able to bind to, or wet the nanoparticle scaffold such that the nanoparticles form the nodes of the network.

Taking these requirements into account, gold was chosen as a suitable material for the nanoparticle scaffolds because it is a good conductor, is generally inert, and is expected to dewet on our chosen substrate materials (see section 5.1.2). Additionally, polymers can be easily bound to gold, for example using thiols[110].

5.1.2 Substrate materials

The most important requirement for a substrate for a percolation network of polymers is that it must be a good insulator. Furthermore, since the nanoparticle scaffolds described in this chapter are created by dewetting a gold thin film, the relative surface energies of the substrate, the metal, and their interface, have to be such that the dewetted

state is the energetically most favourable state (see section 4.1). Adsorption of various metals, including gold, and the formation of films and supported particles have amongst others been studied on Al_2O_3, SiO_2, ZrO_2, TiO_2, ZnO, and MgO[82].

Four different substrate materials have been used for the work described in this thesis: MgO, SiO_2, glass, and $SrTiO_3$. These four substrate materials all have different advantages and disadvantages, and have therefore been used in different parts of this thesis.

MgO is an interesting material for sensors because it is a very good insulator. Furthermore, MgO allows for single crystal substrates, and thus the possibility of epitaxial growth. Although this might give more control over the sample, this is not required for the metal nanoparticle scaffolds. MgO has, for example, been used as a substrate for NbN nanowire based single-photon detectors[111].

SiO_2 is also a good insulator. Additionally, it is compatible with existing complementary metal-oxide-semiconductor (CMOS) technologies, which could give more options for the ways in which the sensor could be used and controlled. SiO_2 has already been used as a substrate for various sensor, including examples based on graphene and carbon nanotubes[56, 112-113]. Single crystalline quartz can be used as a substrate material, however it is more common to use an oxide layer on a silicon wafer. Silicon wafers have a thin native oxide layer, of a few nanometres thick, however a thicker oxide layer is usually needed to ensure that the substrate is sufficiently insulating. A thicker oxide layer can be created through thermal oxidation, under wet or dry conditions, resulting in an oxide layer of tens or hundreds of nanometres thick[114]. For the work described in this chapter 635-675 µm Si wafers with a 80-100 nm thermal oxide layer were purchased from Pi-KEM and used after dicing and thorough cleaning with acetone, isopropyl alcohol, and water.

Glass substrates were used because small electrode separations, in the form of interdigitated electrodes (IDEs) are readily available on glass substrates. A possible disadvantage of glass is that it is not as smooth as some of the other substrates. However, this did not affect the experiments described in this chapter, as no effects due to the difference in surface smoothness between glass and MgO or SiO_2 were observed. The glass substrates with IDEs were purchased from DropSens and used after cleaning with acetonitrile and concentrated nitric acid.

Additionally, gold nanoparticles were formed on Nb-doped $SrTiO_3$ substrates. Since this substrate is not insulating it cannot be used as a substrate for this sensor. However, because this material is conductive these samples can be imaged with STM, and imaged more easily with SEM. For this reason Nb-doped $SrTiO_3$ was chosen as the substrate material for initial STM and UHV-SEM imaging of Au nanoparticles.

5.1.3 Electrode material and separation

The electrode material has to be a good conductor, wet the substrate, and have a melting point that is high enough to ensure that it is not affected by the high temperatures involved in the metal nanoparticle formation. Platinum, which has a higher melting point than gold, was used as the electrode material. An adhesion layer, for example made of titanium, can be used to improve the adhesion of the electrodes to the substrate and limit damage when handling the sample and making electrical connections to the electrodes.

Experiments have shown that the electrode separation plays an important role in the gold deposition experiments. It was observed that, when depositing a thin film of gold on an insulating substrate the resistance decreased as the gold layer thickness was increased (see section 5.4). Initial experiments, on samples with 5 µm, 10 µm, and 1 mm separations, showed that for a larger electrode separation a thicker gold film was needed to observe the

same decrease in resistance. This is in agreement with the expectation that for larger networks the percolation threshold shifts towards a larger number of connections, as will also be demonstrated for conductive polymer networks (chapter 6) and simulations of conductive polymer networks (section 7.3). This indicates that for experiments aimed at observing small changes in the resistance due to the wetting or dewetting of a gold thin film, a smaller electrode separation is favourable. However, samples with a smaller electrode separation are also much more sensitive to contamination, as even a small contaminant could connect the electrodes.

For experiments using a 5 or 10 µm electrode separation IDEs, consisting of 250×2 and 125×2 digits respectively, were purchased from DropSens. For samples with a 1 mm electrode separation 10-30 nm Pt was sputtered on SiO_2 or MgO substrates, while masking a 1 mm wide strip in the middle of the substrate (*Figure 5.2*).

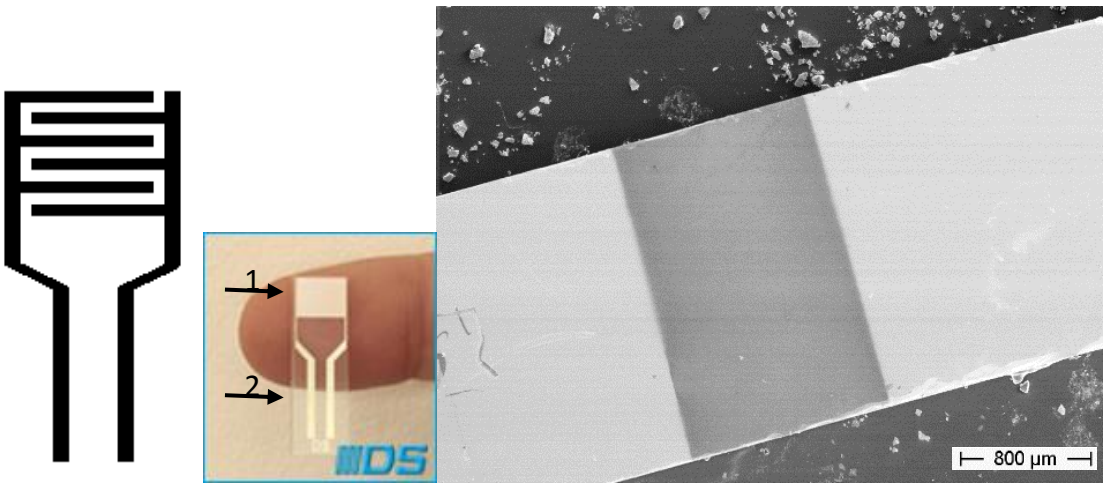


Figure 5.2: Left: Schematic representation of interdigitated electrodes. Centre: Picture of a glass substrate with Pt IDEs. Where 1 indicates the interdigitated electrodes and 2 the connection tracks (adapted from the DropSens catalogue). Right: SEM image of a 2x7 mm SiO_2 substrate, with ~10 nm thick platinum electrodes (bright areas), and a 2x1 mm area between the electrodes (dark). The whole sample is covered with a ~5 nm layer of gold.

5.2 Methods

Several methods can be used to form supported nanoparticles, including methods to deposit pre-existing particles and the *in situ* formation of supported particles. The formation of supported nanoparticle by dewetting a thin film is an especially interesting method because it, by definition, results in a (sub-)monolayer of particles. Furthermore, it does not require additional materials such as ligands that might be unwanted for further use of the supported nanoparticles. The two steps of this method, gold deposition and annealing, will be discussed in this section.

5.2.1 Gold thin film deposition

First, a gold thin film is deposited on a substrate. A straightforward method to do so is to use thermal evaporation. In this case evaporation took place for example in a vacuum chamber, at ~10^{-4} Pa, depositing gold at ~0.15-0.3 Å/s (see chapter 2). Using this method, it is possible to deposit a gold layer of a few nanometres in thickness. The advantages of this method include the large range of sample sizes and shapes that can be used, and the possibility of depositing gold on multiple samples at the same time. However, early experiments showed that samples prepared in this way tend to contain defects (*Figure 5.3*).

To eliminate the defects a new deposition method was developed. This method uses a K-cell in a ultrahigh vacuum (UHV) chamber, at 10^{-6}-10^{-7} Pa, to deposit a gold thin film at ~0.02-0.03 Å/s. Apart from the cleaner UHV environment, this method allows for gold deposition and annealing to take place in the same UHV chamber, eliminating the possibility of contaminating the sample between the different steps of the process.

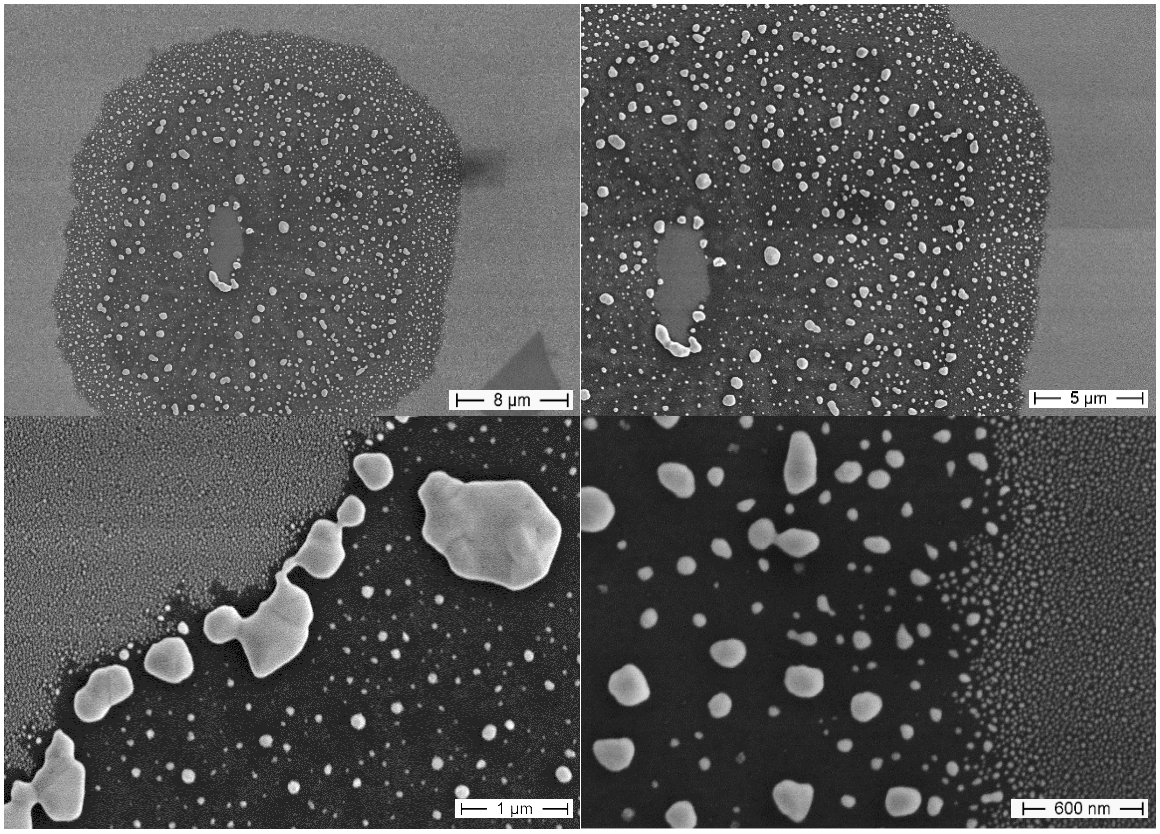


Figure 5.3: SEM images of gold particles on SiO_2, formed by annealing 5 nm gold thin film deposited by thermal evaporation in vacuum. The sample was annealed at 700°C for ~14 hours. Samples produced in this way contained defects, consisting of areas with large particles of various sizes in samples that otherwise consist of relatively regular, much smaller supported nanoparticles.

5.2.2 Annealing

After gold deposition the samples are annealed using an indirect heating holder (see chapter 2). The heating current is slowly increased until the desired temperature in reached. The sample in kept at that temperature for the desired duration, after which the heating current is slowly decreased. Annealing causes the film to break up into individual gold particles and increases the separation between the particles (see section 5.4). The annealing time and temperature that are required for a sample, are determined by the materials as well as the thickness of the metal thin film. It has been shown that thicker films require a higher annealing temperature or longer annealing time to dewet[76, 115] (*Figure 5.4*). When the annealing temperature is too high or the annealing time too long the particles cluster

together. This means that, to create uniform nanoparticle scaffolds, the annealing conditions have to be optimised for each gold film thickness.

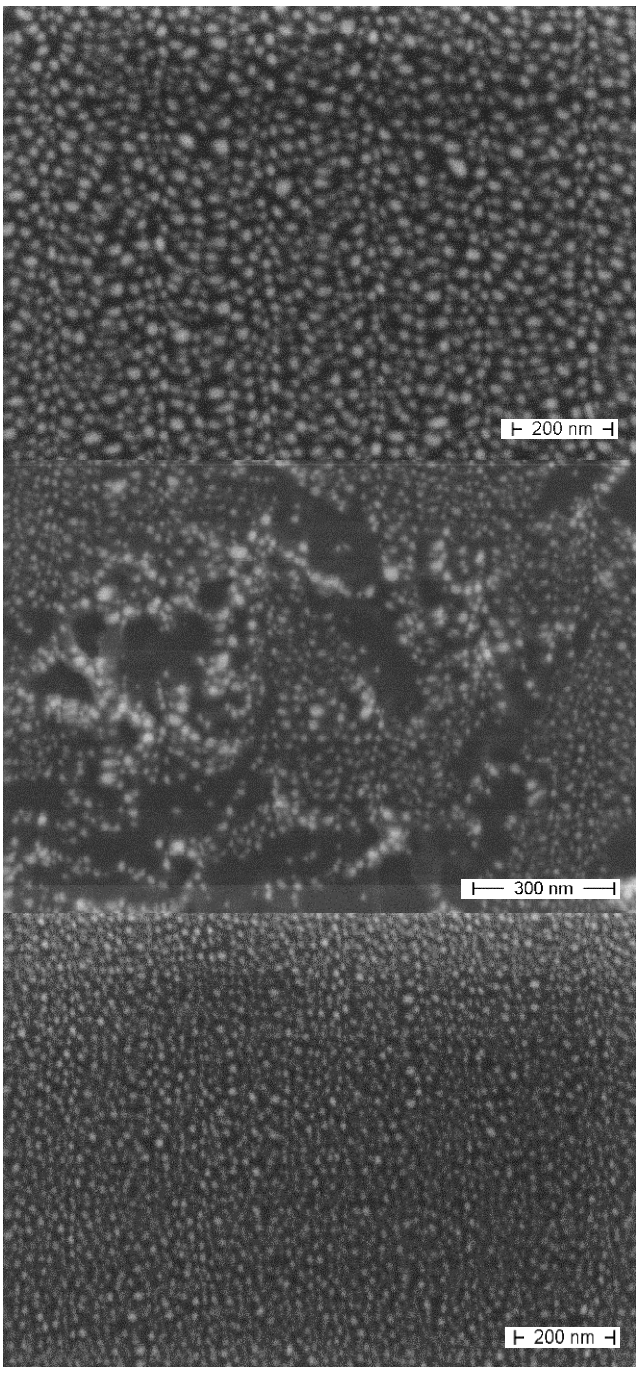


Figure 5.4: SEM images of nanoparticles formed by annealing a gold thin film that was deposited on SiO_2 by thermal evaporation in vacuum: A 5 nm thin film annealed at 700°C for ~15 hours (top), a 3 nm thin film annealed at 700°C for ~3 hours (middle), and a 3 nm thin film heated to 700°C and cooled down immediately (bottom). These examples demonstrate that different film thicknesses require different annealing conditions to create supported nanoparticle scaffolds with even size and particle distributions.

5.3 Particle size and separation

Controlling the size and separation of supported metal nanoparticles can play an important role for various applications. For the formation of a sensor based on a network of conductive polymer on a nanoparticle scaffold, it is important that the conductive polymer is able to bridge the separation between the nanoparticles. The ability to control the nanoparticle size and separation, makes it possible to tailor the nanoparticle scaffolds to the chosen conductive polymer and deposition method, and might play a role in optimising the sensor.

To study the influence of the initial gold film thickness on the resulting nanoparticles, gold thin films of various thicknesses were deposited and subsequently annealed to form supported nanoparticles. 5, 8, 10, 15, and 20 nm thick gold films were deposited on glass substrates with Pt interdigitated electrodes (IDEs) with a 5 µm electrode separation, using the UHV deposition method described in section 5.2. Next the samples were annealed for 1 at 200°C, 2 hours at 200°C, 16 hours at 200°C, 16 hours at 350°C followed by 2 hours at 500°C, and 16 hours at 350°C followed by 6 hours at 500°C, respectively. Different annealing conditions are required for the different gold film thicknesses, as explained in section 5.2. The annealing time and duration had to be optimised for each film thickness, as demonstrated by the example in *Figure 5.4*.

In samples of all thicknesses it was observed that annealing promotes the formation of individual particles, and increases the particle separation. Furthermore, thicker initial gold layers result in larger particles (*Figure 5.5*). The relative surface energies determine the wetting angle (see chapter 4), which is thus independent of the initial gold film thickness. It follows that, to accommodate the larger amount of material while maintaining the same wetting angle, thicker films result in larger particles (*Figure 5.6*). The average nanoparticle

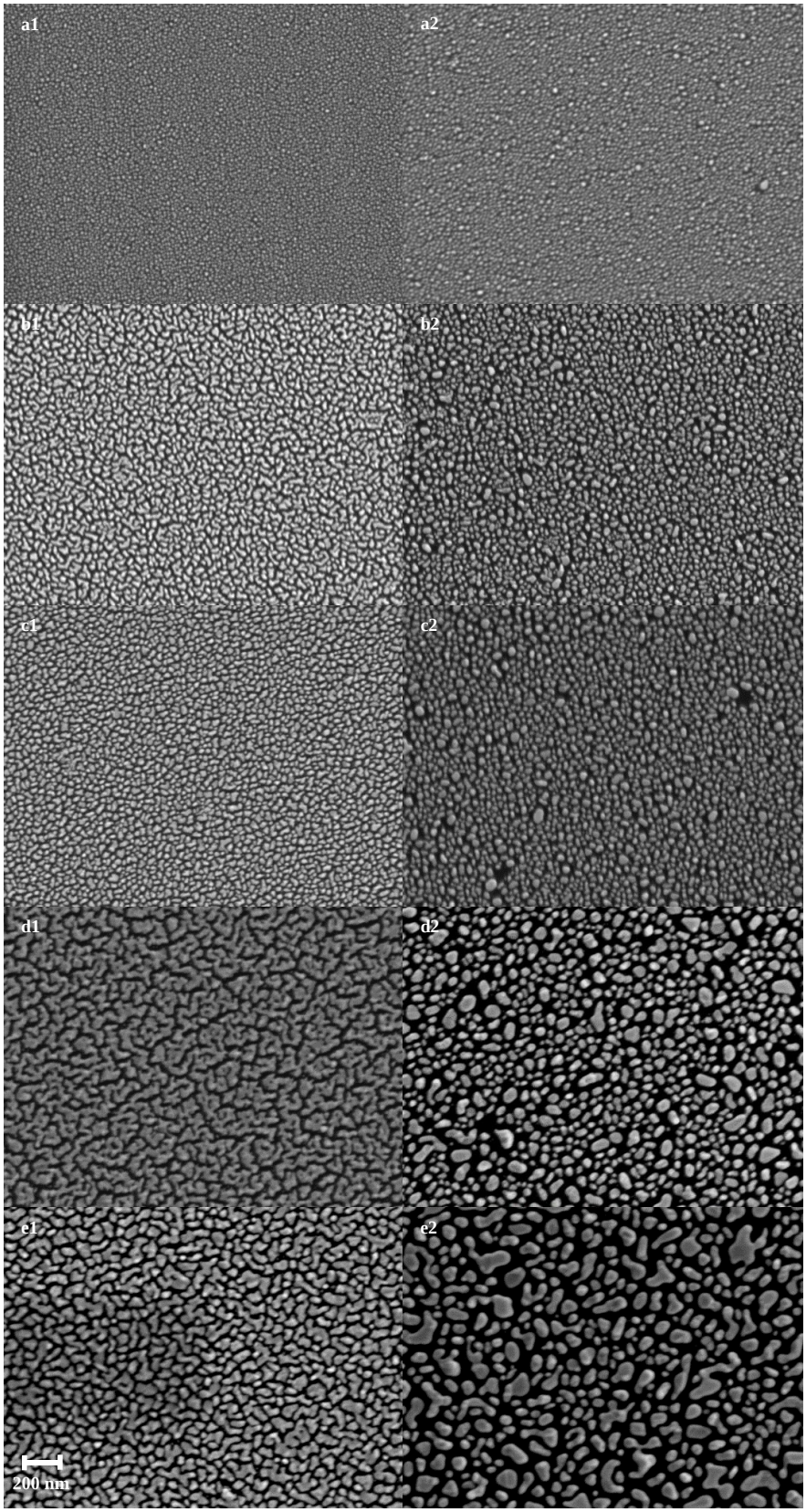


Figure 5.5: SEM images of Au deposited on glass substrates, for Au layer thicknesses of (a) 5, (b) 8, (c) 10, (d) 15, and (e) 20 nm as deposited (1) and after annealing for 1 hour at 200°C, 2 hours at 200°C, 16 hours at 200°C, 16 hours at 350°C followed by 2 hours at 500°C, and 16 hours at 350°C followed by 6 hours at 500°C, respectively (2).

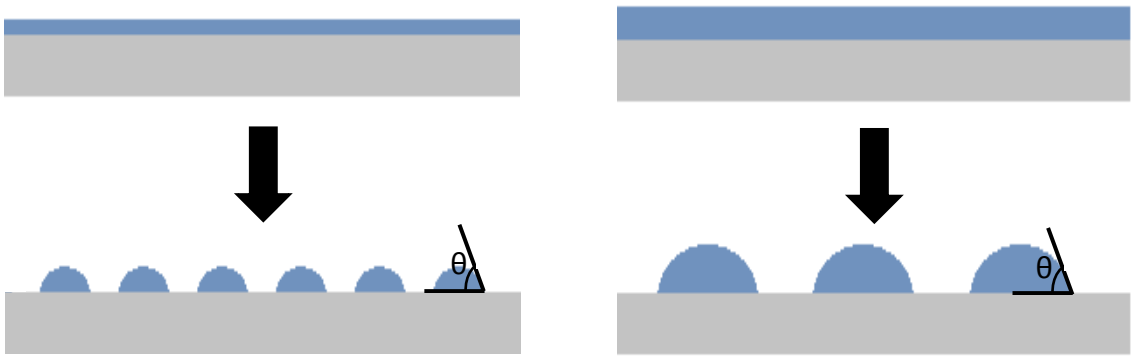


Figure 5.6: Schematic representation of the dewetting of a thinner (left) and thicker (right) film of the same material, resulting in smaller (left) and larger (right) particles with the same wetting angles.

sizes resulting from the 8, 10, 15, and 20 nm thick gold layers were 27±11, 19±13, 44±18, and 74±29 nm respectively (*Figure 5.7*). These average diameters were determined by analysing the SEM images in (*Figure 5.5*), under the assumption that the particles are on average circular, using ImageJ. One factor influencing the precision of these measurements is that the black/white threshold, used to determine the edges of the particles in the images, was determined by eye. Furthermore, there is a large range of particles sizes present in each sample. In samples with larger particles fewer particles are measured and contribute to the average because fewer particles are visible in an image with the same magnification.

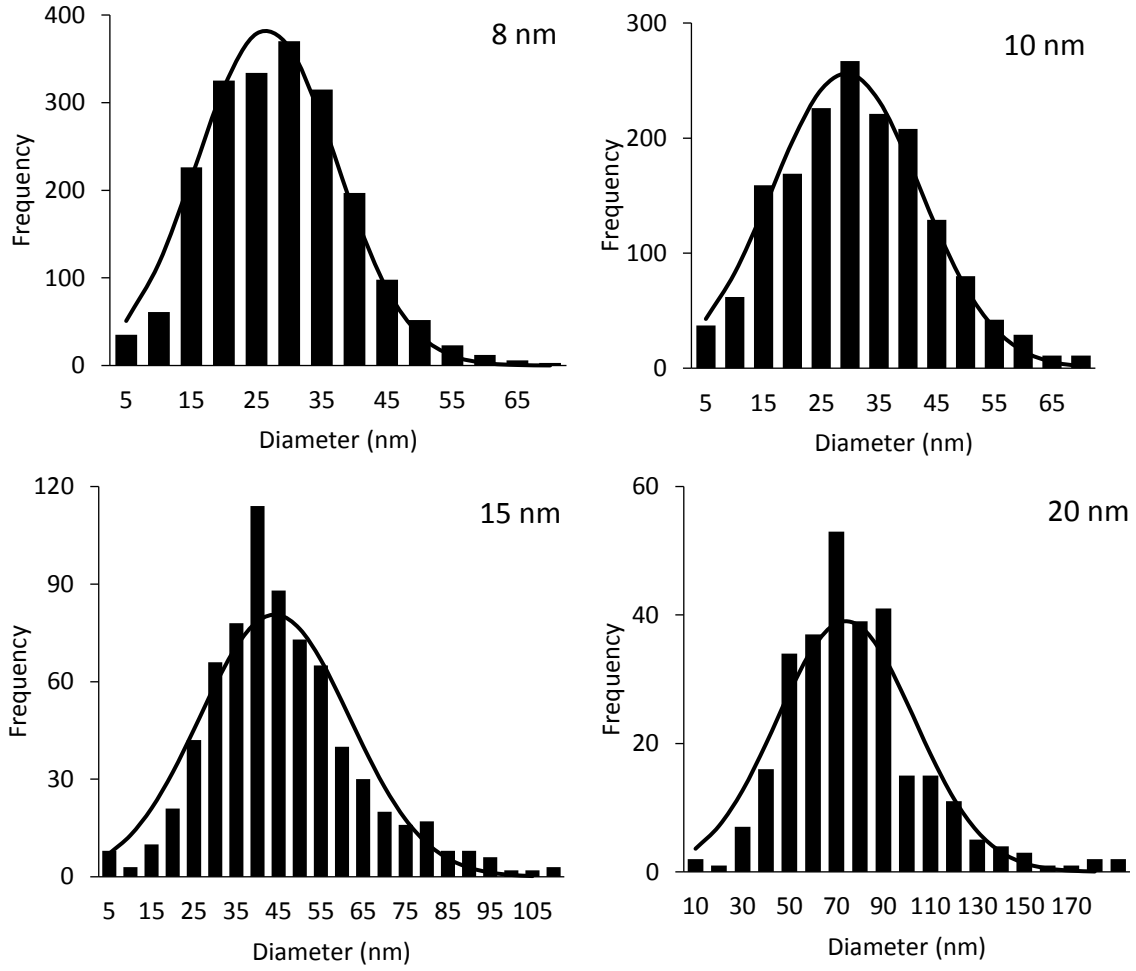


Figure 5.7: Particle size distributions after annealing 8, 10, 15, and 20 nm thick gold layers on glass, determined by analysis of SEM images a2, a3, a4, and a5 (see Figure 5.5).

5.4 Resistance

To further study the gold layer, the resistance of the samples was monitored during gold deposition and annealing. Because the gold is deposited on an insulating substrate, it is possible to measure the resistance of the gold layer itself. Previous research has shown that the resistance of a metal film decreases with increasing film thickness[116-117]. However, to our knowledge, this resistance change has never been studied for very thin films, thinner than 16-20 nm, nor at a resolution sufficient to observe more than the general trend of the resistance change.

Our experimental setup allows us to study the resistance of very thin gold films with high precision, *in situ*, during gold deposition in UHV. Nanoparticles were created on glass substrates with Pt IDEs with a 5 µm electrode separation as described in the previous sections. Additionally, the resistance of the gold layer was determined by applying 1V and measuring the current through the sample. At the start of gold deposition the resistance of the samples was very high, on the order of 100s of MΩ, as expected for an insulating substrate. This is very close to the measurement limit of the multimeter, and is thus subject to a relatively large amount of noise.

It was observed that as more gold is deposited the resistance of the gold layer decreases, which is consistent with previous work on thicker metal thin films[116-117] (*Figure 5.8*). In addition, it was observed that the resistance change during gold deposition is not a smooth, gradual process. Two regimes can be identified. In the first regime, up to an equivalent film thickness of approximately 11 nm, there is a smooth decrease in resistance. However, in the second regime, from approximately 11 nm, step wise changes were observed. These step changes can be attributed to parts of the gold film becoming electrically connected, to form a more continuous film. This is in agreement with SEM images taken of gold layers of various thicknesses (*Figure 5.5*), showing very thin films that seem to consist of small particles (for example the 8 and 10 nm thick films) and slightly thicker films where the particles within the gold layer have become more interconnected (for example the 15 and 20 nm thick films). If the observed step were due to measurement artefacts, such as range changes of the multimeter, one would expect the steps to occur every couple of orders of magnitude as specified in the user manual, which is not the case. Furthermore, the first few connections made in the gold layer cause a much larger decrease in the resistance of the gold layer than later connections, resulting in smaller steps for a thicker film, as observed (*Figure 5.9*). To our knowledge this is the first time that these step wise changes have been observed.

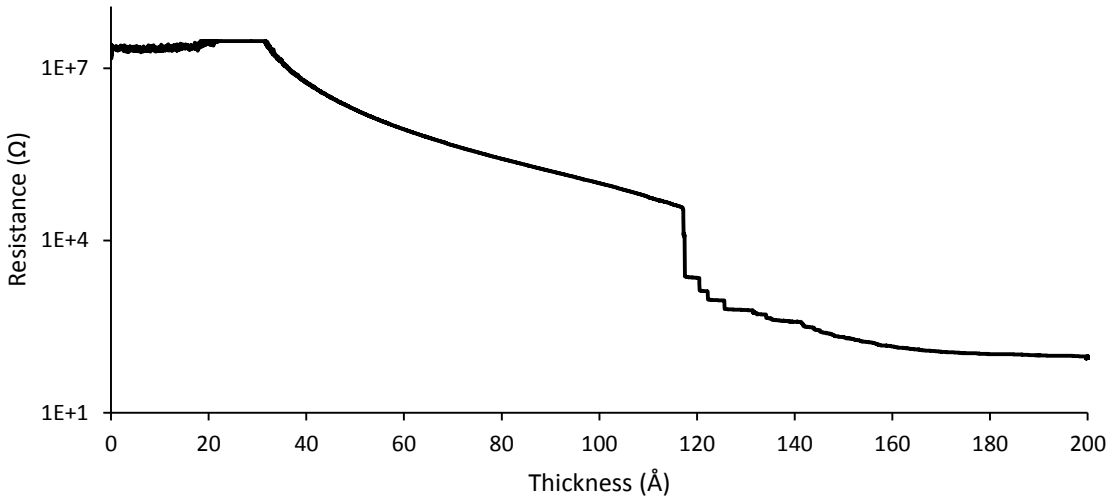


Figure 5.8: Resistance measured during deposition of a 20 nm thick gold layer, showing a decrease in resistance with increasing film thickness. Initially the resistance creases gradually, however from a film thickness of approximately 11 nm the resistance change becomes stepwise.

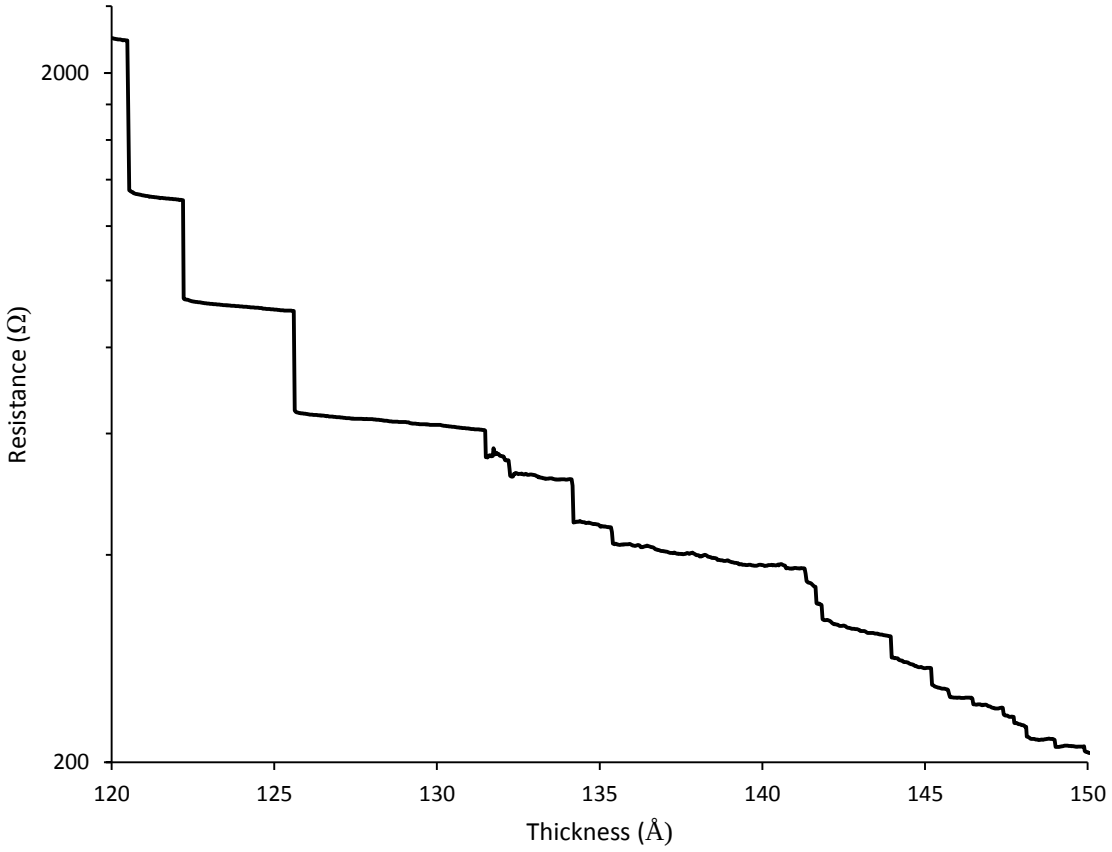


Figure 5.9: Magnified section of Figure 5.8 showing the stepwise change in resistance during gold deposition, and the decreasing step size with increasing gold layer thickness.

After demonstrating the step wise resistance change during gold deposition, one would expect similar step wise changes, but in reverse direction, to occur during the annealing of a gold layer. SEM images in the previous sections of this chapter have shown that annealing causes the gold layer to dewet, which should result in a higher resistance. However, it is practically more challenging to monitor the resistance during annealing over a similarly large resistance range. This would require a higher annealing temperature than can currently be achieved with our set up, and would risk melting the glass substrates.

It is possible to fully dewet a thinner gold layer, of for example 8 nm, and monitor its resistance. However, such a sample already has a high resistance, on the order of a MΩ, at the start of the annealing process. Furthermore, steps in the resistance change during gold deposition were not observed for films as thin as 8 nm, and can thus also not be expected during annealing of such a sample.

Despite it not being possible to fully dewet a thicker gold film in the regime were steps would be expected, stepwise resistance changes were observed during the initial phase of the annealing of thicker films, at temperatures achievable with this set up (*Figure 5.10).* It was observed that, during annealing, the resistance of the film initially decreases, after which it starts to increase. This suggests that, as the sample is heated, it initially recrystallizes to become a more ordered, more conductive layer, before it starts to dewet.

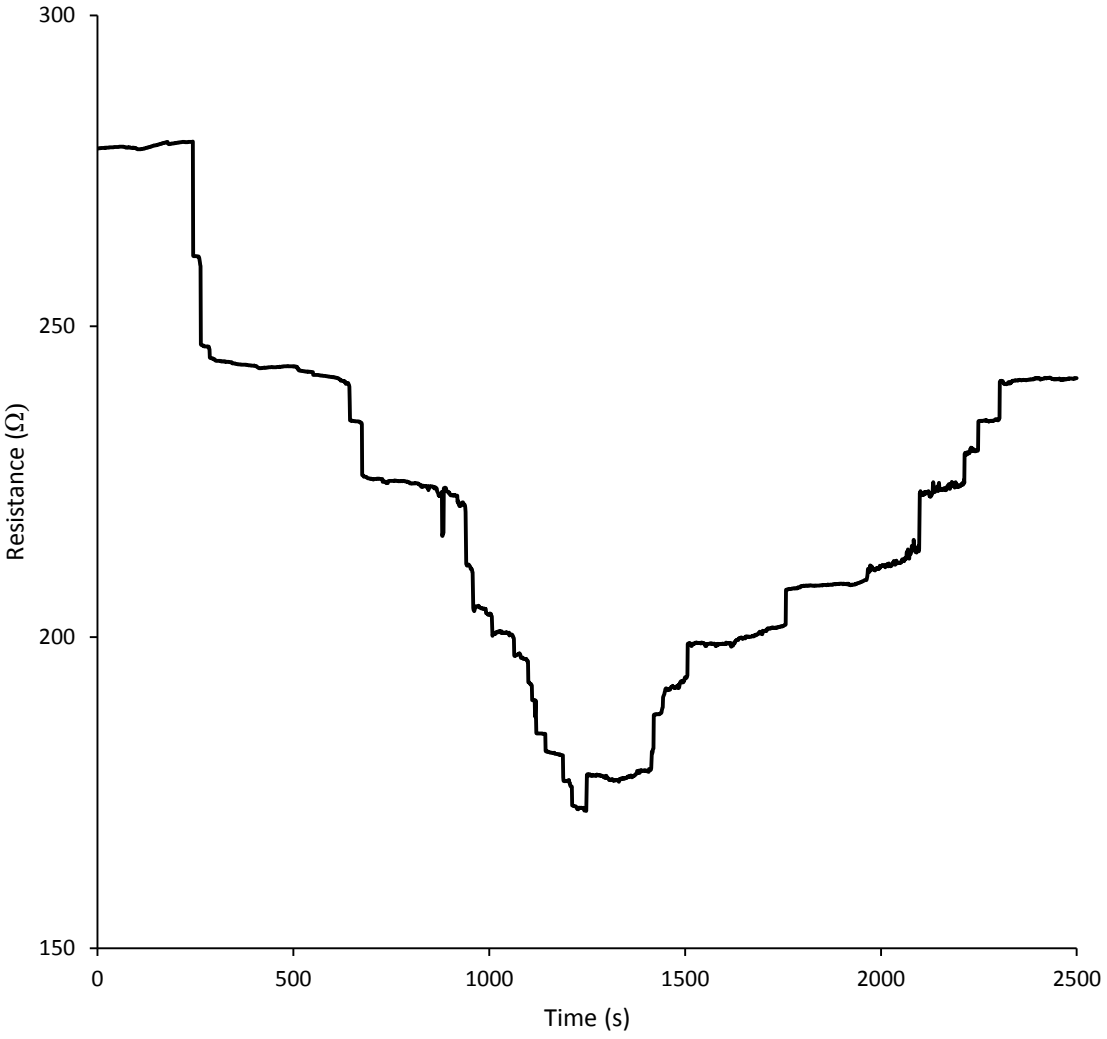


Figure 5.10: Resistance during the initial 2500 seconds of the annealing of a 20 nm thick gold layer at 350°C. An initial decrease in resistance is observed, possibly due to grain growth and the elimination of vacancies, before the resistance increases due to dewetting of the Au layer.

5.5 Summary and outlook

Supported gold nanoparticles of various sizes were created by depositing a thin layer of gold on an insulating substrate and annealing the sample. It was shown that the particle size can be controlled by controlling the initial gold layer thickness, where thicker gold films result in larger nanoparticles. Furthermore, annealing causes the film to break up into individual particles and the particle separation to increase. Controlling the size and separation of supported nanoparticles in this manner makes the use of additional materials such as ligands and sacrificial layers unnecessary, which is advantageous for various applications. The supported nanoparticles created by annealing 5-8 nm thick gold films will be used as a scaffold on top of which conductive polymers will be deposited, as described in chapter 6, to create the vapour sensors used for the sensor testing described in chapter 8.

Apart from being able to create gold nanoparticle scaffolds, these results demonstrate the possibility to controllably create gold layers with resistances ranging from a few Ω to more than a MΩ. Resistance measurements conducted during gold deposition show a decrease in resistance with increasing gold film thickness. Furthermore, it was found that this resistance change is stepwise, with a decreasing step size with increasing film thickness. The steps can be attributed to parts of the gold layer connecting to each other to form a more uniform conductive gold film. To our knowledge this is the first time that the stepwise decrease in resistance was observed.

Future work could be aimed at monitoring the resistance increase during the dewetting of a gold film, for example by using a different substrate and a higher annealing temperature, or a smaller electrode separation. Furthermore, understanding of the wetting and dewetting of this system could be increased by *in situ* imaging of the sample during gold deposition and annealing, for example using UHV-SEM.

Chapter 6

Conductive polymer networks

To create a sensor based on a percolation network of conductive polymers, polymers are deposited on top of the gold nanoparticle scaffolds described in chapter 5 (*Figure 1.1*). The conductive polymers are the active component of the sensor, interacting with the analyte molecules. The resistance of the network, and its position relative to the percolation threshold, will play an important role in the sensitivity of the resulting sensor.

In this chapter I will describe polymer layers deposited on insulating substrates, with and without gold nanoparticles. Deposition methods used for the work described in this chapter, include thermal evaporation, drop casting, dip coating, spin coating, and electrochemical polymerisation. The resulting polymer networks consist of thin strands of polymer that form connections between individual gold particles.

6.1 Materials

In this section I will describe the materials used for the formation of conductive polymer networks. I will start with the conductive polymers that were used, followed by the samples that the polymers were deposited onto, consisting of a substrate, electrodes, and supported gold nanoparticles.

6.1.1 Conductive polymers

The polymers used for the networks have to satisfy several requirements. First of all, the polymers have to be conductive. It must also be possible to process the polymer in such a way that they can be deposited on the nanoparticle scaffolds. Furthermore, they have to chemically react with the analyte material, resulting in a measurable change in resistance.

The polymers must also wet, or form a connection with, the gold nanoparticle scaffold. Early experiments showed that not all polymers are stable on the gold nanoparticle scaffold. For example, thin sexithiophene films dewetted from the gold nanoparticle scaffold after having been stored under ambient conditions for a few weeks (*Figure 6.1*).

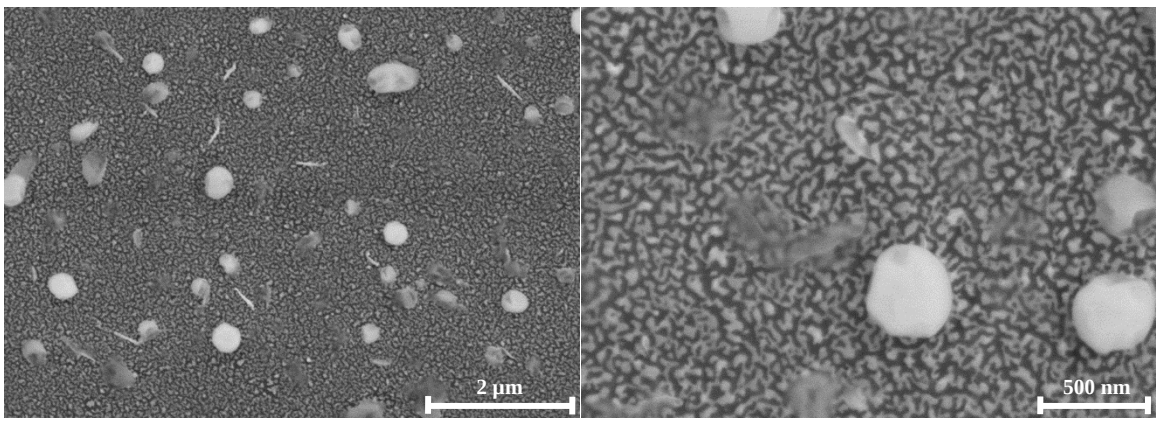


Figure 6.1: SEM images of sexithiophene on a partially dewetted gold nanoparticle scaffold on MgO. After having been stored under ambient conditions for a few weeks, the sexithiophene film has dewetted and formed big clusters of polymer on the gold scaffold.

Finally, it could be advantageous if the polymer can be modified to change its side groups or selectivity. In that case, a polymer could be functionalised to react with a different analyte molecule, without causing significant changes to the deposition method or the electrical properties of the polymer network.

The initial focus of this project will be on the formation of percolation networks of conductive polymers, using polymers that are easy to process and have good conductivity. Then, the focus will move to polymers that react with analyte vapours that can be relatively easily acquired by and used at the university, before using polymers that react with specific explosives.

The conductive polymers used for the work described in this chapter are sexithiophene (6T), poly(3-hexylthiophene-2,3-diyl) (P3HT), polypyrrole (PPY), and poly(3,4-ethylenedioxythiophene) (PEDOT) (*Figure 6.2*). These polymers have primarily been chosen because they have a relatively high conductivity.

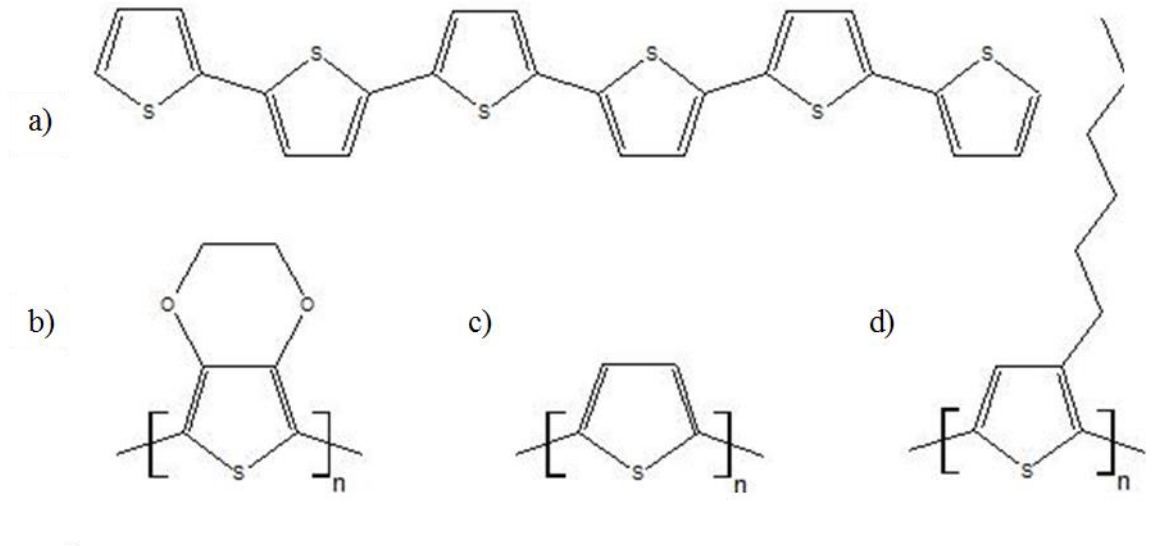


Figure 6.2: Structural formulas of a) sexithiophene (6T), b) poly(3-hexylthiophene-2,3-diyl) (PEDOT), c) polypyrrole (PPY), and d) poly(3,4-ethylenedioxythiophene) (P3HT).

6.1.2 Substrates, electrodes, and gold nanoparticles

The substrates and electrodes that were described in chapter 5 were also used for the polymer networks in this chapter, including SiO_2, MgO, and glass substrates with Pt electrodes, with 1 mm, 10 µm, and 5 µm electrode separations.

In the initial polymer deposition experiments polymer was deposited directly on substrates without gold nanoparticles, to limit unnecessary costs and time needed to produce the supported gold nanoparticles. Once enough control was gained over the deposition of very small amounts of polymer on the substrates, polymer was deposited on the gold nanoparticle scaffolds. Despite the different interactions between the polymer and the gold, and the polymer and the substrate, the initial deposition experiments without gold particles helped optimise the deposition process. From the point of view of polymer deposition, the addition of the gold nanoparticles could be viewed as simply a decrease in the size of the gap that the polymer has to bridge, from the electrode separation to the particle separation.

A range of nanoparticle sizes were used for the initial electrochemical polymerisation experiments. However, the use of smaller particles makes it possible to create nanoparticles scaffolds with a high resistance, higher than approximately 100 MΩ, which is required to be able to measure the resistance through the polymer networks. Therefore, smaller particles, formed by annealing a 5 or 8 nm thick gold film, were used for experiments aimed at creating percolation networks of conductive polymer.

6.2 Polymer deposition methods

There are many different methods that can be used to deposit polymers on the gold nanoparticle scaffolds. For this application the main challenge is to deposit a small enough quantity of polymer to be able to form a polymer network, instead of a thin film. In this section I will describe all deposition methods that were trialled for the formation of a percolation network of conductive polymers.

6.2.1 Thermal evaporation

Thermal evaporation is a convenient deposition method because the layer thickness can be easily controlled through the deposition rate and time. Furthermore, deposition can take place on multiple samples at the same time. However, this method is also quite restrictive because only relatively small molecules can be deposited without breaking bonds within the molecule before the molecule is evaporated. This limits this method to relatively short oligomers, eliminating a large range of conductive polymers. Additionally, to form a network, it might then be necessary to match the oligomer length to the nanoparticle separation.

Vapour deposition of sexithiophene (6T) on gold nanoparticle scaffolds was tested. It was shown that it is possible to create very thin 6T films, of the order of a couple of nanometres. However, it was also shown that under ambient conditions the deposited 6T layer dewetted from the gold particles over time (*Figure 6.1*). Taking all limitations into account, this deposition method was abandoned.

6.2.2 Drop-casting

Drop-casting is probably the most straightforward polymer deposition method. However, it does not allow for a lot of control over the deposition. Control can be gained through the concentration and quantity of the polymer solution that is used. Drop-casting of

1 mg/mL P3HT in chloroform yielded thick polymer layers. Furthermore, these layers were often, to the bare eye visibly, not uniform and did not always cover the entire sample.

6.2.3 Dip-coating

Dip-coating allows for more control over the deposited layer, through the concentration of the polymer solution and the extraction speed. Initial experiments with 1-20 mg/mL solutions of P3HT in chloroform, extracting the 7 mm long sample in 1-10 s, resulted in visibly relatively thick films (*Figure 6.3*). The filament like structure into which the polymer is expected to order is clearly visible. As expected, faster extraction of the sample from the solution resulted in thicker films than slower extraction[118]. Although polymer monolayers created by dip-coating have been reported[119], we have been unable to create sub-monolayer networks of polymer using this method.

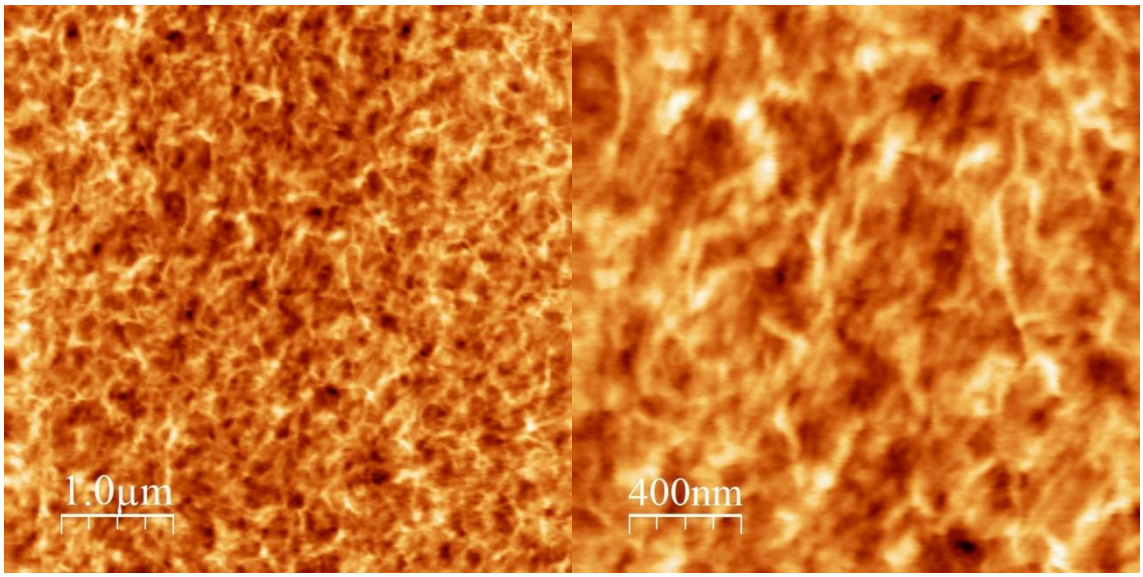


Figure 6.3: AFM images of a P3HT layer created by dip-coating a SiO_2 substrate in a 20 mg/ml solution of P3HT in chloroform. The randomly oriented filaments, into which the polymer orders, are clearly visible.

6.2.4 Spin-coating

Spin-coating allows for additional control over the polymer film thickness through the spin speed as well as the concentration of the polymer solution. P3HT dissolved in chloroform at various concentrations was deposited on SiO_2 substrates without gold nanoparticles at various spin speeds (*Figure 6.4*). At relatively high concentrations the resulting polymer films are similar to the films created by dip-coating, as described above. However, films created by depositing less concentrated polymer solutions were thinner. Furthermore, a higher spin speed also resulted in a thinner film, as expected. These thinner films have pinholes in them. The pinholes in the 1mg/mL samples are 8-12 nm and 4-6 nm deep for the 1000 rpm and 4000 rpm deposition respectively. Which is in agreement with the inverse proportional relationship between the film thickness and the square root of the spin speed[120]. This suggests that the depth of the pinholes is representative of the film thickness.

Since relatively thin polymer films were achieved by spin-coating, compared to the previously described methods, these experiments were repeated on SiO_2 substrates with gold nanoparticles. One would expect that if the polymer film is thinner than the gold nanoparticle height, the particles might show through the polymer film, or otherwise affect the polymer film. However the AFM images show no difference between the polymer films deposited on samples with and without gold particles. This suggests that the polymer film, despite being a lot thinner than previously described films, is still too thick compared to the size of the nanoparticles (*Figure 6.5*).

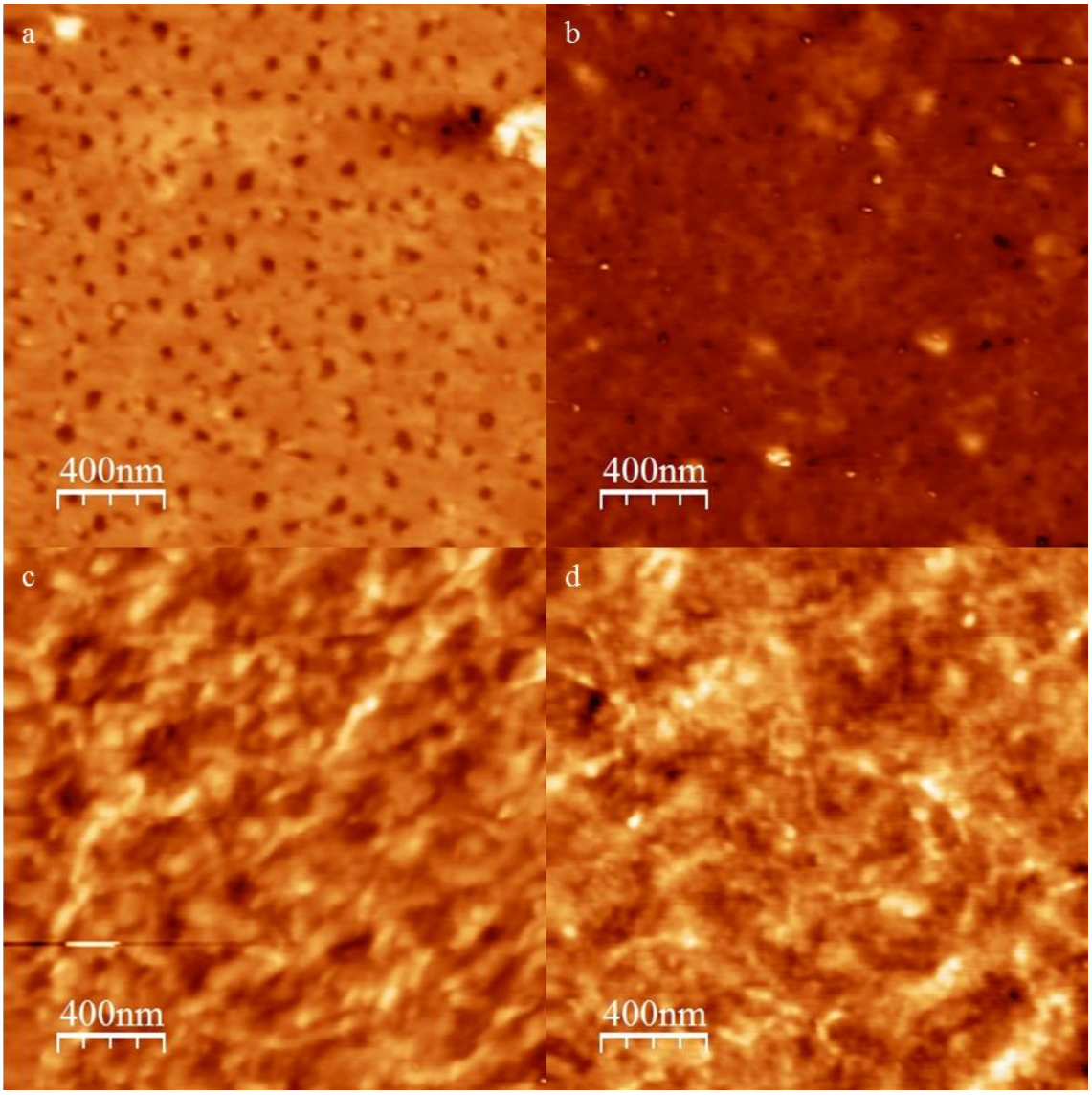


Figure 6.4: AFM images of P3HT deposited on SiO_2 from a a) 1 mg/mL solution by spin coating at 1000 rpm, b) 1 mg/mL solution by spin coating at 4000 rpm, c) 10 mg/mL solution by spin coating at 1000 rpm, and d) 10 mg/mL solution by spin coating at 4000 rpm. Deposition from a 10 mg/mL solution resulted in thicker films with visible filaments, whereas deposition from a 1 mg/mL solution resulted in thinner polymer films with pin holes.

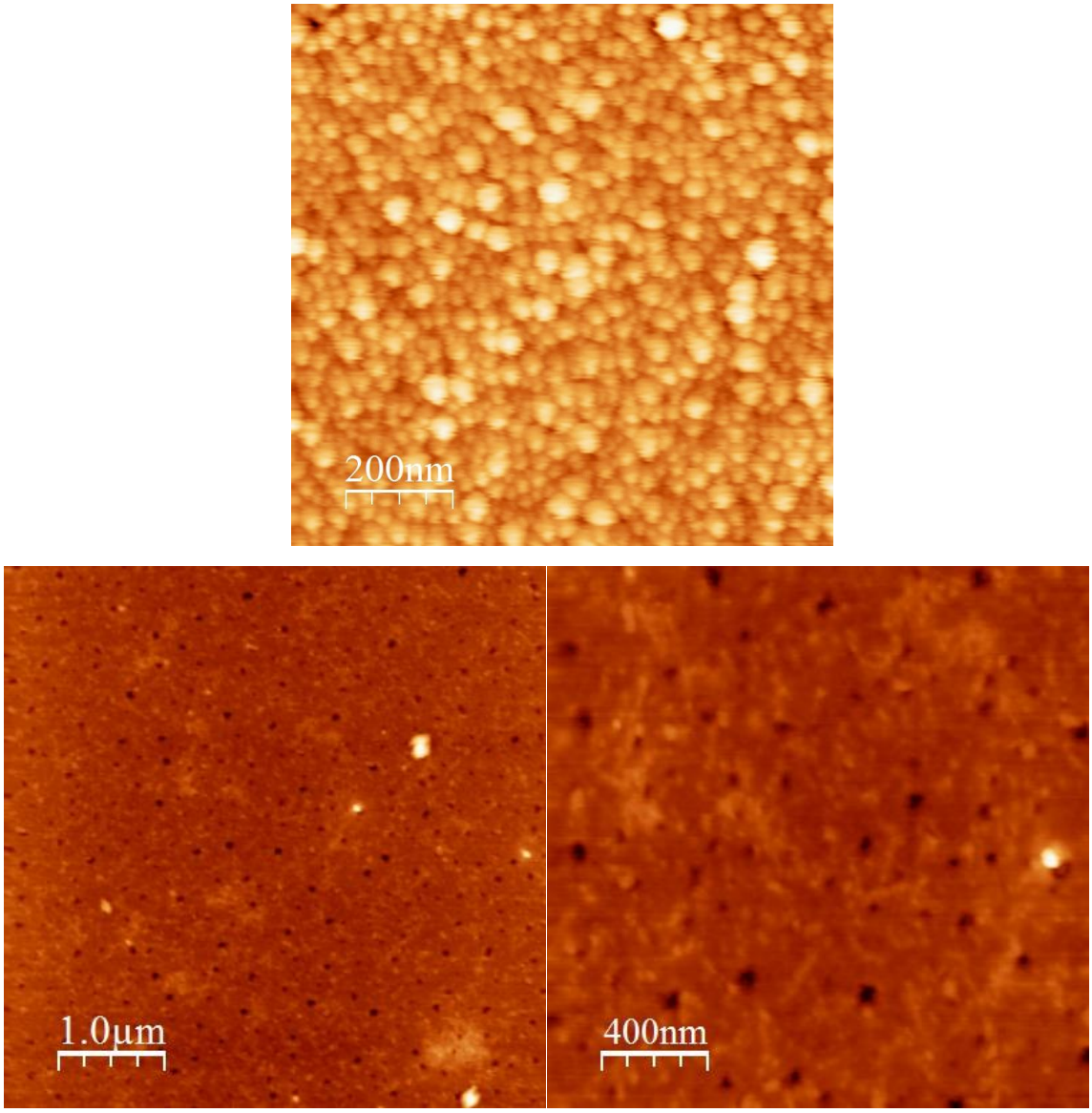


Figure 6.5: Top: AFM image of 3 nm Au on SiO_2, annealed by heating to 700 °C and left to cool as soon as that temperature was reached. Bottom: AFM images of P3HT on gold nanoparticles on SiO_2, deposited from a 1 mg/mL solution by spin coating at 1000 rpm. This image illustrates that, despite the holes in the polymer layer, the layer is still too thick to form a network where the gold nanoparticles are used as nodes. The holes and the separation between them are both much larger than the gold nanoparticles and the separation between the gold nanoparticles (as observed in the SEM images of gold nanoparticles in chapter 5). Furthermore, these holes are also visible in some of the samples without gold nanoparticles (see Figure 6.4), and can therefore not be correlated to the existence of the nanoparticles.

6.2.5 Electrochemical deposition

All the previously described methods resulted in polymer layers that were too thick to form a percolation network. So far the approach to creating a polymer network has been top-down, aiming to decrease the polymer layer thickness. However, using these methods, the polymer layer did not become thin enough. The problem can be approached differently by using a bottom-up method, starting without polymer and then slowly adding polymer to build up a network a few connections at a time. This can be achieved with electrochemical polymerisation methods. Previous work in our group has shown that electrochemical polymerisation can be used to form polymer connections between interdigitated electrodes with various electrode separations. Since the gold nanoparticles decrease the distance that has to be bridged by the polymer, it is expected that samples with supported gold particles will be bridged more easily.

For the work described in this chapter two electrochemical deposition methods were used: cyclic voltammetry (CV), in which a range of potentials is cycled across the sample, and chronoamperometry (chrono) in which the sample is kept at a set potential for a certain amount of time. In both cases the sample is held in a salt solution with the monomer and a counter and reference electrode, as described in chapter 2. The potential at which polymerisation is initiated is specific to each polymer.

Before resistance measurements and sensing experiments were conducted, all samples were doped for 5 minutes using chrono in a salt solution without monomer. This ensured that all samples were in an approximately equally doped state before the resistance was measured.

The initial electrochemical deposition work focussed on CV deposition of PEDOT. The initial CV deposition results were promising because the gold particles were visible

through the polymer layer (*Figure 6.6*). Furthermore, PEDOT grows in such a way that polymer strands connect the gold particles, forming a network. As expected, the polymer grows outward from the electrode.

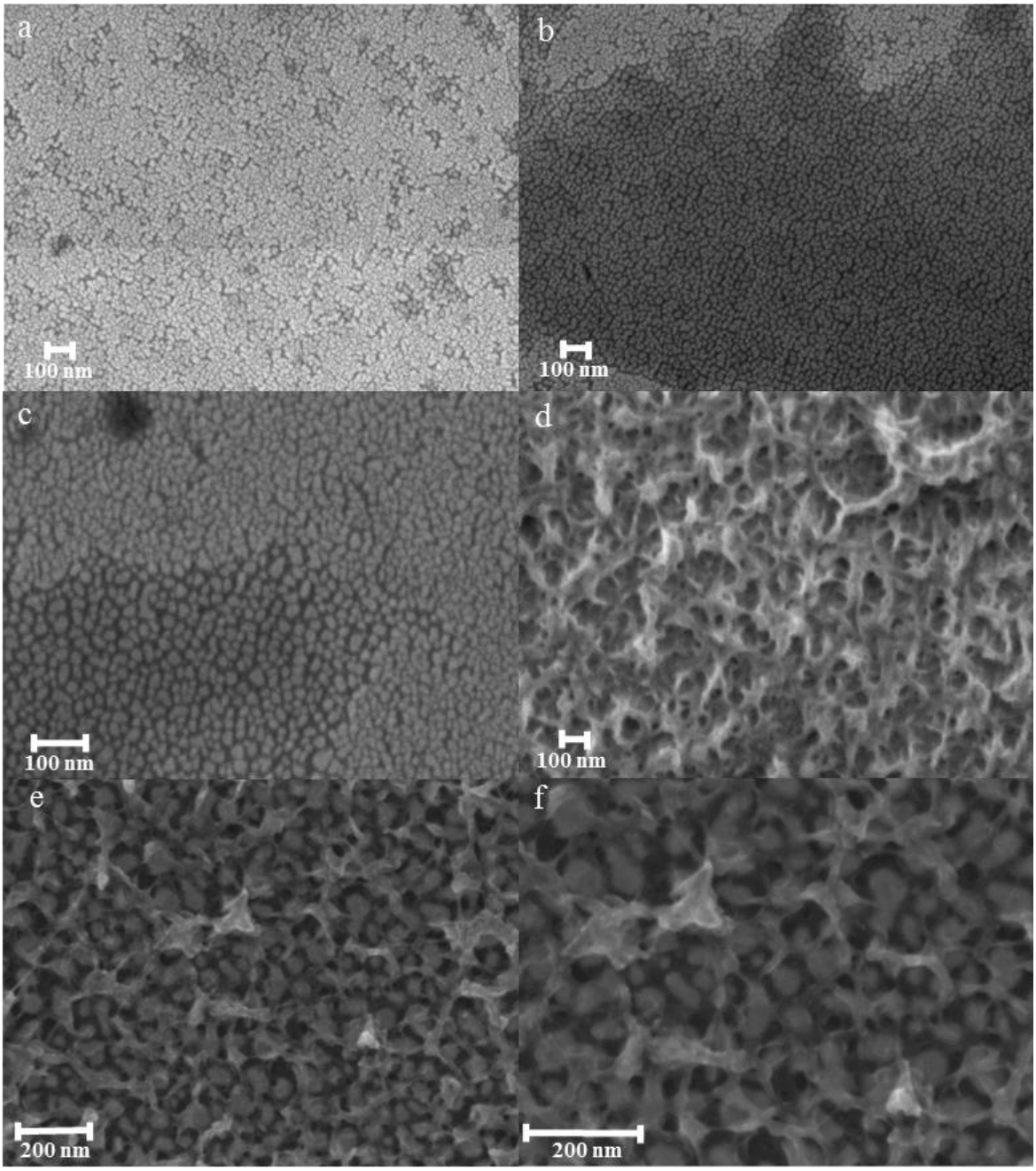


Figure 6.6: SEM images of PEDOT on glass with Pt IDEs and gold nanoparticles, deposited through CV: a) Au particles and polymer. b) & c) Au particles with partial polymer coverage (the brighter areas closer to the edges of the images). The polymer grows outward from the electrodes, connecting the Au particles closest to the electrodes first. d) A thicker polymer layer, which looks similar to the polymer layers that were deposited using the other deposition methods. e) and f) thin strands of polymer, connecting individual gold particles, are visible.

6.3 Polymer networks

In the previous section it was shown that it is possible to create fine polymer networks, bridging the gold nanoparticle scaffolds, using electrochemical polymerisation. The aim of the work described in this section is to gain more control over the polymer deposition process and use electrochemical polymerisation to create conductive polymer networks with a range of resistances, both close to the percolation threshold and in the thin film regime.

Cyclic voltammetry (CV) was used to deposit PEDOT on gold nanoparticles, formed by annealing an 8 nm thick gold layer between Pt IDEs on a glass substrate. The number of CV scans was varied to create conductive polymer networks with different amounts of polymer connecting the gold nanoparticles. PEDOT was deposited in 1, 2, 3, and 4 scans. All 4 resulted in polymer networks that bridged the gold particles. Furthermore, the SEM images show that scanning more often indeed results in more polymer being deposited, as expected (*Figure 6.7*).

The resistances of the 1, 2, 3, and 4 scans samples were 395, 71, 70, and 30 Ω respectively. As expected, samples with less polymer have a higher resistance than samples with more polymer. However, the resistances of these 4 polymer thicknesses are relatively similar. Furthermore, only 1 CV scan changes the resistance of the sample from >50 MΩ to 395 Ω. To create a conductive polymer network that has a higher resistance or is closer to a percolation network we need more control over the polymer deposition than CV deposition can provide.

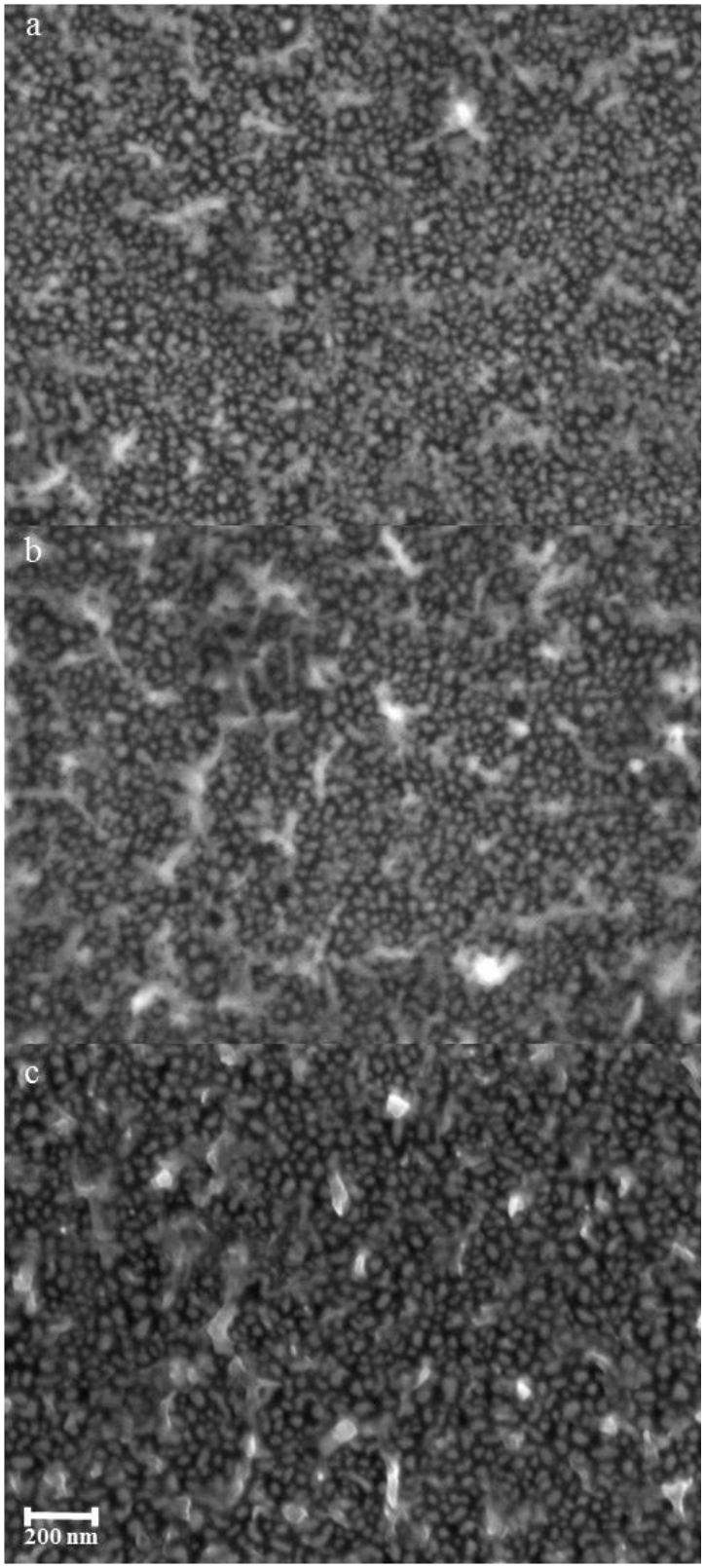


Figure 6.7: PEDOT deposited on gold particles, created by annealing a 8 nm Au layer, using CV for a) 2, b) 3, and c) 4 scans. Strands of PEDOT are visible on the Au nanoparticle scaffolds, with an increasing amount of polymer visible for an increasing number of CV scans.

To gain more control over the polymer deposition and try to create a network that is closer to the percolation threshold PEDOT was also deposited using chronoamperometric (chrono) deposition. Previous work in our group depositing conductive polymer on IDEs without gold nanoparticles has shown that a few seconds of chono deposition equates to 1 scan in CV. Furthermore, while CV is limited to full scans, the chono deposition time can be specified up to a precision of 0.1 second. This means that chrono might provide more control over the deposition and might make it possible to deposit even smaller quantities of polymer.

Using chrono, PEDOT was deposited on gold particles for 1, 3, 5, and 10 seconds. To the trained eye the SEM images show that, as expected, longer deposition times result in more polymer on the sample. It is especially clear that the 10 s sample has more polymer than the 1, 3, and 5 s samples (*Figure 6.8*). The resistances for these samples were 115, 86, 73, and 69 Ω respectively. The resistance values for networks with different deposition times are again quite similar. However, since the polymer networks look quite different for different deposition times, the thinner polymer networks might still be closer to the percolation threshold. This means that, despite having resistances similar to those of the thicker films, they might have different sensor responses. However, these polymer networks are all situated on the shallower part of the percolation graph, closer to the thin film regime.

Since the chemical differences between different polymers cause them to have different resistances and to deposit differently when using electrochemical polymerisation, they will form different networks for the same number of CV scans or chrono deposition time. Since PPY is less conductive than PEDOT[121], more PPY has to be deposited to create networks with a similar resistance to the PEDOT networks. Furthermore, PPY and PEDOT do not grow in the same way when they are electrochemically polymerised onto the sample.

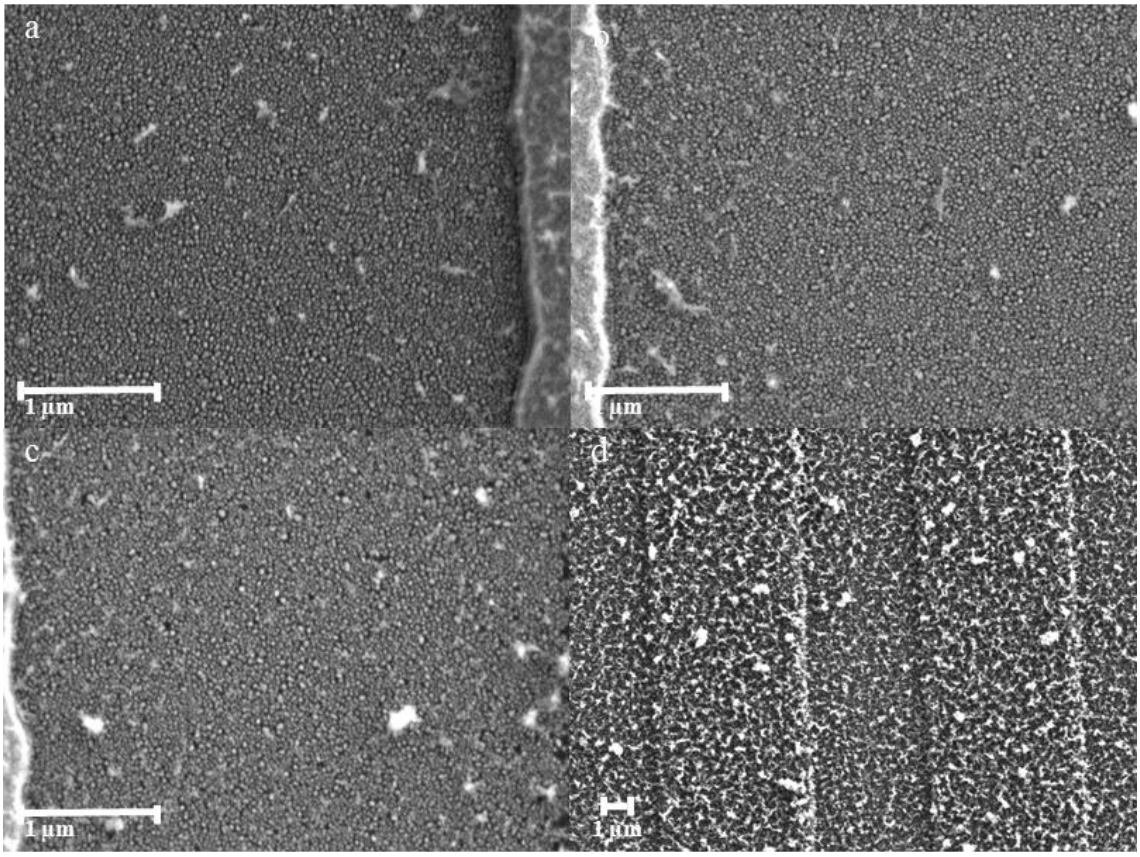


Figure 6.8: SEM images of PEDOT deposited on supported Au particles, created by annealing a 8 nm Au film, on glass by chrono deposition for a) 1, b) 3, c) 5, and d) 10 seconds. For samples with a longer chrono deposition time, more PEDOT filaments are visible on the gold nanoparticles. The edges of electrodes are visible as bands on the side of the images in images a, b, and c, and two electrodes run vertically through image d.

This is another opportunity to gain more control over the conductive polymer network and create networks closer to the percolation threshold, or with different resistances.

PPY was deposited on gold particles, created by annealing a 5 nm gold film, for 1, 3, 5, and 60 seconds using chrono. The 1, 3, and 5 s samples had so little polymer on them that it was not possible to see the polymer using SEM. The 60 s sample, on the other hand, had a polymer film that was visible with the bare eye. The resistance values of theses samples were 1.7 MΩ, 27 kΩ, 318, and 78 Ω respectively. These resistance values clearly put the first two of these samples in the steeper part of the percolation graph. The 1 and 3 seconds chrono sample in particular are close to the percolation threshold for a network of conductive

polymer on a gold nanoparticle scaffold. This shows that with PPY it is possible to create a range of conductive polymer networks with different resistances, both close to the percolation threshold and in the thin film regime.

Chrono deposition of PPY results in networks that are closer to the percolation threshold than chrono deposition of PEDOT, with the same deposition time. This difference between PPY and PEDOT could be due to two factors: the different resistances of these two materials, or a difference in the way these two materials deposit. The differences in resistance between the 1, 3, and 5 seconds chrono samples are much larger for the PPY sample than for the PEDOT samples. At long deposition times the PPY and PEDOT samples have relatively similar resistances, whereas at short deposition times the differences in resistance between the PPY and PEDOT samples are much larger. This suggests that the difference between PPY and PEDOT must be primarily due to a difference in the deposition of these two materials, causing them to be in different positions relatively to the percolation threshold. If the difference in resistance was mainly due to the different resistances of the bulk materials, and not a shift towards the percolation threshold, one would expect the resistances of samples with different deposition times to shift by similar amounts.

6.4 Summary

Several methods were used to deposit polymer on insulating substrates with and without gold nanoparticles scaffolds. Most methods, including drop-casting, dip-coating, and spin-coating resulted in polymer thin films that were too thick to create a percolation network. The electrochemical polymerisation methods used in this chapter, cyclic voltammetry and chronoamperometry, resulted in polymer networks that connected the gold nanoparticles. Especially chronoamperometric deposition gives a lot more control over the polymer deposition and makes it possible to create barely connected networks.

PEDOT and PPY networks with resistances between 50 Ω and 2 MΩ were created on gold nanoparticle scaffolds. As expected, polymer networks with less polymer have a higher resistance than networks with more polymer. Furthermore, the PEDOT networks have a lower resistance than the PPY networks with the same deposition times. Because the resistances of the PPY networks with deposition times of 1, 3, and 5 seconds are much further apart than the resistances of the PEDOT networks with deposition times of 1, 3, and 5 seconds, it can be concluded that the PPY networks are much closer to the percolation thresholds that the PEDOT networks. PPY networks deposited by chrono for 1 or 3 seconds were especially close to the percolation threshold. These networks will be used as vapour sensors based on a percolation network of conductive polymers in chapter 8.

Future work should be aimed at studying a larger range of polymers at a large range of coverages, and the networks and resistance values that can be achieved with those polymers. This will make it possible to plot the percolation curves for those polymers, which will give insight in the polymers and polymer coverages that would be suitable for use as vapour sensors based on percolation networks of conductive polymers. Furthermore, the combination of the nanoparticle size, separation, and material, and the polymer and polymer thickness should also be optimised.

Chapter 7

Simulations of a sensor based on a percolation network

To simulate a sensor based on a percolation network of conductive polymers on a metal nanoparticle scaffold, a two dimensional system of interconnected nodes was simulated. Furthermore, the conductance through such a simulated network was calculated. The code used to simulate the sensor was developed in collaboration with Sid Visser and implemented in MatLab[122].

The simulations can be used to gain further understanding of a sensor based on a percolation network of conductive polymers and the influence of various parameters on such a network. This information can in turn be used to optimise the physical system that is being developed in the laboratory. In this chapter I will discuss the following parameters: the node distribution, the network size, the maximum connection length, the magnitude of change in conductance caused by the interaction with an analyte molecule, and the dwell time of the analyte molecule.

7.1 Simulated conductive network

A two dimensional interval [0, W] × [0, H], where W and H are the width and height of the interval, represents the area of the sensor between the electrodes. On this interval points are chosen to represent the nodes of the network. The nodes are the intersections of the wires that make up the network, analogous to the nanoparticles in the sensor. The nodes can be chosen in random positions or such that they form a regular lattice.

To form a network, connections are made between the nodes. Delaunay triangulation is used to find the nearest neighbours of each node. If the distance between two nearest neighbours is shorter than or equal to a set value, the maximum connection length, a connection can be made between those nodes. In this way a network is formed, where the nodes represent the metal nanoparticles and the connections represent the conductive polymers.

Once a network has been formed, the conductance through that network can be calculated. Two extra nodes are added, one on each side of the network, to represent the electrodes. All nodes within a distance R0 from the electrode-nodes are connected to the electrode-nodes. In these simulations the connections between the electrode-nodes and the normal nodes do not interact with analyte molecules and can thus not be opened and closed. The conductance between the two electrode-nodes is determined. In these simulations it is assumed that nodes are perfectly conducting points, such that no losses occur at the nodes. Every connection between the nodes is treated as a resistor.

For each simulation the system size, the number of nodes per unit area, and the maximum connection length between those nodes are used as input parameters. Then the conductance through the network is calculated for various values of β (*Figure 7.1*). The conductance is calculated by considering each connection in the network as a small resistor.

As expected for a percolation network there is no conductance if there are no connections, or just a few connections, in the network. When more connections are added there is a sharp increase in conductance through the network, after which the conductance levels off. The values of β for which the conductance has levelled off correspond to the beginning of the thin film regime.

Where input parameters are not mentioned the following values have been used: 1×1 system size, 400 particles per unit area, a maximum connection length of 0.1 of a length unit, and $\alpha = 1$.

In these simulations α is defined as the rate at which connections are broken, or equivalently the rate at which analyte molecules start their interaction with the network. β is defined as the rate at which connections are made, or equivalently the rate at which analyte molecules leave the network after interacting. The ratio of α and β can thus be interpreted as the dwell time of the analyte molecule. In the physical system the dwell time depends on the properties of both the polymer and the analyte molecule, as well as environmental conditions such as temperature. When the conductance of the network is studied over time, there is a dynamic equilibrium, depending on the values of α and β, between analyte molecules interacting with the network and leaving again (see section 7.6). If a snapshot is taken of a simulation at one point in time and for a constant α, β can be used as a measure of how connected the nodes in the network are to each other. In this case the ratio of β and α can be interpreted as being proportional to the probability of having a connection between two nodes.

In the physical system the interaction between an analyte molecule and a conductive polymer molecule causes a decrease in the conductance of the conductive polymer, as will be demonstrated in chapter 8. When the analyte molecule dissociates from the polymer

molecule, the conductance through this polymer returns to its original level. The change in conductance through an individual connection upon interaction between that connection and an analyte molecule depends on the properties of both the analyte molecule and the polymer. In most of the simulations in this chapter the change in conductance is approximated by completely switching a connection off upon interaction with an analyte molecule and switching it back on after its dissociation. This is equivalent to removing that connection from the network and putting it back in the network after the interaction. The degree to which the conductance is reduced upon interaction with an analyte molecule is included as a variable parameter in section 7.5. However, because connections are made and broken in the simulations, many different networks with the same α and β are explored over time. This allows the error bars in the simulations to be determined.

There is a limit where the simulations, while still describing a realistic percolation network, cannot realistically describe the sensor. This is due to the way in which the simulations describe molecular adsorption to the network. When $\alpha << \beta$, the simulations do not realistically describe the sensor. When the rate at which connections are made is much larger than the rate at which connections are broken, more connections are being added to the network than have been broken by interaction with an analyte molecule. This is not possible in a physical sensor, as it would describe a network to which connections are continuously added. On the other hand, for $\alpha >> \beta$ the code is realistic. When the rate at which connections are broken is much higher than the rate at which connections are made, the resistance of the network is quenched. This is equivalent to the sensor being flooded with an excess of analyte molecules.

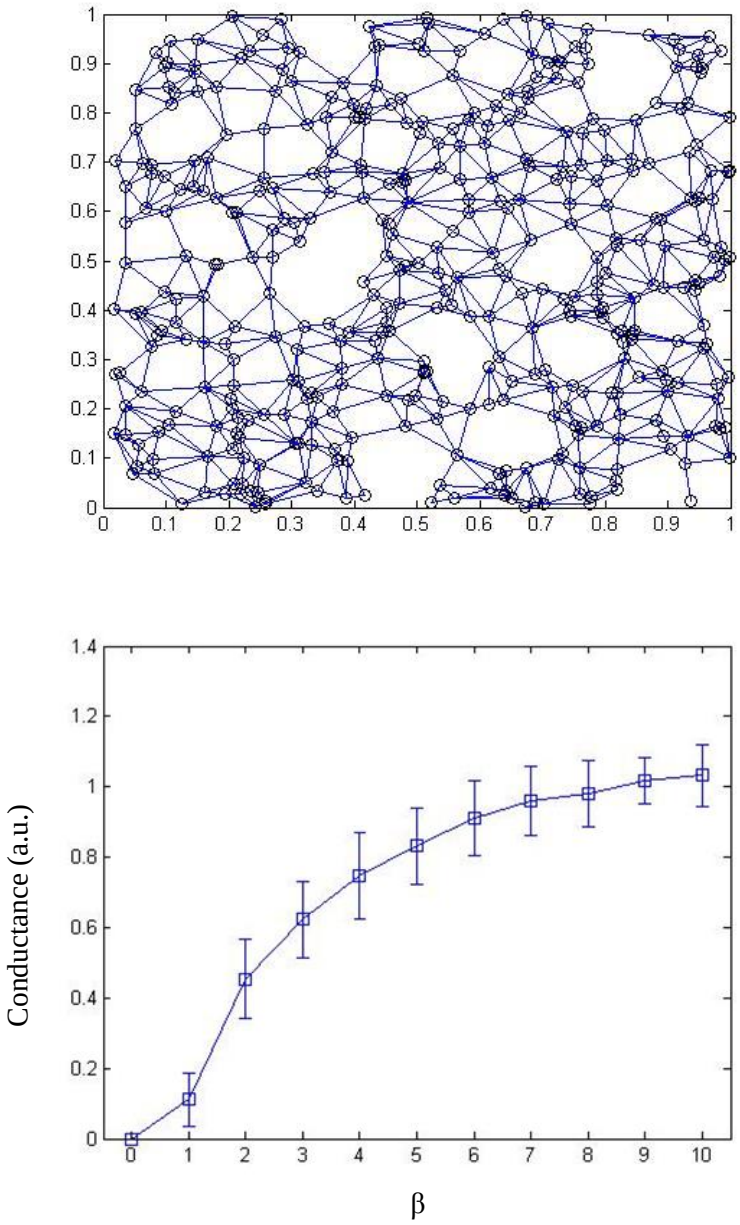


Figure 7.1: *A random network of size 1×1, with 400 particles per unit area, and a maximum connection length of 0.1 (top). Conductance through the network shown above at various values of β (bottom). 100 realisations were used for each point in this graph and all other conductance versus β figures in this chapter. The error bars give the standard deviation, determined using the 100 different networks used for each point.*

7.2 Node distribution

To realistically simulate a sensor based on a percolation network of conductive polymers, the network used in the simulations has to be similar to that in the physical system. Since it is known that regular lattices with different geometries have different critical probabilities[96], we can assume that the relative positions of the nodes affects some of the properties of the network.

The gold nanoparticles created by dewetting a thin gold film on an insulating substrate are irregular. The positions of the nanoparticles formed in this way are determined by the location of holes, grooves, and grain boundaries in the initial gold thin film (see section 4.1.2). Since the substrates are flat and do not have patterning to guide the dewetting, the resulting nanoparticles are relatively randomly distributed. For this reason, the initial simulations were set up to have a random node distribution. However, when comparing the simulated random networks to SEM images of gold nanoparticles created in the laboratory, it is clear that the random networks are more irregular than the gold nanoparticles (*Figure 7.2*). For this reason, networks based on square, hexagonal, and triangular lattices were also used for simulations (*Figure 7.3*). Regular lattices are at the other end of the scale, and are clearly a lot more regular than the gold nanoparticle scaffolds created in the laboratory. By adding a small amount of noise to the regular lattices, by randomly displacing the nodes, a more realistic network can be created. When too much noise is added the network becomes too irregular (*Figure 7.4)*.

As expected, all of these networks behave like percolation networks. The exact shape of each curve, the position of each percolation threshold, and the value of the maximum conductance reached at high values of β differ slightly from one network to another. Some of these differences can be attributed to the random nature of the networks.

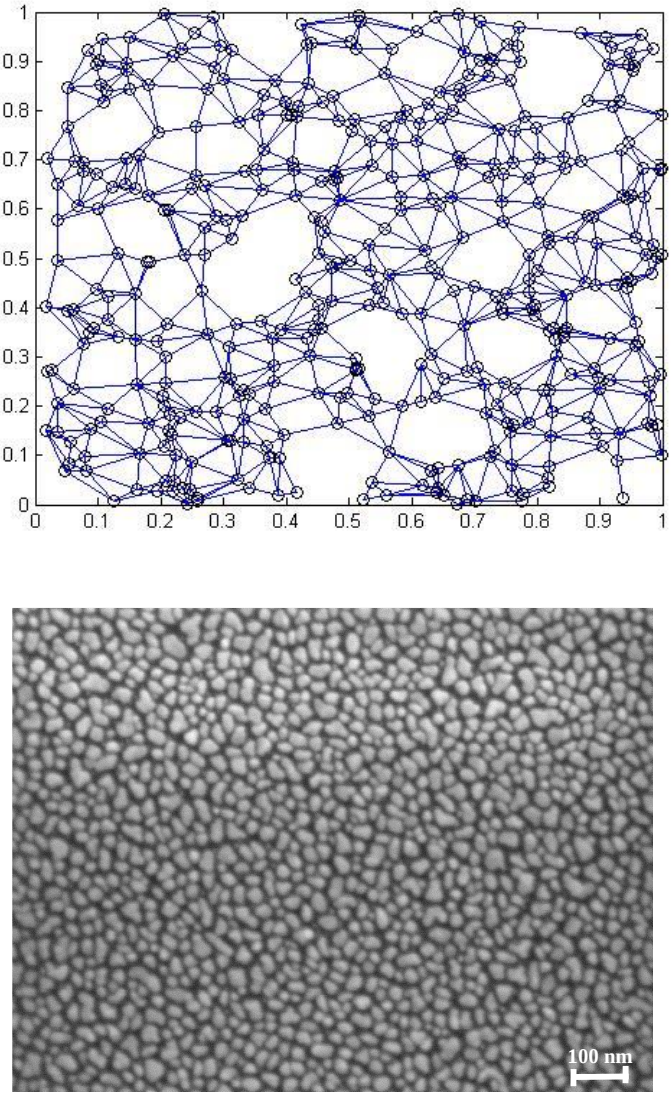


Figure 7.2: Simulation of a random network (top). SEM image of gold nanoparticles on a SiO_2 substrate (bottom). A comparison of these two images illustrates that the node distribution of the simulated random network is more random than the nanoparticle distribution of the nanoparticle scaffolds created in the laboratory.

Furthermore it is know that percolation networks based on regular lattices have different critical probabilities. As expected (see *Figure 4.5*), out of the three regular networks shown in Figure 7.3, the hexagonal network has a percolation threshold at the lowest value of β, followed by the square network and finally the triangular network. Finally, the conductance through the network changes when the nodes of regular lattices are slightly displaced by adding random noise to their positions. Because of the displacements the total numbers of nodes and edges included in the network change. Furthermore, because of the random nature of the displacements, the overall shape of the network changes, which also affects the conductance through the network.

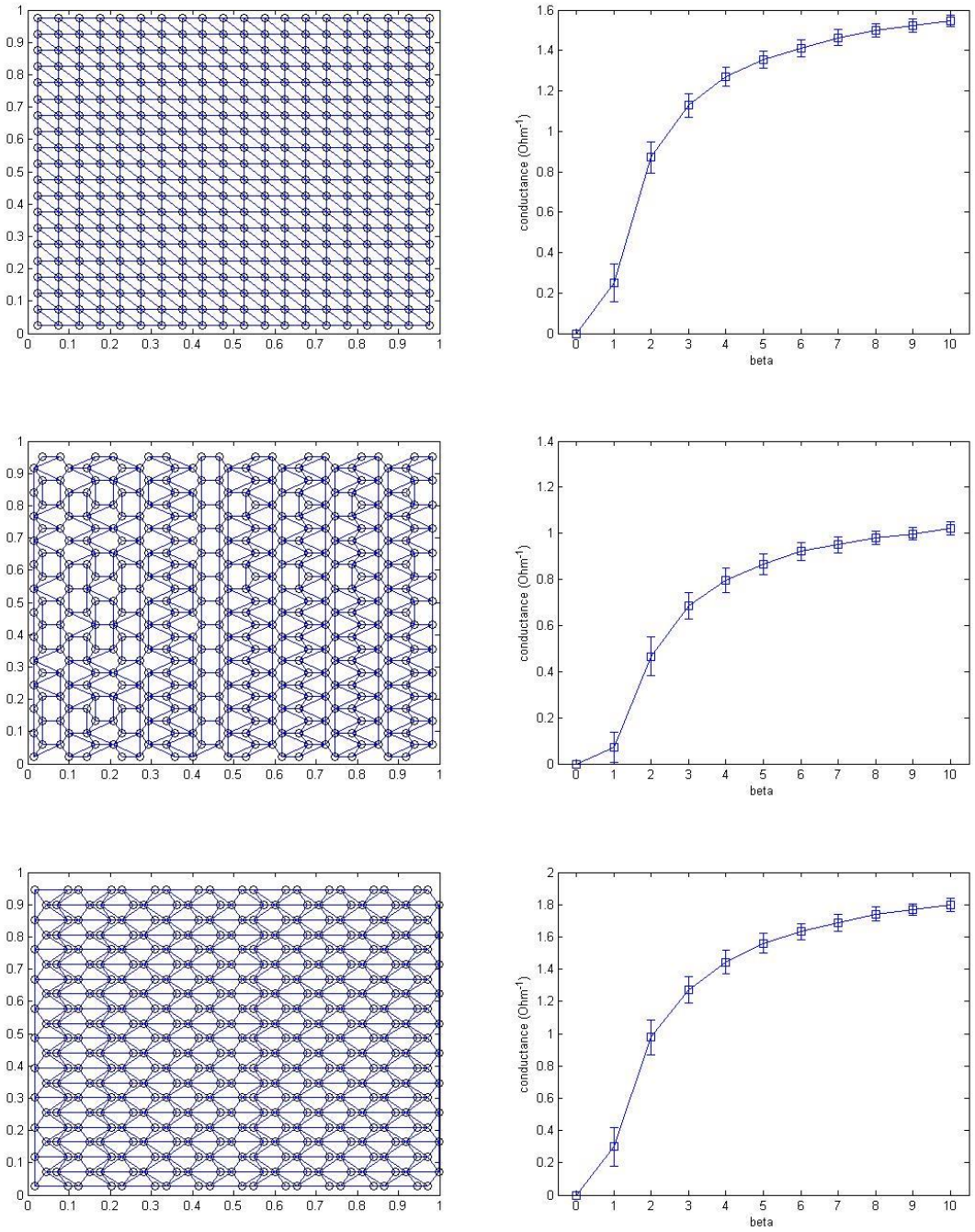


Figure 7.3: Simulations of networks based on regular (from top to bottom) square, hexagonal, and triangular lattices, illustrating that networks based on regular lattice can also be used as percolation networks. Furthermore, the critical probability of networks based on a triangular lattices is lower than that of a square lattice, which is lower than that of a hexagonal lattice.

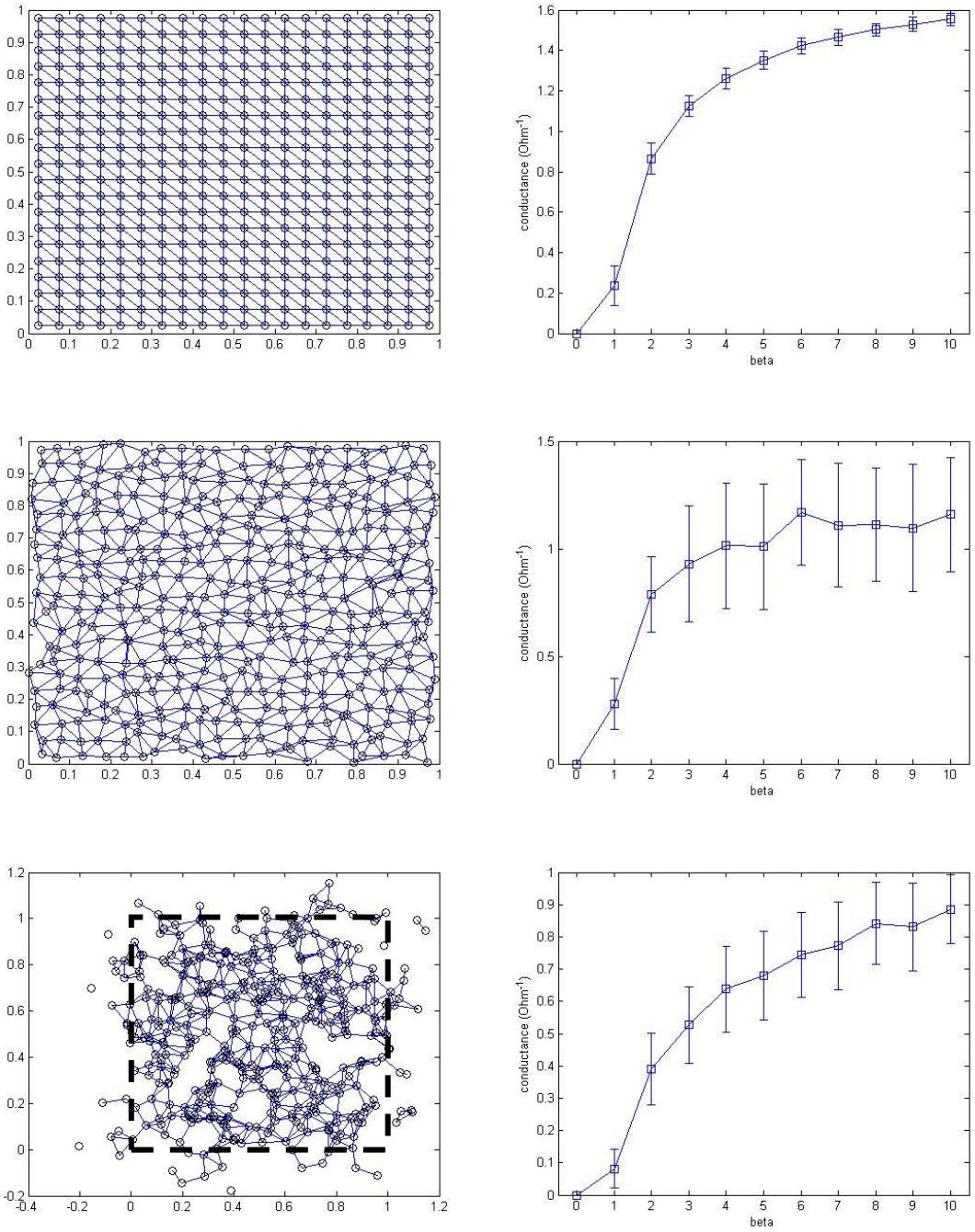


Figure 7.4: Simulations of a network based on a square lattice (from top to bottom) without added noise, with 1% noise, and 10% noise, where the dashed lines indicate the 1×1 unit area between the electrodes, between which the resistance through the network is calculated.

7.3 System size

The networks used for most simulations in this chapter have 400 nodes. However, a small nanoparticle scaffold of 5×5 μm has at least ~30,000 nanoparticles. To investigate the effect of the size of the system on the percolation behaviour of the network, simulations were run for systems of various sizes while the number of particles per unit area and the maximum connection length were kept constant. The simulations were run for systems of 1×1, 2×2, 4×4, and 8×8 length units (*Figure 7.5*). A system of size 8×8 has 25600 nodes. Even in the case of a conservative estimate this is less than the number of particles in a 5×5 μm nanoparticle scaffold, and considerably less than the number of particles in a system larger than 5×5 μm, or with smaller nanoparticles. However, simulated systems of a more realistic size could not be handled by this setup, limiting the size of our simulated networks to 8×8 length units.

The systems of various sizes all behave like percolation networks. However, there are a few differences between networks of different sizes. Larger networks become conductive at slightly larger values of β. This is a small shift that has very little implication for the production and no implications for the operation of a sensor based on such a network. For the sensor it is important that there is a percolation threshold, but not at which value of β this threshold occurs. The sensor can be produced such that it operates close to the percolation threshold, independent of the value of β for which the threshold occurs. Furthermore, larger networks have a slightly decreased maximum conductance compared to smaller networks. This is due to the fact that a larger network has more connections between the electrodes, meaning more resistors, and thus a lower maximum conductance.

Because of the similarities between the systems of different sizes, we can assume that despite the small differences between those networks, networks that are larger than 8×8

length units will behave in a similar way. This indicates that this concept should work on the size scale of the nanoparticles scaffolds described in chapter 5.

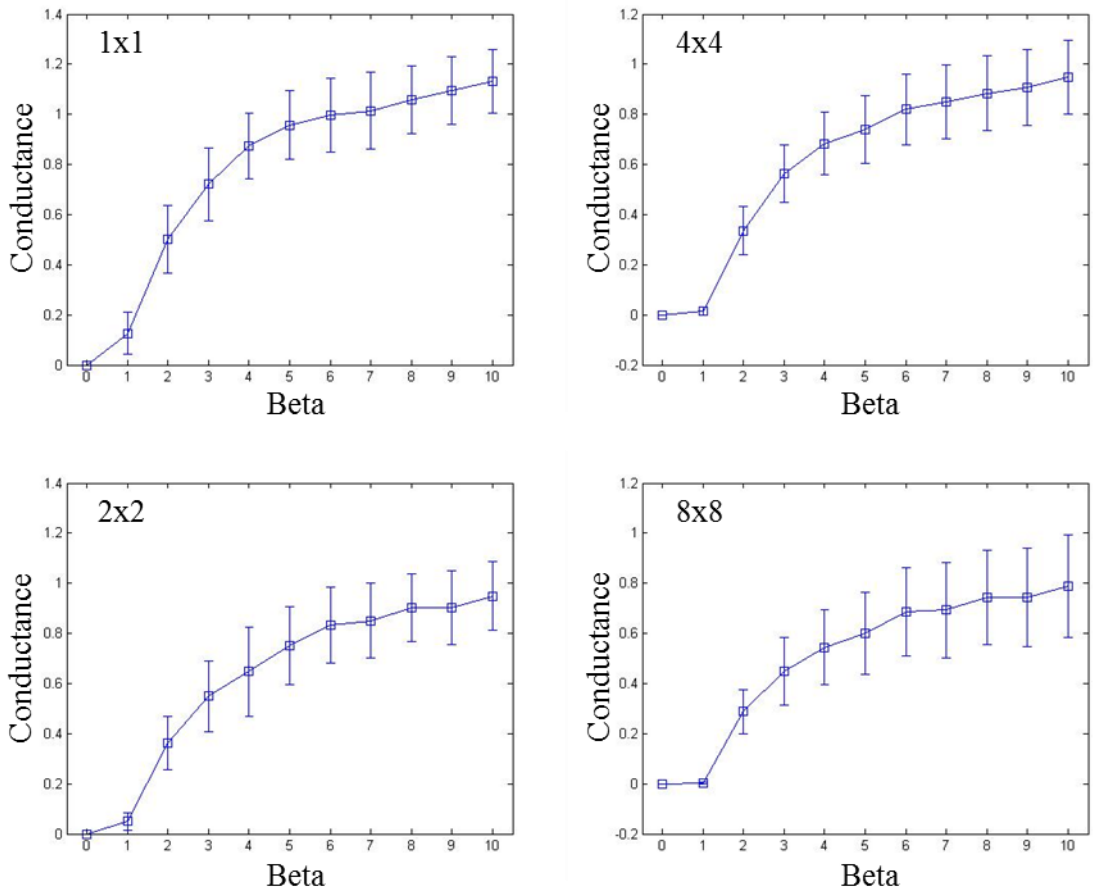


Figure 7.5: Conductance versus beta for random networks with a size of 1×1, 2×2, 4×4, and 8×8 length units. The differently sized networks are all percolation networks. However, the total conductance through larger networks is lower because there are more resistors between the two electrodes. Furthermore, the percolation threshold shifts to higher values of β for larger networks because more connections are needed to connect the electrodes.

7.4 Maximum connection length

The maximum connection length between the nodes is another important variable. In the physical system this corresponds to the maximum distance between the nanoparticles that can be bridged by the polymers. This is less important in networks where the polymers are grown onto the nanoparticle scaffold from a solution of monomers, or when multiple polymer chains can together form one connection.

Starting at one extreme end of the scale, it is clear that if the connections are very short, relative to the distance between the nodes, they cannot connect the nodes. In that case there is no network, and thus no conductance between the two electrodes (*Figure 7.6*). When the connections are longer, a network is formed that behaves as expected from a percolation network. When the connections are very long, there are connections that nearly directly connect the two electrodes (*Figure 7.7*). This causes a large amount of background conductance, which would make it difficult to detect any changes in conductance due to a percolation effect if such a network would be used as a sensor. Furthermore, for longer connections, the percolation threshold shifts to a smaller value of β because fewer connections are needed to connect the two electrodes.

Even at high values of the maximum connection length, there still is a percolation effect because the code uses the maximum connection length instead of the length required to connect nearby nodes. This means that in addition to the very long connections there are shorter connections, and those still cause the system to behave like a percolation network, despite the larger background signal. This is an extreme case and is not realistic for the physical system, because such a large spread in connection lengths is not realistic. Furthermore, this situation is avoidable by matching the electrode to nanoparticle separations and the polymer chain length.

Networks based on regular lattices respond in a similar way to changes in the maximum connection length as those based on random networks. However in the case of the regular lattices there is a finite number of solutions (*Figure 7.8)*. The connection lengths required to make connections in the network are always the same because the lattices and thus the distances between the nodes are regular. The number of solutions and the length of the connections needed for each of those solutions can be found for each lattice. In the case of random networks, the positions of the nodes and thus the lengths of the connections needed to connect the nodes and form a network are random. For this reason there is no finite number of solutions for random networks. It is also interesting to note that for a square lattice with a maximum connection length of 0.07 there is no strong percolation effect. This is due to the geometry of this particular network, resulting in a conductance change similar to that expected for two electrodes that are directly connected by a large number of parallel wires that do not form a network.

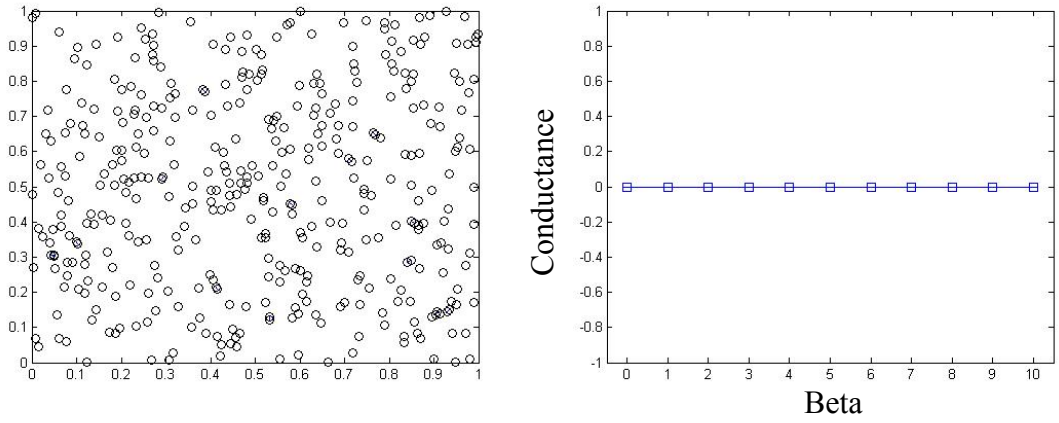


Figure 7.6: Simulations of randomly distributed nodes and a maximum connection length of 0.01 of a length unit. These connections are too short to connect enough nodes to form a network. There is no conductance between the electrodes.

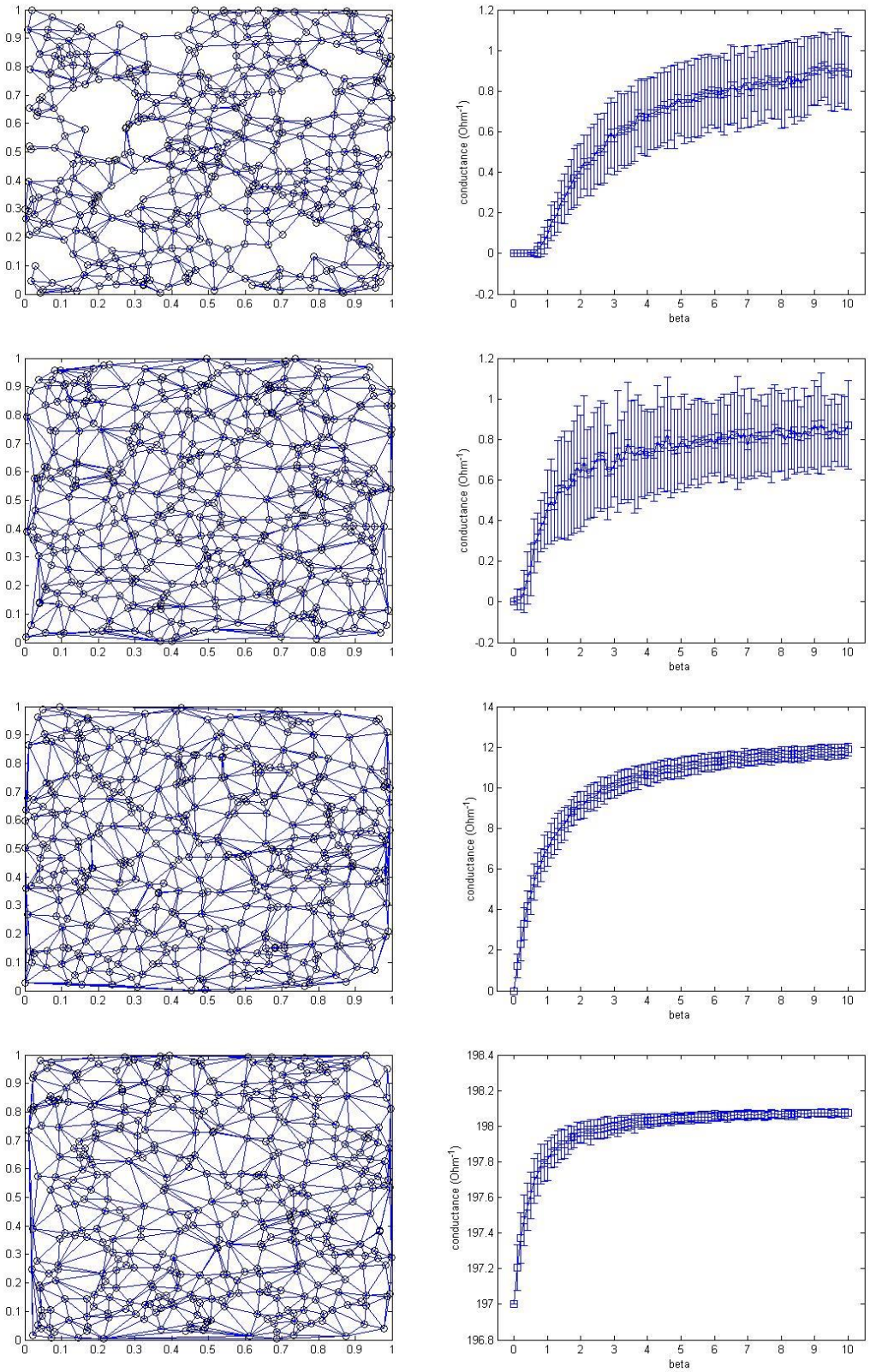


Figure 7.7: A random network (left) and the conductance through the network for different values of beta (right) at different maximum connection lengths: (from top to bottom) 0.1, 0.3, 0.5, and 0.99. In addition to a large background conductance, longer connections cause the percolation threshold to shift to lower values of β.

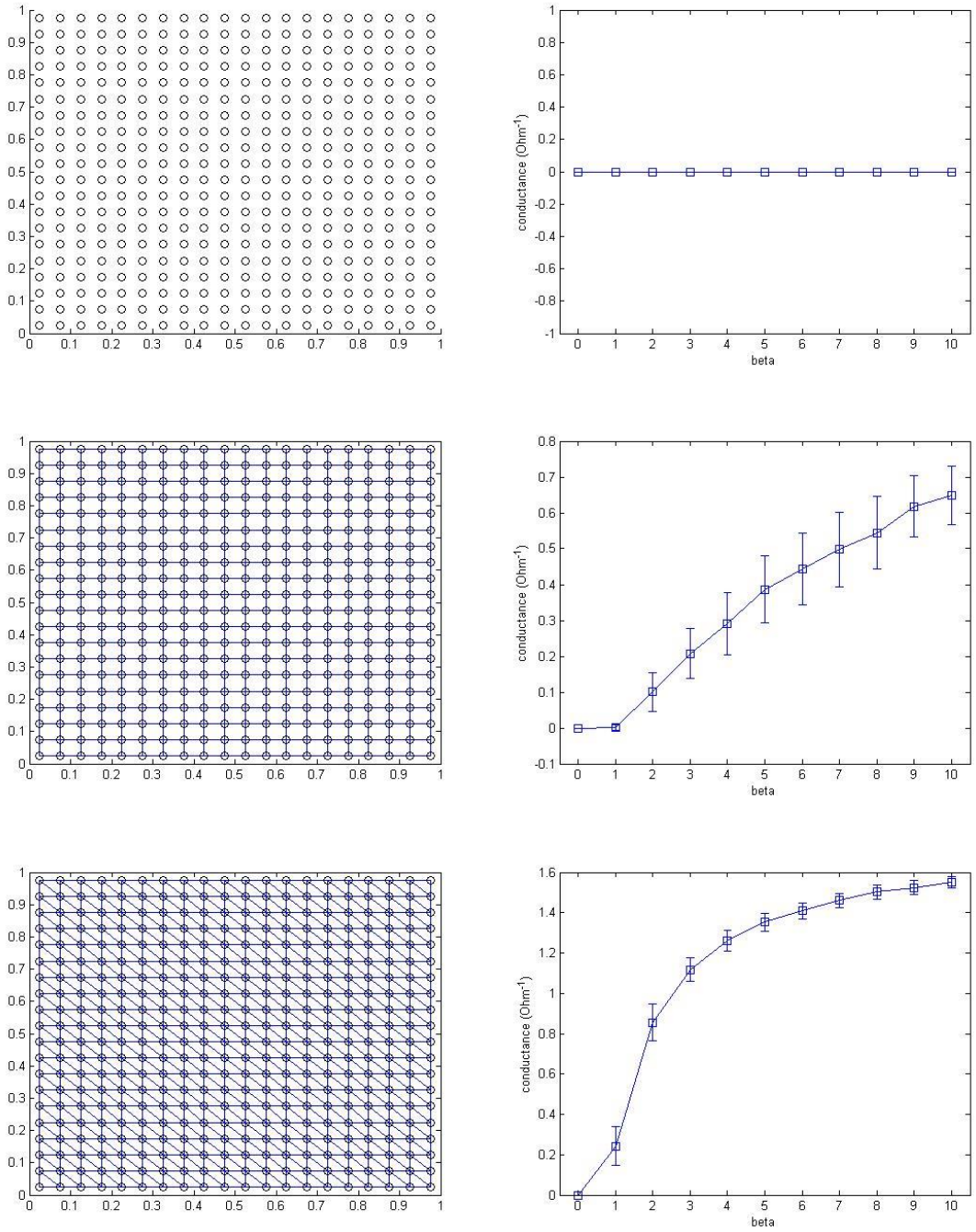


Figure 7.8: Simulations of a square lattice for different maximum connection lengths: (from top to bottom) 0.04, 0.07, and 0.08. A connection length of 0.04 is too short to form connections between the nodes, this means that there is no network. For longer connection lengths percolation networks can be formed. Because the network is based on a regular lattice, there are a number of discrete solutions for different networks that can be formed.

7.5 Change in conductance upon interaction

For the simulations in this chapter it was assumed that upon interaction with an analyte molecule the conductance through the interacting polymer molecule becomes zero. However, in the physical system this is not the case. In the physical system, upon interaction with an analyte molecule the conductance through the bond is changed but not completely switched off. It depends on various factors, including the properties of the polymer and the interaction between the polymer and the analyte molecule, and how big the change in conductance through a connections is.

In the simulations in this section the amount of change in conductance through a single bond upon interaction is varied (*Figure 7.9*). Here 0.0 indicates that the bond is completely switched off, there is no conductance through this bond, and 1.0 means that the conductance is not changed when there is interaction with an analyte molecule. As expected there is no change in conductance when 1.0 is used. The conductance changes with β for a percolation network for values smaller than 1.0. When the change in conductance upon interaction is such that the interacting connection is not completely switched off, the conductance of the network can never be completely quenched. Even for very small β the conductance is larger than zero. Note that the curves are similar to the curve for a maximum connection length of 0.99 in figure 7.7, in which case there also is a background conductance.

At first glance the shape of the curves in *Figure 7.9* for low values of β, other than $\beta = 0$, looks different from what would be expected. However, zooming in on the $0 \leq \beta \leq 1$ interval shows that the percolation threshold has only been shifted to lower values of β (*Figure 7.10*). This is most likely due to the way in which the code handles connections that have been switched of and can potentially be added to the network. This could be improved in future simulations by using simulations that distinguish between network formation and

molecular adsorption, instead of making use of the ratio of the rate at which connections are made and the rate at which connections are broken.

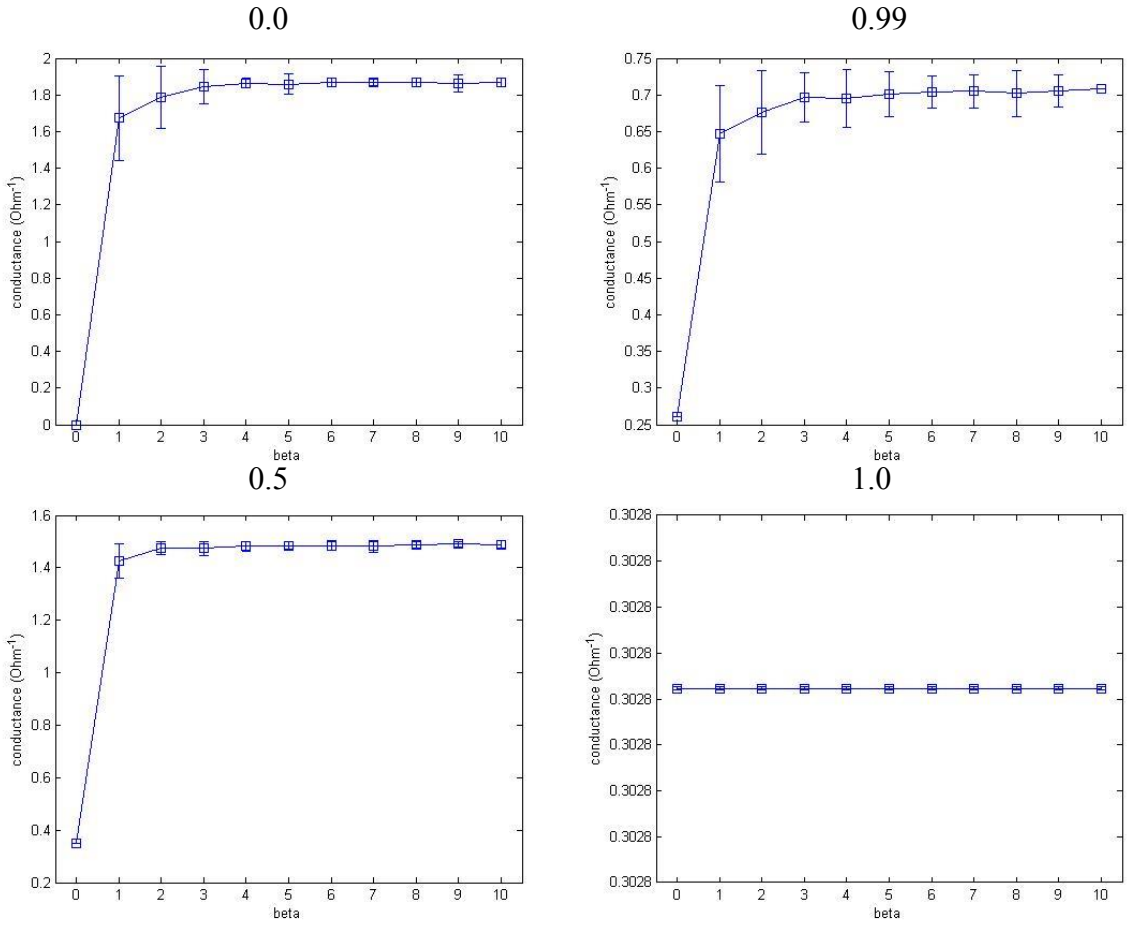


Figure 7.9: Beta versus conductance for different interaction strengths. Where 0.0 means that a connection is completely switched off upon interaction with an analyte molecule, and 1.0 means that the conductance is not changed by the presence of analyte molecules. A partial resistance change upon interaction causes a background signal, the conductance can never be completely quenched. If there is no change upon interaction, as in the 1.0 case, the conductance does not change at all.

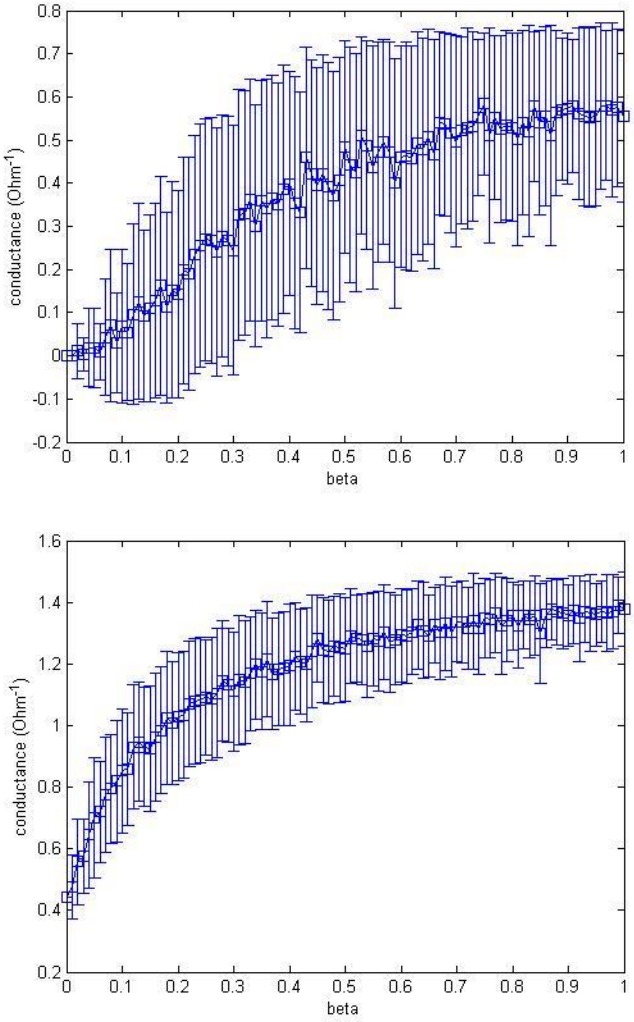


Figure 7.10: Beta versus conductance for a 0.0 conductance though a closed connection (top) and a 0.9 conductance through a closed connection (bottom). Points are taken at 0.01 intervals for $0 \leq \beta \leq 1$. Focusing on this β interval illustrates that networks with a larger conductance through a closed bond have a percolation threshold at a lower β.

7.6 Dynamics

To study the behaviour of a sensor based on a percolation network of conductive polymers while it is interacting with an analyte vapour, changes in conductance during interaction have to be calculated. In that case there is a dynamic equilibrium of analyte molecules coming and going, or connections being broken and connections being made, influencing the conductance through the network over time.

To calculate the conductance over time the parameters α and β are kept constant. The value of β, the rate at which connections are made, is chosen close to the percolation threshold as determined by the simulations earlier in this chapter, for example β=2. The value of α, the rate at which connections are broken, was varied from 0 to 5. The ratio of α and β is equivalent to the dwell time of the analyte molecule on the network. In the physical system this depends on the properties of the analyte molecule and the polymer. Running the simulations for various values of α gives the conductance over time for various dwell times (*Figure 7.11*).

When α is 0, there are no analyte molecules interacting with the network. This is equivalent to the state of the sensor before it starts to interact with analyte molecules. For other values of α, analyte molecules interact with the network and leave again. For α equals 1 and 2, the conductance decreases upon interaction, as expected, and as the analyte molecules leave again the conductance increases again. For larger values of α analyte molecules arrive on the network at a higher rate than they leave again, causing the conductivity to be quenched.

This effect is the same for random networks and networks based on regular lattices. However, the dynamic equilibrium of regular lattices looks slightly less random than that of

the random lattices. In the case of regular lattices there seem to be peaks, instead of completely random fluctuations, as shown in *Figure 7.12*.

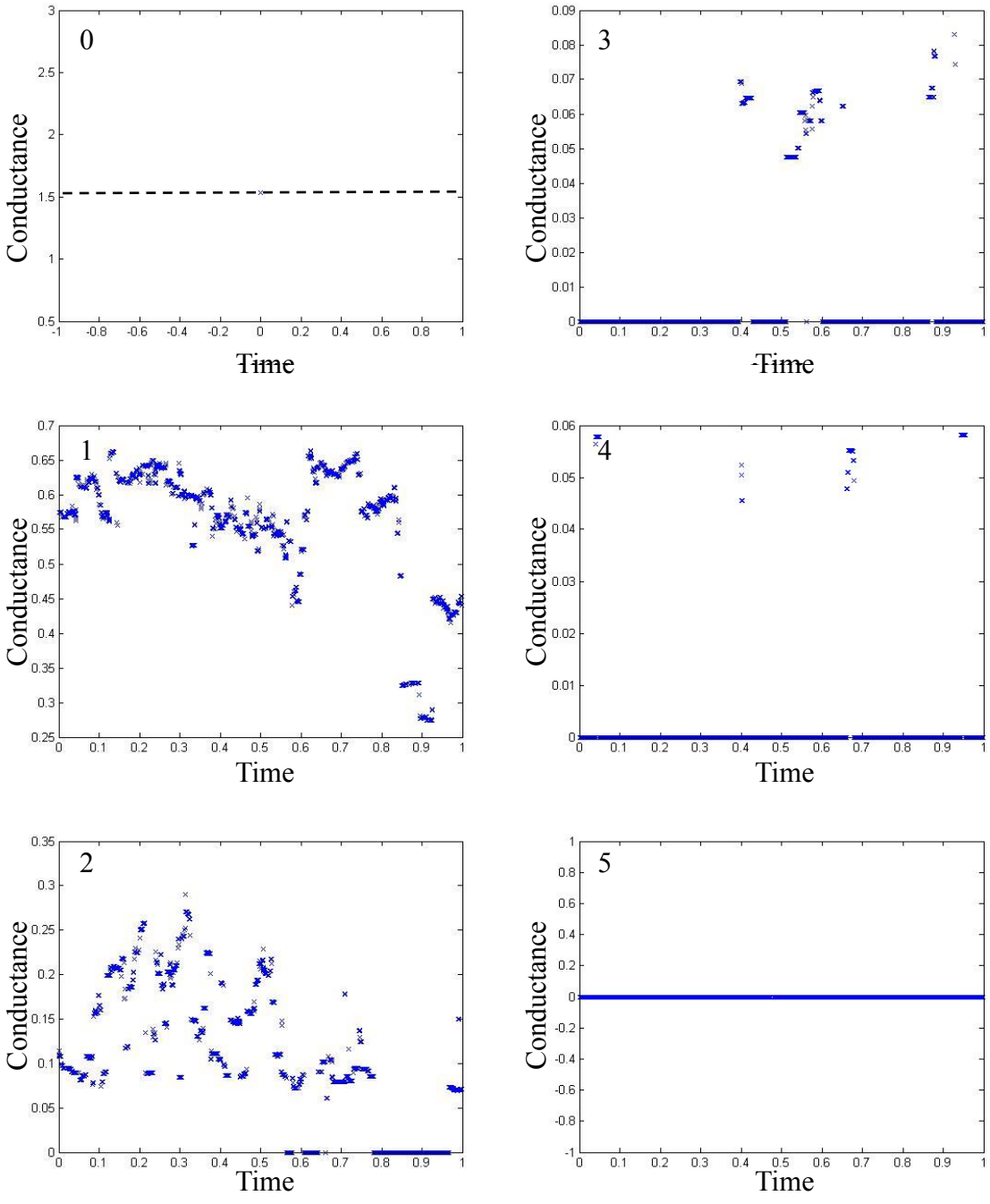


Figure 7.11: The conductivity over time for various values of alpha, ranging from 0 to 5. Beta is fixed at 2. The dashed line in the alpha equals 0 case represents the static situation caused by the lack of interacting analyte molecules, as described by alpha equals 0. The conductance decreases with increasing alpha, until the conductance is completely quenched.

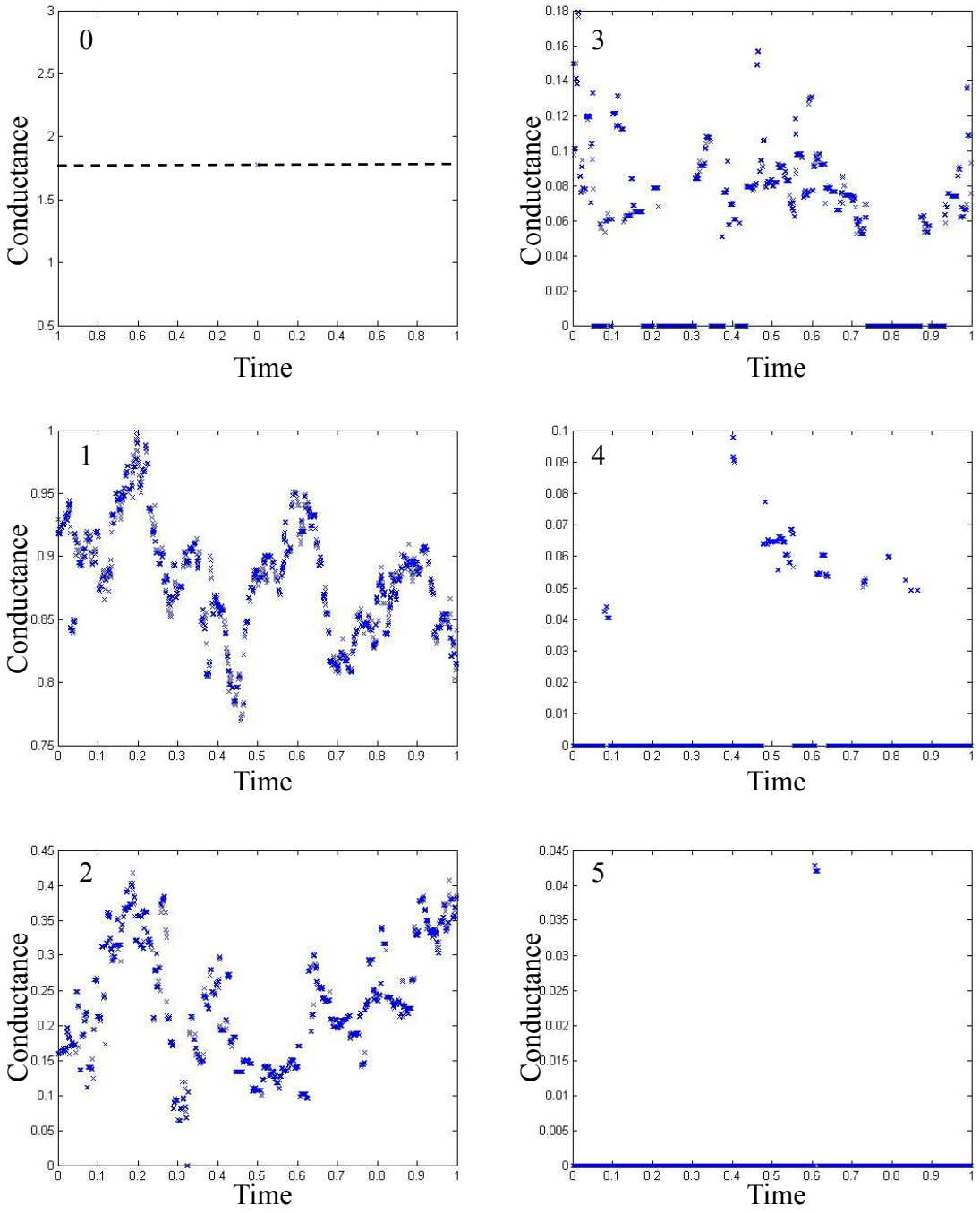


Figure 7.12: Simulations for square lattices giving the conductance over time for a dynamic equilibrium of bonds opening and closing, for α ranging from 0 to 5 and β=2. The dashed line in the alpha equals 0 case represents the static situation caused by the lack of interacting analyte molecules, as described by alpha equals 0. The conductance decreases with increasing α, until the conductance is completely quenched.

7.7 Summary and outlook

A sensor based on a percolation network of conductive polymers was simulated. Simulations were run for networks with random node distributions, as well as square, hexagonal and triangular lattices with and without added noise. The influences of various parameter on the behaviour of the systems were studied.

The node distribution was studied because the random networks used for the initial simulations were more random than the nanoparticle scaffolds created in the laboratory. Networks based on various node distributions can all behave as percolation networks. Some small differences in the critical probability and maximum conductance of these networks were observed. This confirms that networks based on the randomly distributed gold nanoparticles described in chapter 5 are suitable as the basis of a sensor based on a percolation network of conductive polymers. To make future simulated networks more similar to the nanoparticle scaffolds, information from SEM images of the nanoparticles scaffolds could be used to create networks for simulations. This information could, for example, be in the form of a distribution function or coordinates extracted from SEM images.

The system size was studied because a realistic nanoparticle scaffold is larger than most simulated networks. These simulations showed that despite small changes in the critical probability and the maximum conductance, larger networks are very similar to smaller ones, indicating that also beyond the size limit of the simulations in this chapter percolation behaviour is expected. This means that the size of the conductive polymer percolation networks described in chapter 6 will not affect the operation of the sensor, as long as the network itself is close to the percolation threshold.

As expected, when the maximum connection length is varied, the connections within the network are varied. When the maximum connection length is too short, there is no network and thus no conductance. Longer connections allow for a network to form. When the connections are too long, there is a background conductance in addition to the changes in conductance around the percolation threshold.

For most simulations the bonds between the nodes are completely switched off and on upon interaction with and dissociation of an analyte molecule. However, further simulations have shown that when there is a partial change in conductance through a bond upon interaction the percolation effect still holds as expected. However, when there is a partial change in conductance upon interaction there is a background conductance. In that case, even when all connections are interacting with analyte molecules simultaneously the conductance can never be zero. This shows that the concept of the percolation network based sensor still holds in a more realistic case, in which the conductance through a connection changes upon interaction, but is not completely switched off.

Finally, the conductance was calculated over time while the network is in a dynamic equilibrium with analyte molecules interacting with the network and dissociating again. This was simulated for various dwell times. This can be interpreted as exposing the sensor to an increasing analyte molecule concentration (an increasing α/β ratio). Resulting in a decreasing conductance for an increasing analyte concentration, until the sensor is completely flooded with analyte molecules (as will also be demonstrated for the sensors described in chapter 8).

To conclude, a sensor based on a percolation network of conductive polymers was simulated and the influence of various parameters on the conductance through the network was studied. Future work should focus on making the simulations more similar to the sensors

studied in the laboratory. This could for example be done by using SEM images of the nanoparticles scaffolds to obtain more realistic node distributions, and by including more details, for example by including information about specific polymers and their interactions with specific analyte molecules, or by giving the nodes a finite size. Furthermore, simulations will be set up in such a way that it is possible to distinguish between network creation and molecular adsorption on an existing network.

Chapter 8

Sensor testing

The aim of this thesis is to develop a vapour sensor based on a percolation network of conductive polymers (*Figure 8.1*). By using a percolation network, instead of a polymer thin film, a more sensitive sensor can be developed. This sensor was described using simulations in chapter 7. In this chapter the sensor, of which the development was described in chapters 5 and 6, will be tested. The sensors will be exposed to a range of ammonia concentrations. Furthermore, sensors with different polymer coverages, ranging from close to the percolation threshold to a polymer thin film, will be compared.

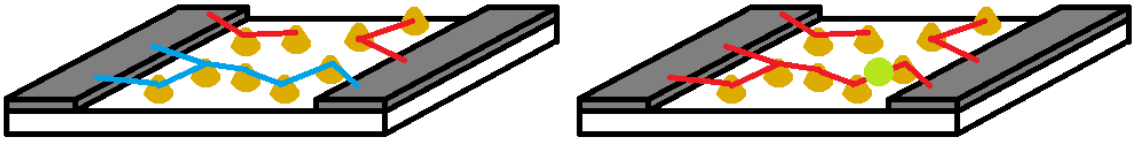


Figure 8.1: Schematic representation of a sensor based on a percolation network of conductive polymer on a gold nanoparticle scaffold (gold), between two electrodes (grey), on an insulating substrate (white), before (left) and after (right) interaction with an analyte molecule (green). Sections of the polymer network that contribute to the connection between the two electrodes are given in blue, and in red when they do not contribute to a connection between the electrodes.

8.1 Materials and Methods

Sensors were developed as described in chapters 5 and 6. First, 5 nm gold was deposited on a glass substrates with Pt interdigitated electrodes (IDEs) with a 5 μm separation, after which the sample was annealed at 200 ºC for 1 hour (see chapter 5). A 5 nm gold film was used because this is thin enough to always result in dewetted samples with a resistance larger than approximately 100 MΩ after annealing. This allows us to measure the resistance of the conductive polymer network.

Next, a conductive polymer was electrochemically deposited on the samples, as described in chapter 6. Samples with different polymer coverages were created by chronoamperometric deposition of polypyrrole (PPY) for 3 to 60 seconds. PPY was used as the conductive polymer because a range of polymer coverages, from close to the percolation threshold to a thin film can be achieved with PPY. Furthermore, PPY-based sensors are known to respond to ammonia[123], the analyte vapour used for the work described in this chapter.

Ammonia was chosen as the analyte vapour for these experiments because it is easily available at a large range of concentrations, and can be safely used in a laboratory environment. Furthermore, ammonia is of interest for the detection of improvised explosive devices (IEDs) and is a useful first step towards detecting explosives that are more difficult to detect or not as easily used in a laboratory environment.

The samples were placed in the sensor testing rig (see chapter 2) under N_2 flow. After allowing the sample to stabilise in the N_2 environment, ammonia was introduced into the system, while keeping the total gas flow constant. The sensor response was monitored by applying 1 V and measuring the current through the sample. After exposing the sample to ammonia for 20 minutes, the sample was left under N_2 flow for 70 minutes to recover.

Control experiments, without ammonia present, were conducted to confirm that the observed sensor responses were not caused by other factors, such as changes in pressure or gas flow.

8.2 Results and discussion

8.2.1 Sensor response

As expected all PPY-based sensors responded to ammonia (*Figure 8.2*). The resistance of the samples increased when ammonia was introduced into the sensor testing chamber. The initial response is instantaneous. As the sensor starts to become saturated, the change in resistance slows down. Complete saturation of the sensors was not reached in the 20 minutes during which the samples were exposed to ammonia. The response time, typically defined as the time required to reach 90% of the magnitude of the response, is approximately 10 minutes for these sensors. However, this is not a particularly useful measure in this case because the maximum response of the sensors is not achieved in the 20 minutes during which the sensors were exposed to ammonia.

Furthermore, the response is reversible. Reversing the response takes longer than the response itself. When the ammonia flow is stopped and the sensor is kept under N_2 flow, the resistance decreases again. The first measurement in a series of exposures tends to start from a lower baseline than later experiments, suggesting that the sample has not fully recovered before the next exposure.

8.2.2 Ammonia concentration and limit of detection

A comparison of the sensor responses to various ammonia concentrations shows that a lower ammonia concentration causes a smaller sensor response than a larger ammonia concentration. More ammonia means more interactions with the polymer network, and thus

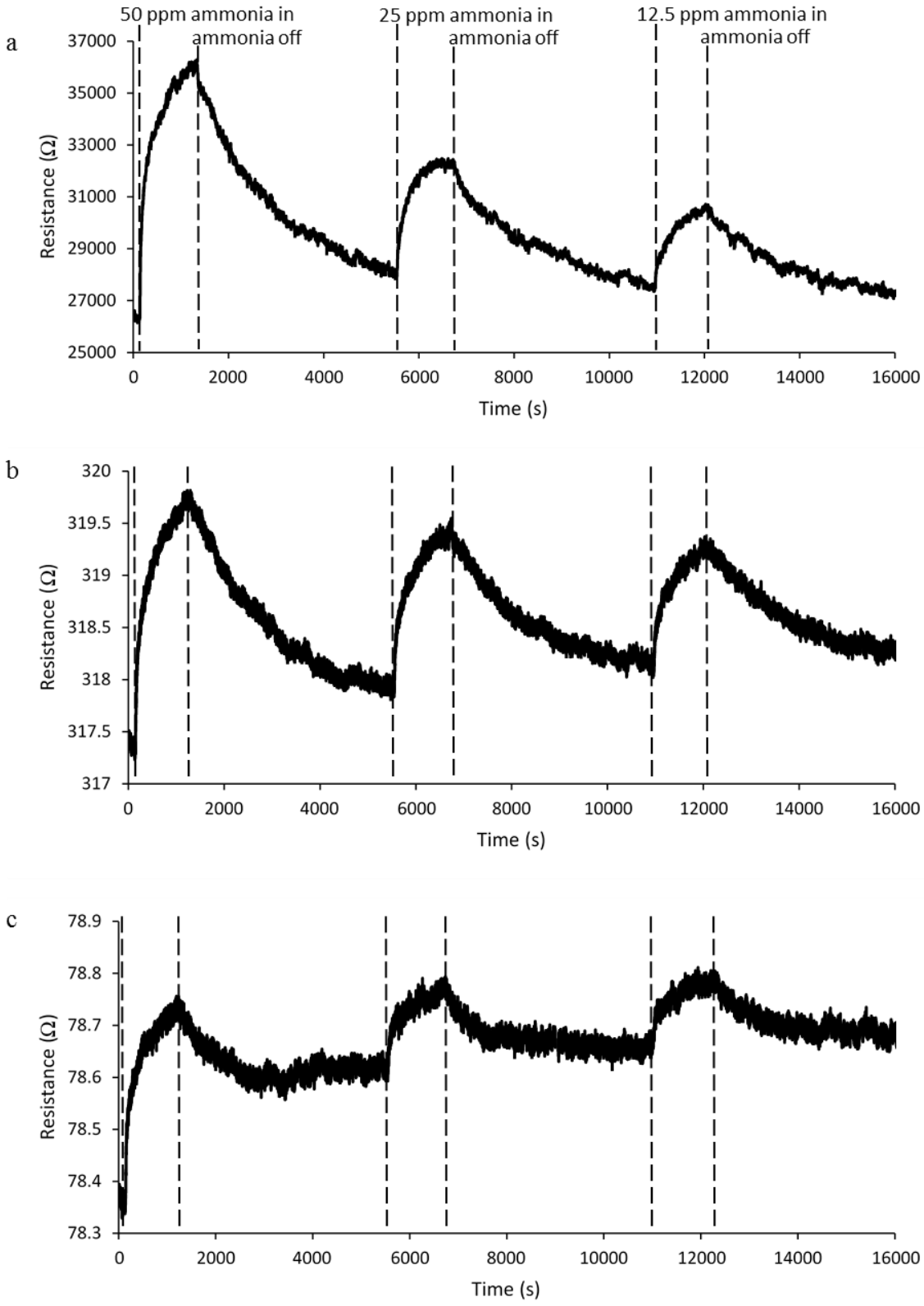


Figure 8.2: Sensor responses to, from left to right, 50, 25, and 12.5 ppm ammonia of samples with PPY chronoamperometrically deposited for a) 3, b) 5, and c) 60 s. For all 3 plots a moving average, averaging over 1 second, has been used. For all three PPY coverages the magnitude of the response decreases with decreasing ammonia concentration. Furthermore, samples with less PPY have a larger sensor response than samples with more PPY.

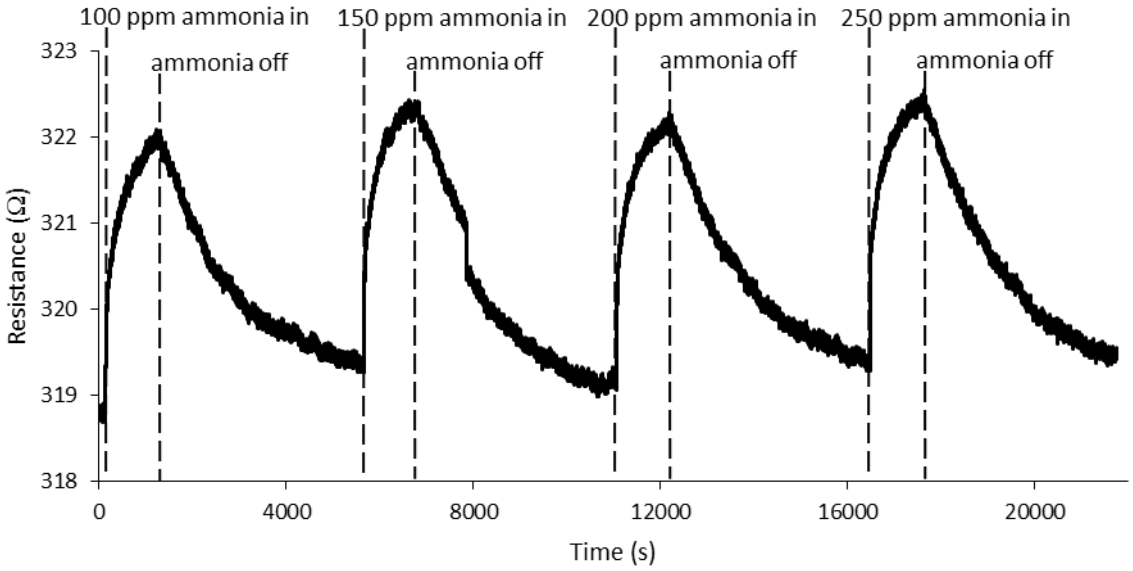


Figure 8.3: Sensor responses to, from left to right 100, 150, 200, and 250 ppm ammonia of a sample with PPY deposited using chronoamperometry for 5 seconds. A moving average over 1 second has been used. The sensor response to these ammonia concentrations does not increase with increasing ammonia concentration, indicating that at these ammonia concentrations the sensor is saturated.

a more strongly disrupted network, as expected. However, for concentrations of approximately 50 ppm and above, the sensor becomes saturated (*Figure 8.3*). Higher concentrations do not result in a larger response.

The lowest concentration used in these experiments was 12.5 ppm. This experimental limit was caused by the 500 ppm ammonia cylinder that, with the current setup, could not be diluted any further. However, the sensor response to 12.5 ppm is large enough to suggest that the sensor will be able to detect significantly lower concentrations as well.

The limit of detection of these samples was estimated by dividing 3× the standard deviation of a blank measurement, under N_2 flow and without ammonia present, by the gradient of the linear trend line through the sensing responses to 12.5-50 ppm ammonia (*Figure 8.4*). This gives an estimate of the limit of detection, here defined as the ammonia

concentration for which the sensor response will have the same magnitude as 3× standard deviation of a blank measurements, which gives a good indication of the noise. The resulting limits of detection are 0.69, 2.4, and 6.5 ppm for the 3, 5, and 60 s PPY sensors respectively. This is a very conservative estimate because only a few concentrations below the saturation limit of the sensors were tested.

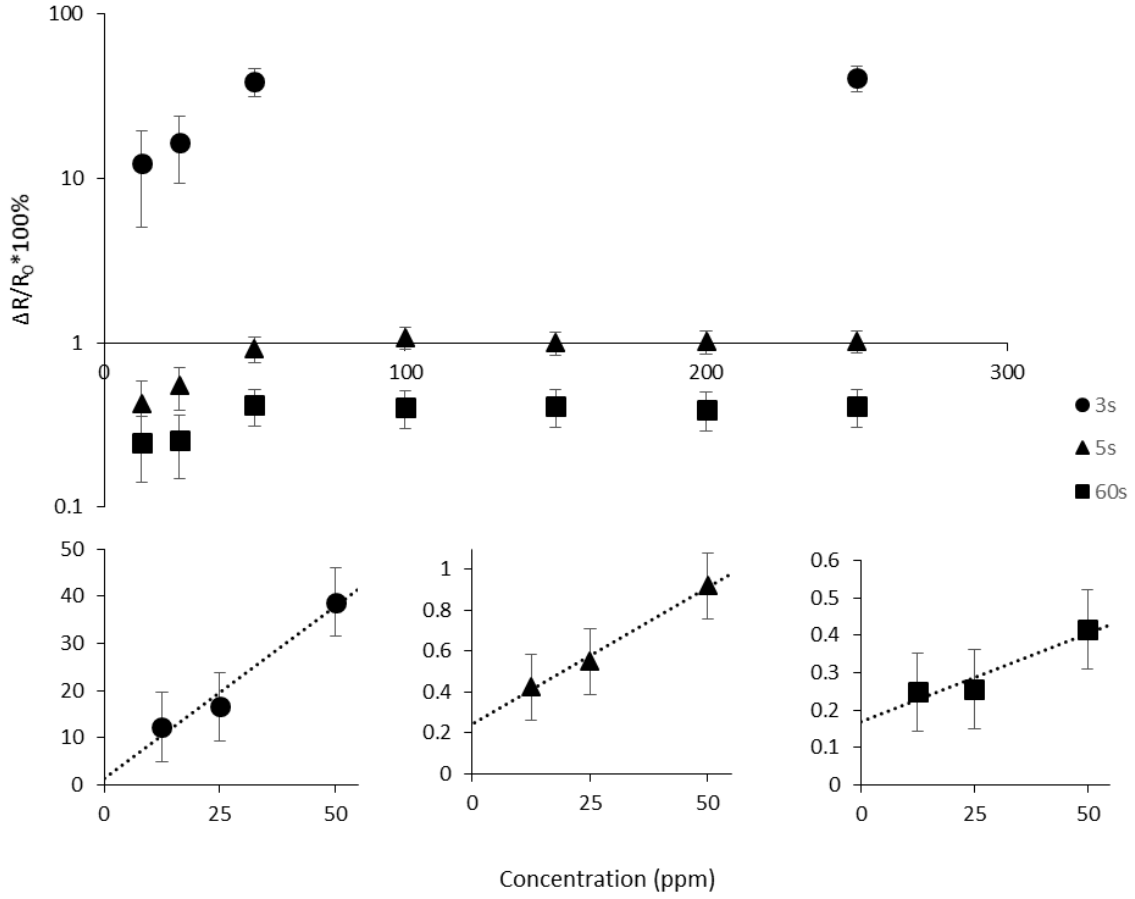


Figure 8.4: Sensor response, in percentage change with respect to the starting resistance, to 12.5-250 ppm ammonia for samples with 3, 5, and 60 s PPY. Linear trend lines were determined for the results for 12.5-50 ppm, shown in the bottom three plots. The error bars were estimated based on the sum of the standard deviation of a blank measurement for each sample and the standard deviation of repeat measurements of the response of that sample to 50 ppm ammonia.

8.2.3 Percolation network vs. thin film

Comparing samples with different polymer covers shows that sensors with less polymer have a much stronger response than sensors with more polymer. This shows that sensors that are closer to the percolation threshold, such as the 3 s sensor, are much more sensitive than thin film based sensors, such as the 60 s sensor. Furthermore, sensors closer to the percolation threshold recover more rapidly after ammonia exposure, have a lower predicted limit of detection, and a better signal to noise ratio than thin film based sensors.

8.3 Summary

Sensors based on a percolation network of PPY were created and their response to ammonia was tested. The PPY based sensors are responsive to ammonia. Furthermore, the sensors show a larger response to higher concentrations, up to approximately 50 ppm, after which the system is saturated. The response to ammonia is reversible.

A comparison of samples with different polymer coverage shows that samples with less polymer, which are closer to the percolation threshold, are much more sensitive than samples with more polymer, which are thin film like. This shows that a sensor operated close to the percolation threshold is much more sensitive than a sensor based on a conductive polymer thin film.

Future experiments will be aimed at testing the sensor at lower analyte concentrations and providing a more accurate estimate of the limit of detection. Furthermore, the response of different conductive polymers will be tested to different analyte vapours. The recovery time might be improved by heating the sample during recovery. And the effect of temperature and humidity on the sensor will be investigated. Finally, to improve the selectivity of the sensor, a combination of sensors, using different or differently functionalised polymers, can be used to create an electronic nose type device.

Chapter 9

Summary

Explosives detection is important for many, both military and civilian, applications. However, explosives detection remains challenging, especially because of the low vapour pressures of explosive materials. The work described in this thesis is aimed at developing a small and extremely sensitive sensor for the detection of explosives vapours. This sensor is based on a percolation network of conductive polymers supported on a metal nanoparticle scaffold. By operating the sensor close to the percolation threshold a higher sensitivity can be achieved than with a more traditional polymer thin film based sensor. This thesis describes the development of the two main components of this sensor: the gold nanoparticle scaffold and the conductive polymer network. Furthermore, simulations were performed to further understand the sensor. Finally, the sensor response to ammonia was tested. Sensors with polymer coverage ranging from the thin film regime to close to the percolation threshold were compared.

The first component of a sensor based on a percolation network of conductive polymers is the metal nanoparticle scaffold. The nanoparticles act as the nodes of the conductive polymer network. Supported gold nanoparticles were created on an insulating substrate by annealing a gold thin film, which causes it to dewet into individual nanoparticles. By depositing a thicker initial gold layer larger particles can be created than when a thinner gold layer is deposited. Furthermore, by controlling the annealing time and temperature the amount of dewetting and the particle separation can be controlled. Finally, the resistance of the gold film was monitored during deposition. As expected, the resistance decreases as more gold is deposited. The observed decrease in resistance was stepwise, which can be attributed to separate sections of the film connecting to each other, until a continuous film is present between the electrodes. To our knowledge this is the first time that the resistance changes of such thin films have been studied, and the first time that the stepwise change have been observed. Further work on the gold nanoparticle scaffolds should be aimed at increasing understanding of the wetting and dewetting behaviour of the gold layer by *in situ* imaging of during gold deposition and annealing. Additionally, the resistance changes during the dewetting of such a layer could be studied using a different substrate material and higher annealing temperature, or smaller electrode separation.

The next component of the sensor is the conductive polymer layer. Initial experiments consisted of polymer deposition on insulating substrates. Later polymer was deposited on insulating substrates with gold nanoparticles. Several deposition methods, including thermal evaporation, dip-coating, spin-coating, and electrochemical polymerisation were trailed. Most of these methods resulted in polymer films that were too thick to form a percolation network. However, using electrochemical polymerisation conductive polymer networks were created, in which polymer strands form connections between the gold nanoparticles. Networks of PEDOT and PPY were created with a range of

different polymer coverages, and with resistances ranging from approximately 50 Ω to 2 MΩ. In particular, chronoamperometry of PPY was used to create PPY networks close to the percolation threshold. Future work on the conductive polymer percolation networks should be aimed at creating a networks with various polymer coverages using different polymers. The resulting data can be used to produce percolation graphs for networks of various conductive polymers.

Simulations of a sensor based on a percolation network of conductive polymers were used to gain further understanding of a sensor based on a percolation network. Conductive networks were simulated and the resistance through the networks was calculated. The influence of parameters, such as node distribution, connection length, system size, strength of the change of the conductivity of one bond upon interaction, and the dynamic equilibrium while interacting for different dwell times, were studied. The simulations confirmed that a sensor operated at the percolation threshold is more sensitive than traditional polymer thin film based sensors. Furthermore, the simulations showed that networks with random node distributions and a system size similar to those of the nanoparticles scaffolds described in chapter 5 are suitable for a sensor based on a percolation network. Further work on the simulations should be aimed at making the sensor more similar to the physical system, so that the simulations can be used to further optimise the physical system. For example by using information from the SEM images of the nanoparticle scaffolds to create networks for simulations, by including information about specific polymers and their interaction with specific analyte materials. Futhermore, simulations should be set up in such a way that it is possible to distinguish between the creating of a percolation network and molecular adsorption on an existing network.

Finally, the response of sensors with PPY networks on gold nanoparticles, to various concentrations of ammonia, was tested. The sensor response to ammonia was instantaneous and reversible. A comparison of sensors with different PPY coverages showed that sensors with less polymer, being closer to the percolation threshold, are significantly more sensitive than those in the thin film regime, proving the concept of a percolation sensor. Furthermore, the sensors had a stronger response to higher ammonia concentrations, as expected, but were saturated for concentrations higher than approximately 50 ppm. Due to limitations of the equipment, the lowest concentration at which the sensor was tested was 12.5 ppm. The response to 12.5 ppm ammonia was sufficiently strong to suggest that the percolation sensor will respond to much lower concentrations as well.

The work described in this thesis has shown that vapour sensors operated close to the percolation threshold are more sensitive than vapour sensors operated closer to the thin film regime. This opens up opportunities for significant improvements on existing polymer thin film based sensors. To further develop vapour sensors based on a percolation network, future work should be aimed at testing a range of different polymers and testing their response to various analyte materials. The sensors should also be tested at lower concentrations and the detection limit should be determined. Furthermore, an array of sensors, all with different polymers, could be created to obtain more selectivity using an electronic nose type approach.

Chapter 10

Summary for a broad audience

This thesis describes a novel type of sensor for the detection of vapours of explosive materials. Explosives vapour detection is challenging because explosives vapours are usually only present in very small quantities. Furthermore, techniques for hiding explosives are improving, thus making it more difficult to detect them. For this reason, it is important to continue to develop more sensitive sensors. In addition, it is important to keep developing technologies to be able to decrease the sensor size and make it easier to use them for various applications. The sensor described in this thesis is based on a novel concept that allow us to make a very small and very sensitive sensor.

This summary roughly follows the outline of this thesis: starting with background of explosives detection, followed by an explanation of the sensor concept. Next, the two main components of the sensor, the metal nanoparticles and the polymer network, are discussed, followed by simulations, and finally sensor testing.

10.1 Explosives detection

Explosives detection plays an important role in both military and civilian environments, and has many applications ranging from airport security to demining. When thinking of existing detection methods, sniffer dogs are perhaps the first that come to mind. And perhaps surprisingly, despite all modern technologies that are available, sniffer dogs are the most sensitive detection method available. However, it is not always practical to use animals; they need care and rest, can be quite intimidating, and cannot be used in every situation. Everybody also knows the bulky detection systems that are used at airports (*Figure 10.1*). Their size is a big disadvantage. A large amount of research is aimed at, not only improving existing detection methods, but also using novel and small scale materials to develop new sensor technologies.

10.2 Novel vapour sensor concept

The sensor described in this thesis makes use of small scale materials and can be developed into a small and very sensitive device. The basic principle of the sensor is based on that of a chemiresistive sensor. A chemiresitive sensor is a sensor in which changes in



Figure 10.1: Examples of well-known explosives detection methods: a sniffer dog (left) and an example of an explosives detector used at airports (right). The device in the image is based on ion mobility spectroscopy, a method in which the sample is ionised and the different ions in the sample are separated and analysed.

electrical resistance, caused by chemical interactions between the active material in the sensor and the analyte molecules, are used as a detection mechanism. There are many different types of materials that can react with the analyte molecules, so there are many different materials that can be used as the active material of the sensor. However, one group of materials that is especially interesting to use as the active materials are conductive polymers.

Polymers are very long chain molecules, consisting of repeated units. Those units are called monomers. Everyday examples of polymers include plastics, DNA, and protein molecules. Most polymers do not conduct electricity. However, some do, which makes them especially interesting for a large range of applications (*Figure 10.2*). Conductive polymers are an interesting group of materials because of the large range of different polymers that are available. This means that, the properties of the polymers can be tailored to meet the requirements of a lot of different applications. Furthermore, polymers are relatively easy to process.

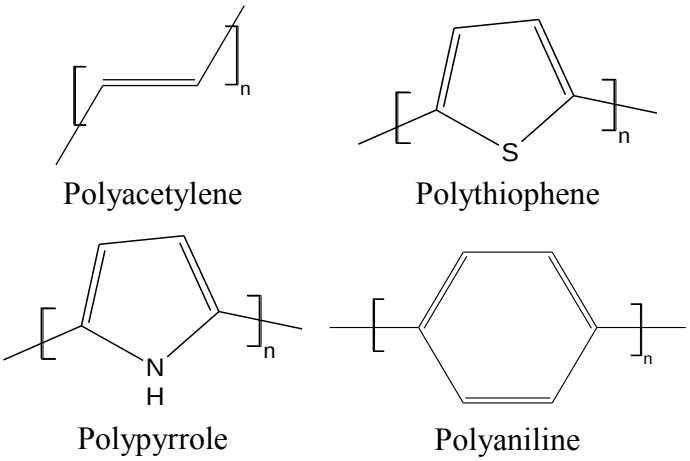


Figure 10.2: Examples of conductive polymers. For each polymer the monomer is give between brackets, which is repeated n times, where n indicates the number of times the monomer is repeated in the polymer chain.

Traditional conductive polymer based sensors make use of a thin film of conductive polymer between two electrodes (*Figure 10.3*). When an analyte molecule interacts with a polymer molecule in a thin film based sensor, the resistance of the polymer changes which changes the overall resistance of the polymer film.

The aim of the work described in this thesis is to develop a more sensitive sensor by using a percolation network of conductive polymer, instead of a polymer film. A percolation network is a network that is close to the percolation threshold. If there are no connections in a network, below the percolation threshold, electricity cannot flow from one electrode to the other. If enough connections are added to make a network that connects the two electrodes, above the percolation threshold, electricity can flow from one side of the network to the other side. Those first few connections make a big difference to the network, causing the conductivity to increase sharply. If more connections are added, the later connections have a much smaller effect on the conductivity of the sensor (*Figure 10.4*). Imagine adding 1 connection to a network that has only 10 connections, compared to adding 1 connection to a network that already has 1000 connections. It is clear which will cause a larger change to the network.

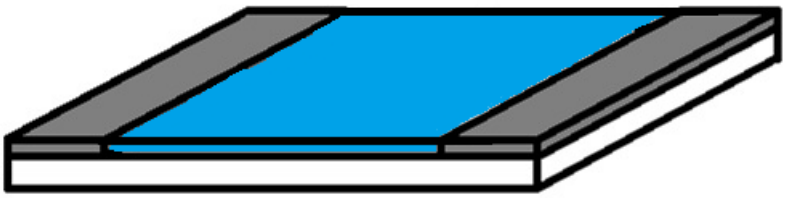


Figure 10.3: Schematic representation of a chemiresistive sensor based on a polymer thin film. The white layer is the substrate, the grey bands at the sides are the electrodes and the blue layer between the electrodes is the conductive polymer film that acts as the active part of the sensor by changing its resistance when it interacts with the explosives vapour.

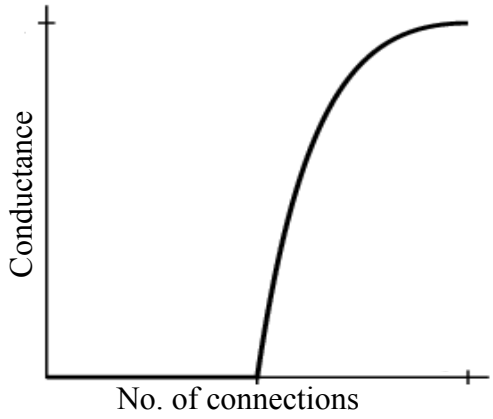


Figure 10.4: This curve gives the conductance for the number of polymer connections in the network. If there are very few connections, there are not enough connections to connect to the two electrodes so the conductivity is zero. When more connections are added the conductivity increases sharply, until it starts to level off.

This concept can be used to make a very sensitive sensor. A traditional conductive polymer thin film based sensor has a polymer layer consisting of many polymer connections. If an explosives molecule interacts with one of those many connections it will locally change the conductance of the polymer, but the effect on the film as a whole will be relatively small. However, if a sensor with a network close to the percolation threshold is used, each individual interaction has a much larger effect on the sensor as a whole. In this way it is possible to make a much more sensitive sensor (*Figure 10.5*).

10.3 Practical implementation

In practice, the sensor consists of a few different components. The basis of the sensor is an insulating substrate. Because the sensor itself makes use of changes in the conductance it is important that the substrate doesn't interfere with this, by also conducting electricity. I used SiO_2, MgO, and glass as substrate materials. On top of the substrate there are two electrodes, these electrodes are used to measure the resistance (the inverse of conductance) through the network.

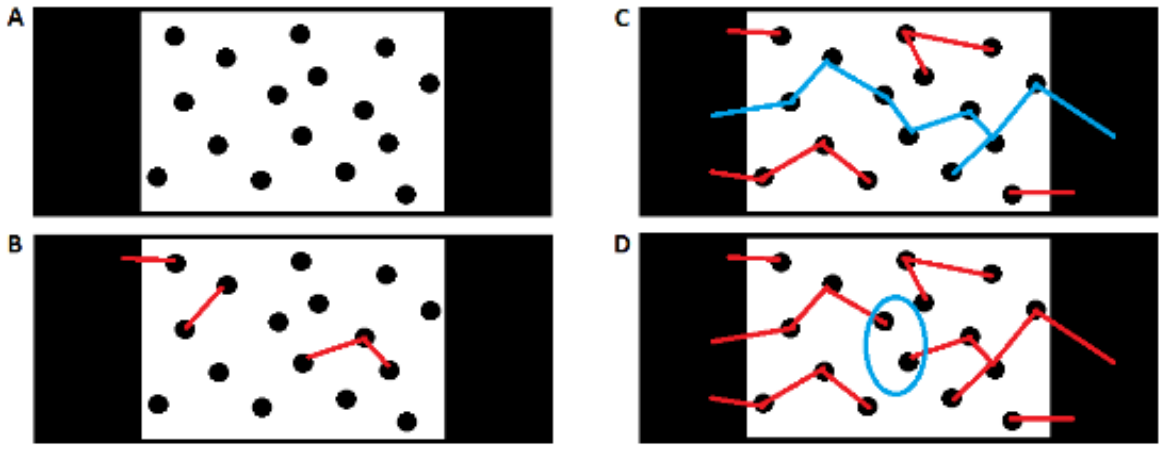


Figure 10.5: Schematic representations of a sensor based on a percolation network of conductive polymers. The black bars on the sides of each sensor are the electrodes, and the black dots are the nanoparticles that will form the nodes of the network. A) A substrate with electrodes and nanoparticles. B) A few polymer connections have been made, but not enough to connect the two electrodes. C) There are just enough polymer connections to connect the two electrodes. In this image blue lines represent polymer connections that contribute to the connection between two electrodes, whereas red lines represent polymer connections that do not contribute. D) If one of the connections is removed from the network, indicated by the blue circle, the whole network could be interrupted. This means that one small local change can have a large effect on the entire network.

First the gold nanoparticles, that form the nodes of the network, are created. Nanoparticles are particles that are a few to a few hundred nanometres in size. 100 nanometres is approximately a thousandth of the width of a human hair. In this case the gold nanoparticles are created by depositing a 5 to 20 nm layer of gold on the substrate. The sample is then heated, which causes the gold layer to separate into individual particles. The initial thickness of the gold layer and the heating time and temperature can be used to control the nanoparticle size and separation. This, as well as some interesting changes in the resistance of the gold layer during these processes, is described in chapter 5.

Next, the polymer is deposited on the gold particles. This process is described in chapter 6. Conductive polymer networks, with various quantities of polymer, ranging from networks close to the percolation threshold to polymer films, were created.

In chapter 7 simulations of a sensor based on a percolation network are described. The influence of various parameters, including the system size, connection length, and dwell time of the analyte molecules, were studied. The simulations confirmed that a sensor based on a percolation network will be more sensitive than a sensor based on a thin film.

Finally, the sensor response to ammonia was tested in a controlled environment, as described in chapter 8. A comparison of the sensor responses of sensors with different polymer covers showed that sensors with less polymer, closer to the percolation threshold, are a lot more sensitive than sensors with more polymer, a polymer film. This proves the concept of a sensor based on a percolation network of conductive polymers.

Future work will amongst others be aimed at testing the sensor at lower analyte vapour concentrations, investigating the influence of humidity and temperature on the sensor, and using different polymers and analyte vapours. Furthermore, the selectivity could be improved by using an array of sensors with different polymers.

Acknowledgements

First of all I'd like to thank my supervisor Martin Castell. Thank you for steering me in the right direction, for your support and advice (and the never ending search for 'steps'). I'd also like to thank the other members of the Surface Nanoscience group. I'd especially like to thank Yakun, with whom I shared an office and many lunch breaks. And the entire sensor group: Krish, for collaborating on the sensor project, teaching me about electrochem, and for taking the SEM images in *Figure 5.5, Figure 6.6, Figure 6.7,* and *Figure 6.8.* Ben, who will spend the next few years further developing the sensor. Tabby, who investigated the electrochemical deposition of various polymers on IDEs. And of course Chen and Shams for showing me the ropes at the start of this project.

I'm very grateful to Dstl for financially supporting this work (project number DSTLX-1000081077). I'd especially like to thank Matt Brookes, Pete Hickey, Carrina Turner, and Mike Jones for many interesting discussions and suggestions.

I'd also like to thank Sid Visser for collaborating on the simulations described in chapter 7 of this thesis, and our discussions on the modifications of the code.

I'd like to thank Chris Spencer for maintaining the UHV equipment, helping with modifications, and always replying promptly when something wasn't working the way it should.

I'd like to thank everybody else at the Materials Department. I want to thank Andrew Watt and his group for allowing me to use their equipment and lab space. I'd like to thank the SEM and AFM staff and users for support, and for teaching me how to use the equipment. I'd also like to thank Jason Smith, for being my college advisor and for many MCR/SCR dinners.

Finally, this thesis would not have been possible without everybody who supported (and distracted) me in more casual settings: specifically the Oxford University Women's Boat Club 2014 and 2016 Boat Race squads, my Mansfield College Boat Club friends, non-rowing friends, housemates, and family.

References

1. Steinfeld, J. I.; Wormhoudt, J., Explosives detection: a challenge for physical chemistry. *Annual review of physical chemistry* **1998,** *49* (1), 203-232.
2. JEOL, JEOL JSPM-4500S/TM-51021 user manual. **2004**.
3. Fischer, C., CreaTec Fischer SFC-H-5-SH user manual. **2000**.
4. Lu, C.; Czanderna, A. W., *Applications of piezoelectric quartz crystal microbalances*. Elsevier: 2012.
5. JEOL, JEOL indirect heating holder TM-51320 instruction manual. **1996**.
6. Hall, D. B.; Underhill, P.; Torkelson, J. M., Spin coating of thin and ultrathin polymer films. *Polymer Engineering & Science* **1998,** *38* (12), 2039-2045.
7. Yimsiri, P.; Mackley, M., Spin and dip coating of light-emitting polymer solutions: Matching experiment with modelling. *Chemical engineering science* **2006,** *61* (11), 3496-3505.
8. Smith, K. C.; Wells, O. C.; McMullan, D., The fiftieth anniversary of the first applications of the scanning electron microscope in materials research. *Physics Procedia* **2008,** *1* (1), 3-12.
9. Seiler, H., Secondary electron emission in the scanning electron microscope. *Journal of Applied Physics* **1983,** *54* (11), R1-R18.
10. Lloyd, G. E., Atomic number and crystallographic contrast images with the SEM: a review of backscattered electron techniques. *Mineralogical Magazine* **1987,** *51* (359), 3-19.
11. Binnig, G.; Quate, C. F.; Gerber, C., Atomic force microscope. *Physical review letters* **1986,** *56* (9), 930.
12. Meyer, E., Atomic force microscopy. *Progress in surface science* **1992,** *41* (1), 3-49.
13. Garcia, R.; San Paulo, A., Attractive and repulsive tip-sample interaction regimes in tapping-mode atomic force microscopy. *Physical Review B* **1999,** *60* (7), 4961.
14. Giessibl, F. J.; Quate, C. F., Exploring the nanoworld with atomic force microscopy. *Physics today* **2006,** *59* (12), 44.
15. Hallowell, S. F., Screening people for illicit substances: a survey of current portal technology. *Talanta* **2001,** *54* (3), 447-58.
16. Singh, S., Sensors—an effective approach for the detection of explosives. *Journal of hazardous materials* **2007,** *144* (1), 15-28.
17. Moore, D. S., Recent Advances in Trace Explosives Detection Instrumentation. *Sense Imaging* **2007,** *8*, 9-38.
18. Toal, S. J.; Trogler, W. C., Polymer sensors for nitroaromatic explosives detection. *Journal of Materials Chemistry* **2006,** *16* (28), 2871-2883.
19. Urbanski, T., Chemistry and Technology of Explosives Vol. 1. 1964.
20. Parmeter, J. E. In *The challenge of standoff explosives detection*, Security Technology, 2004. 38th Annual 2004 International Carnahan Conference on, IEEE: 2004; pp 355-358.
21. Senesac, L.; Thundat, T. G., Nanosensors for trace explosive detection. *Materials today* **2008,** *11* (3), 28-38.
22. Walker, D. B.; Walker, J. C.; Cavnar, P. J.; Taylor, J. L.; Pickel, D. H.; Hall, S. B.; Suarez, J. C., Naturalistic quantification of canine olfactory sensitivity. *Applied Animal Behaviour Science* **2006,** *97* (2), 241-254.
23. Furton, K. G.; Myers, L. J., The scientific foundation and efficacy of the use of canines as chemical detectors for explosives. *Talanta* **2001,** *54* (3), 487-500.

24. Quignon, P.; Rimbault, M.; Robin, S.; Galibert, F., Genetics of canine olfaction and receptor diversity. *Mammalian Genome* **2012,** *23* (1-2), 132-143.
25. Otto, J.; Brown, M. F.; Ill, W. L., Training rats to search and alert on contraband odors. *Applied animal behaviour science* **2002,** *77* (3), 217-232.
26. Shaw, J. A.; Seldomridge, N. L.; Dunkle, D. L.; Nugent, P. W.; Spangler, L. H.; Bromenshenk, J. J.; Henderson, C. B.; Churnside, J. H.; Wilson, J. J., Polarization lidar measurements of honey bees in flight for locating land mines. *Optics express* **2005,** *13* (15), 5853-5863.
27. King, T. L.; Horine, F. M.; Daly, K. C.; Smith, B. H., Explosives detection with hard-wired moths. *IEEE Transactions on Instrumentation and Measurement* **2004,** *53* (4), 1113-1118.
28. Collin, O. L.; Niegel, C.; DeRhodes, K. E.; McCord, B. R.; Jackson, G. P., Fast Gas Chromatography of Explosive Compounds Using a Pulsed-Discharge Electron Capture Detector*. *Journal of forensic sciences* **2006,** *51* (4), 815-818.
29. Collin, O. L.; Zimmermann, C. M.; Jackson, G. P., Fast gas chromatography negative chemical ionization tandem mass spectrometry of explosive compounds using dynamic collision-induced dissociation. *International Journal of Mass Spectrometry* **2009,** *279* (2), 93-99.
30. Bertsch, W., Two-Dimensional Gas Chromatography. Concepts, Instrumentation, and Applications–Part 1: Fundamentals, Conventional Two-Dimensional Gas Chromatography, Selected Applications. *Journal of High Resolution Chromatography* **1999,** *22* (12), 647-665.
31. Stefanuto, P.-H.; Perrault, K. A.; Focant, J.-F.; Forbes, S. L., Fast Chromatographic Method for Explosive Profiling. *Chromatography* **2015,** *2* (2), 213-224.
32. Moore, D. S., Instrumentation for trace detection of high explosives. *Review of Scientific Instruments* **2004,** *75* (8), 2499-2512.
33. Mullen, C., Detection of explosives and explosives-related compounds by single photon laser ionization time-of-flight mass spectrometry. *Analytical chemistry* **2006,** *78* (11), 3807.
34. Ewing, R. G.; Atkinson, D. A.; Clowers, B. H., Direct real-time detection of RDX vapors under ambient conditions. *Analytical chemistry* **2013,** *85* (1), 389-97.
35. March, R. E., An introduction to quadrupole ion trap mass spectrometry. *Journal of mass spectrometry* **1997,** *32* (4), 351-369.
36. Tam, M., Secondary electrospray ionization-ion mobility spectrometry for explosive vapor detection. *Analytical chemistry* **2004,** *76* (10), 2741.
37. Tabrizchi, M.; ILbeigi, V., Detection of explosives by positive corona discharge ion mobility spectrometry. *Journal of Hazardous materials* **2010,** *176* (1), 692-696.
38. Heeger, A. J., Semiconducting and metallic polymers: the fourth generation of polymeric materials (Nobel lecture). *Angewandte Chemie (International ed.)* **2001,** *40* (14), 2591-2611.
39. Partridge, A. C.; Jansen, M. L.; Arnold, W. M., Conducting polymer-based sensors. *Materials science and engineering C* **2000,** *12* (1), 37-42.
40. Lange, U.; Roznyatovskaya, N. V.; Mirsky, V. M., Conducting polymers in chemical sensors and arrays. *Analytica Chimica Acta* **2008,** *614* (1-26), 1.
41. Bai, H.; Shi, G., Gas sensors based on conducting polymers. *Sensors* **2007,** *7* (3), 267-307.
42. Janata, J.; Josowicz, M., Conducting polymers in electronic chemical sensors. *Nature Materials* **2003,** *2* (1), 19-24.
43. Ram, M. K.; Yavuz, O.; Aldissi, M., NO_2 gas sensing based on ordered ultrathin films of conducting polymer and its nanocomposite. *Synthetic Metals* **2005,** *151* (1), 77-84.

44. McQuade, D. T.; Pullen, A. E.; Swager, T. M., Conjugated polymer-based chemical sensors. *Chemical Reviews* **2000,** *100* (7), 2537-2574.
45. Rajesh; Ahuja, T.; Kumar, D., Recent progress in the development of nano-structured conducting polymers/nanocomposites for sensor applications. *Sensors and actuators B: Chemical* **2009,** *136* (1), 275-286.
46. Angione, M. D.; Magliolo, M.; Cotrone, S.; Mallardi, A.; Altamura, D.; Giannini, C.; Cioffi, N.; Sabbatini, L.; Gobeljic, D.; Scamarcio, G.; Palazzo, G.; Torsi, L., Volatile general anesthetic sensing with organic field-effect transistors integrating phospholipid membranes. *Biosensors and bioelectronics* **2013,** *40* (1), 303-307.
47. Miasik, J. J.; Hooper, A.; Tofield, B. C., Conducting polymer gas sensors. *Journal of the Chemical Society, Faraday Transactions 1: Physical Chemistry in Condensed Phases* **1986,** *82* (4), 1117-1126.
48. Dhawan, S.; Kumar, D.; Ram, M.; Chandra, S.; Trivedi, D., Application of conducting polyaniline as sensor material for ammonia. *Sensors and Actuators B: chemical* **1997,** *40* (2), 99-103.
49. Díaz Aguilar, A.; Forzani, E. S.; Leright, M.; Tsow, F.; Cagan, A.; Iglesias, R. A.; Nagahara, L. A.; Amlani, I.; Tsui, R.; Tao, N., A hybrid nanosensor for TNT vapor detection. *Nano letters* **2009,** *10* (2), 380-384.
50. Andrew, T. L.; Swager, T. M., A fluorescence turn-on mechanism to detect high explosives RDX and PETN. *Journal of the American Chemical Society* **2007,** *129* (23), 7254-7255.
51. Thomas, S. W.; Joly, G. D.; Swager, T. M., Chemical sensors based on amplifying fluorescent conjugated polymers. *Chemical Reviews* **2007,** *107* (4), 1339-1386.
52. Rakow, N. A.; Suslick, K. S., A colorimetric sensor array for odour visualization. *Nature* **2000,** *406* (6797), 710-713.
53. Kannan, G. K., Adsorption studies of carbowax coated surface acoustic wave (SAW) sensor for 2, 4-dinitro toluene (DNT) vapour detection. *Sensors and actuators. B, Chemical* **2004,** *101* (3), 328.
54. Smith, R. G.; D'Souza, N.; Nicklin, S., A review of biosensors and biologically-inspired systems for explosives detection. *Analyst* **2008,** *133* (5), 571-584.
55. Engel, Y.; Elnathan, R.; Pevzner, A.; Davidi, G.; Flaxer, E.; Patolsky, F., Supersensitive Detection of Explosives by Silicon Nanowire Arrays. *Angewandte Chemie-International Edition* **2010,** *49* (38), 6830-6835.
56. Zhang, T.; Mubeen, S.; Myung, N. V.; Deshusses, M. A., Recent progress in carbon nanotube-based gas sensors. *Nanotechnology* **2008,** *19* (33), 332001.
57. Wang, L.; Wang, L.; Shi, X.; Kariuki, N. N.; Schadt, M.; Wang, G. R.; Rendeng, Q.; Choi, J.; Luo, J.; Lu, S., Array of molecularly mediated thin film assemblies of nanoparticles: correlation of vapor sensing with interparticle spatial properties. *Journal of the American Chemical Society* **2007,** *129* (7), 2161-2170.
58. Chen, Y.-Q.; Lu, C.-J., Surface modification on silver nanoparticles for enhancing vapor selectivity of localized surface plasmon resonance sensors. *Sensors and Actuators B: Chemical* **2009,** *135* (2), 492-498.
59. Boisen, A.; Dohn, S.; Keller, S. S.; Schmid, S.; Tenje, M., Cantilever-like micromechanical sensors. *Reports on Progress in Physics* **2011,** *74* (3), 036101.
60. Godin, M.; Tabard-Cossa, V.; Miyahara, Y.; Monga, T.; Williams, P.; Beaulieu, L.; Lennox, R. B.; Grutter, P., Cantilever-based sensing: the origin of surface stress and optimization strategies. *Nanotechnology* **2010,** *21* (7), 075501.
61. Pinnaduwage, L. A.; Boiadjiev, V.; Hawk, J. E.; Thundat, T., Sensitive detection of plastic explosives with self-assembled monolayer-coated microcantilevers. *Applied Physics Letters* **2003,** *83* (7), 1471-1473.

62. Zuo, G.; Li, X.; Zhang, Z.; Yang, T.; Wang, Y.; Cheng, Z.; Feng, S., Dual-SAM functionalization on integrated cantilevers for specific trace-explosive sensing and non-specific adsorption suppression. *Nanotechnology* **2007,** *18* (25), 255501.
63. Lichtenstein, A.; Havivi, E.; Shacham, R.; Hahamy, E.; Leibovich, R.; Pevzner, A.; Krivitsky, V.; Davivi, G.; Presman, I.; Elnathan, R.; Engel, Y.; Flaxer, E.; Patolsky, F., Supersensitive fingerprinting of explosives by chemically modified nanosensors arrays. *Nature Communications* **2014,** *5*, 1-12.
64. Arshak, K.; Moore, E.; Lyons, G. M.; Harris, J.; Clifford, S., A review of gas sensors employed in electronic nose applications. *Sensor Review* **2004,** *24* (2), 181-198.
65. Thompson, C. V., Solid-state dewetting of thin films. *Annu. Rev. Mater. Res.* **2012**, 399-434.
66. Winterbottom, W., Equilibrium shape of a small particle in contact with a foreign substrate. *Acta Metallurgica* **1967,** *15* (2), 303-310.
67. Tyson, W.; Miller, W., Surface free energies of solid metals: Estimation from liquid surface tension measurements. *Surface Science* **1977,** *62* (1), 267-276.
68. Gilman, J. J., Direct measurements of the surface energies of crystals. *Journal of Applied Physics* **1960,** *31* (12), 2208-2218.
69. Hayakawa, R.; Petit, M.; Chikyow, T.; Wakayama, Y., Interface engineering for molecular alignment and device performance of quaterrylene thin films. *Applied Physics Letters* **2008,** *93* (15), 375.
70. Güleç, H. A.; Sarıogˇlu, K.; Mutlu, M., Modification of food contacting surfaces by plasma polymerisation technique. Part I: Determination of hydrophilicity, hydrophobicity and surface free energy by contact angle method. *Journal of food engineering* **2006,** *75* (2), 187-195.
71. Genin, F.; Mullins, W.; Wynblatt, P., Capillary instabilities in polycrystalline metallic foils: experimental observations of thermal pitting in nickel. *Acta metallurgica et materialia* **1994,** *42* (4), 1489-1492.
72. Danielson, D. T. Anisotropic dewetting in ultra-thin single-crystal silicon-on-insulator films. Massachusetts Institute of Technology, 2008.
73. Brandon, R.; Bradshaw, F. *The mobility of the surface atoms of copper and silver evaporated deposits*; DTIC Document: 1966.
74. Voorhees, P. W., The theory of Ostwald ripening. *Journal of Statistical Physics* **1985,** *38* (1-2), 231-252.
75. Grochowska, K.; Sliwinski, G.; Iwulska, A.; Sawczak, M.; Nedyalkov, N.; Atanasov, P.; Obara, G.; Obara, M., Engineering Au Nanoparticle Arrays on SiO_2 Glass by Pulsed UV Laser Irradiation. *Plasmonics* **2013,** *8* (1), 105-113.
76. Gadkari, P. R.; Warren, A. P.; Todi, R. M.; Petrova, R. V.; Coffey, K. R., Comparison of the agglomeration behavior of thin metallic films on SiO_2. *Journal of Vacuum Science Technology A* **2005,** *23* (4), 1152-1161.
77. Kwon, J. Y.; Yoon, T. S.; Kim, K. B.; Min, S. H., Comparison of the agglomeration behavior of Au and Cu films sputter deposited on silicon dioxide. *Journal of Applied Physics* **2003,** *93* (6), 3270-3278.
78. Silly, F.; Castell, M. R., Fe nanocrystal growth on $SrTiO_3$(001). *Applied physics letters* **2005,** *87* (6), 063106.
79. Erkey, C., Preparation of metallic supported nanoparticles and films using supercritical fluid deposition. *The Journal of supercritical fluids* **2009,** *47* (3), 517-522.
80. Campelo, J. M.; Luna, D.; Luque, R.; Marinas, J. M.; Romero, A. A., Sustainable preparation of supported metal nanoparticles and their applications in catalysis. *ChemSusChem* **2009,** *2* (1), 18-45.

81. Javey, A.; Dai, H., Regular arrays of 2 nm metal nanoparticles for deterministic synthesis of nanomaterials. *Journal of the American Chemical Society* **2005,** *127* (34), 11942-11943.
82. Campbell, C. T., Ultrathin metal films and particles on oxide surfaces: structural, electronic and chemisorptive properties. *Surface Science Reports* **1997,** *27* (1), 1-111.
83. Henry, C. R., Morphology of supported nanoparticles. *Progress in Surface Science* **2005,** *80* (3-4), 92-116.
84. Sato, H.; Shinozaki, S., Morphology of nuclei and epitaxial behavior or Au and Ag on MgO. *Journal of vacuum science & technology* **1971,** *8* (1), 159-163.
85. Hybertsen, M. S.; Venkataraman, L.; Klare, J. E.; Whalley, A. C.; Steigerwald, M. L.; Nuckolls, C., Amine-linked single-molecule circuits: systematic trends across molecular families. *Journal of physics: Condensed matter* **2008,** *20* (37), 374115.
86. Sahimi, M., *Applications Of Percolation Theory*. 1994.
87. Bollobás, B.; Riordan, O., *Percolation*. 2006.
88. Kirkpatrick, S., Percolation and conduction. *Reviews of modern physics* **1973,** *45* (4), 574-588.
89. Dattagupta, S., *Diffusion: Formalism and Applications*. Taylor & Francis: 2013.
90. Broadbent, S. R.; Hammersley, J. M. In *Percolation processes I. Crystals and mazes*, Proc. Cambridge Philos. Soc., 1957; pp 629-641.
91. Frisch, H. L., Hammersley, J. M., Percolation processes and related topics. *Journal of the Society for Industrial and Applied Mathematics* **1963,** *11* (4), 894-918.
92. Suding, P. N.; Ziff, R. M., Site percolation thresholds for Archimedean lattices. *Physical Review E* **1999,** *60* (1), 275-283.
93. Kesten, H., The critical probability of bond percolation on the square lattice equals 1/2. *Communications in Mathematical Physics* **1980,** *74* (1), 41-59.
94. Grimmett, G. R., Stacey, A. M., Critical probabilities for site and bond percolation models. *Annals of probability* **1998,** *26* (4), 1788-1812.
95. Hammersley, J. M., Comparison of atom and bond percolation processes. *Journal of mathematical physics* **1961,** *2* (5), 728-733.
96. Shante, V. K. S., Kirkpatrick, S., An introduction to percolation theory. *Advances in Physics* **1971,** *20* (85), 325-357.
97. Sotta, P.; Long, D., The crossover from 2D to 3D percolation: Theory and numerical simulations. *The European Physical Journal E* **2003,** *11* (4), 375-388.
98. Bashan, A.; Parshani, R.; Havlin, S., Percolation in networks composed of connectivity and dependency links. *Physical review E* **2011,** *83* (5), 051127.
99. Obukhov, S. P., The problem of directed percolation. *Physica A* **1980,** *101* (1), 145-155.
100. Meyers, L. A., Contact network epidemiology: Bond percolation applied to infectious disease prediction and control. *Bulletin of the American Mathematical Society* **2007,** *44* (1), 63-86.
101. King, P. R.; Andrade Jr., J. S.; Buldyrev, S. V.; Dokholyan, N.; Lee, Y.; Havlin, S.; Stanley, H. E., Predicting oil recovery using percolation. *Physica A* **1999,** *266* (1), 107-114.
102. Abeles, B.; Pinch, H.; Gittleman, J., Percolation conductivity in W-Al_2O_3 granular metal films. *Physical Review Letters* **1975,** *35* (4), 247-251.
103. Du, F.; Fischer, J. E.; Winey, K. I., Effect of nanotube alignment on percolation conductivity in carbon nanotube/polymer composites. *Physical Review B* **2005,** (72), 121404.
104. Hu, L.; Hecht, D. S.; Grüner, G., Percolation in transparent and conducting carbon nanotube networks. *Nano letters* **2004,** *4* (12), 2513-2517.

105. Bruno, L.; Pijolat, C.; Lalauze, R., Tin dioxide thin-film gas sensor prepared by chemical vapour deposition: Influence of grain size and thickness on the electrical properties. *Sensors and actuators B* **1994,** *18* (1), 195-199.
106. Sysoev, V. V., Percolating SnO_2 nanowire network as a stable gas sensor: Direct comparison of long-term performance versus SnO_2 nanoparticle films. *Sensors and actuators. B, Chemical* **2009,** *139* (2), 699-703.
107. Sysoev, V. V.; Goschnick, J.; Schneider, T.; Strelcov, E.; Kolmakov, A., A gradient microarray electronic nose based on percolating SnO_2 nanowire sensing elements. *Nano letters* **2007,** *7* (10), 3182-3188.
108. Yoo, K. P.; Lim, L. T.; Min, N. K.; Lee, M. J.; Lee, C. J.; Park, C. W., Novel resistive-type humidity sensor based on multiwall carbon nanotube/polyimide composite films. *Sensors and actuators B* **2010,** *145* (1), 120-125.
109. Bläser, G.; Rühl, T.; Diehl, C.; Ulrich, M.; Kohl, D., Nanostructured semiconductor gas sensors to overcome sensitivity limitations due to percolation effects. *Physica A* **1999,** *266* (1), 218-223.
110. Pensa, E.; Cortés, E.; Corthey, G. n.; Carro, P.; Vericat, C.; Fonticelli, M. H.; Benítez, G.; Rubert, A. A.; Salvarezza, R. C., The chemistry of the sulfur–gold interface: in search of a unified model. *Accounts of chemical research* **2012,** *45* (8), 1183-1192.
111. Miki, S., Large sensitive-area NbN nanowire superconducting single-photon detectors fabricated on single-crystal MgO substrates. *Applied physics letters* **2008,** *92* (6), 061116.
112. Kong, J.; Chapline, M. G.; Dai, H., Functionalized carbon nanotubes for molecular hydrogen sensors. *Advanced Materials* **2001,** *13* (18), 1384.
113. Dan, Y.; Lu, Y.; Kybert, N. J.; Luo, Z.; Johnson, A. C., Intrinsic response of graphene vapor sensors. *Nano Letters* **2009,** *9* (4), 1472-1475.
114. Fitch, J.; Bjorkman, C.; Lucovsky, G.; Pollak, F.; Yin, X., Intrinsic stress and stress gradients at the SiO2/Si interface in structures prepared by thermal oxidation of Si and subjected to rapid thermal annealing. *Journal of Vacuum Science & Technology B* **1989,** *7* (4), 775-781.
115. Müller, C. M., Dewetting of Au and AuPt alloy films: A dewetting zone model. *Journal of applied physics* **2013,** *113* (9), 094301.
116. Chopra, K. L.; Bobb, L. C.; Francombe, M. H., Electrical Resistivity of Thin Single-Crystal Gold Films. *Journal of Applied Physics* **1963,** *34* (6), 1699-1702.
117. Adamov, M.; Perović, B.; Nenadović, T., Electrical and structural properties of thin gold films obtained by vacuum evaporation and sputtering. *Thin Solid Films* **1974,** *24* (1), 89-100.
118. Wang, G.; Hirasa, T.; Moses, D.; Heeger, A. J., Fabrication of regioregular poly (3-hexylthiophene) field-effect transistors by dip-coating. *Synthetic metals* **2004,** *146* (2), 127-132.
119. Sandberg, H. G.; Frey, G. L.; Shkunov, M. N.; Sirringhaus, H.; Friend, R. H.; Nielsen, M. M.; Kumpf, C., Ultrathin regioregular poly (3-hexyl thiophene) field-effect transistors. *Langmuir* **2002,** *18* (26), 10176-10182.
120. Norrman, K.; Ghanbari-Siahkali, A.; Larsen, N., 6 Studies of spin-coated polymer films. *Annual Reports Section" C"(Physical Chemistry)* **2005,** *101*, 174-201.
121. Balint, R.; Cassidy, N. J.; Cartmell, S. H., Conductive polymers: towards a smart biomaterial for tissue engineering. *Acta biomaterialia* **2014,** *10* (6), 2341-2353.
122. Visser, S., Modeling electrical conductivity of porous media. **2014**.
123. Šetka, M.; Drbohlavová, J.; Hubálek, J., Nanostructured Polypyrrole-Based Ammonia and Volatile Organic Compound Sensors. *Sensors* **2017,** *17* (3), 562.